

**UC Davis**

**UC Davis Electronic Theses and Dissertations**

**Title**

2D Digital Image Correlation of Barely Visible Impact Damage of T300 Carbon Fiber-Reinforced Polymer and Residual Compressive Strength Testing

**Permalink**

<https://escholarship.org/uc/item/2wq9m7jf>

**Author**

Guinn, David

**Publication Date**

2023

Peer reviewed|Thesis/dissertation

2D Digital Image Correlation of Barely Visible Impact Damage of T300 Carbon  
Fiber-Reinforced Polymer and Residual Compressive Strength Testing

By

DAVID ALEXANDER GUINN

THESIS

Submitted in partial satisfaction of the requirements for the degree of

MASTER OF SCIENCE

in

Mechanical and Aerospace Engineering

in the

OFFICE OF GRADUATE STUDIES

of the

UNIVERSITY OF CALIFORNIA

DAVIS

Approved:

Dr. Valeria La Saponara

Dr. Ben D. Shaw

Dr. Barbara Linke

Committee in Charge

2023

Copyright © 2023 by

David Alexander Guinn

All rights reserved.

To all my amazing friends and family.

I would not have been able to venture this far into this world without all of you.



## ACKNOWLEDGEMENTS

I would like to give a massive thank you to Dr. Valeria La Saponara for serving as my thesis advisor and providing me with guidance in every manner during my time here at the University of California Davis. I would also like to thank Dr. Ben D. Shaw and Dr. Barbara Linke for serving on my thesis committee. I am truly grateful for the research assistance from the members of the ACRES laboratory, Danny Nelson, Shuhao Wan, Shuchen Ye and Alexander Weinstein.

Furthermore, I am extremely thankful for my mother and father, Jacqueline and Keith Guinn, who have supported me throughout my life and endeavors. Lastly, I would like to thank my girlfriend Briana Tamar Aguilar for all of her love and support.

David Alexander Guinn

## Table of Contents

ACRYONYMNS AND ABBREVIATIONS	viii
ABSTRACT	ix
CHAPTER 1	1
1.1 Motivation	1
1.2 Carbon Fiber-reinforced Polymers	3
1.3 Digital Image Correlation	4
1.4 Preliminary Work	6
CHAPTER 2	7
2.1 Manufacturing of T300/epoxy plates by VARTM	7
2.2 Impact testing	11
2.3 Digital Image Correlation Setup	14
2.4 Digital Image Correlation (DIC) Capturing and Processing	15
2.5 Residual Compression Testing Setup	20
CHAPTER 3	22
3.1 Preliminary Testing of CFRP Panels	22
3.2 Impact Damage	26
3.3 DIC Analysis	28
3.4 Testing of Residual Compressive Strength	33
CHAPTER 4	38
References	40
Appendix A – Impact Testing Results	44
Appendix B – Residual Compressive Results	52
Appendix C – Digital Correlation Results	59

List of Figures and Tables

<b>Figure 1: Sketch of a typical VARTM setup (courtesy of Dr. La Saponara)</b> .....	7
<b>Figure 2: T300 fiber texturing during the preparation of the panel</b> .....	8
<b>Figure 3: Initial VARTM bag setup and testing for leaks</b> .....	9
<b>Figure 4: Resin infiltrating the panel</b> .....	10
<b>Figure 5: As-manufactured T300/epoxy panel and preparation of the panel for tile saw cuts</b> .....	11
<b>Figure 6: Impact testing setup with the CFRP panel inside the fixture</b> .....	12
<b>Figure 7: Impact load and energy curves of sample 1</b> .....	13
<b>Figure 8: Experimental setup to acquire Digital Image Correlation</b> .....	14
<b>Figure 9: Capturing images with sample outside (right) and inside (left) the T slot fixture</b> .....	16
<b>Figure 10: Post impact image capturing outside with front side (right) and back side (left)</b> .....	16
<b>Figure 11: Focal plane of an object (plate) (Sutton, 2009)</b> .....	16
<b>Figure 12: Digital Image Correlation AOI and Grid layout</b> .....	20
<b>Figure 13: Residual compression fixture with sample (sample is 95mm x 95mm)</b> .....	21
<b>Figure 14: Preliminary strain results Exx for impacted/ front (left side) and back (right side) surface.</b> .....	23
<b>Figure 15: Preliminary Eyy results for front (left side) and back (right side) surfaces</b> .....	23
<b>Figure 16: Preliminary Exy results for front (left side) and back (right side) surfaces</b> .....	24
<b>Figure 17: Preliminary first principal strain (E1) results for front (left side) and back (right side) surfaces</b> .....	24
<b>Figure 18: Preliminary second principal strain [E2] results for front (left side) and back (right side) surfaces</b> .....	25
<b>Figure 19: Preliminary strain angle [Gamma] results for front (left side) and back (right side) surfaces</b> .....	25
<b>Figure 20: Preliminary Sigma results for front (left side) and back (right side) surfaces</b> .....	26
<b>Figure 21: Impact locations (not to scale) and post-impact thickness measurement locations</b> .....	27
<b>Figure 22: Close-up of sample 1 impacted surface (left) and back surface (right): the silver marker was added post impact to aid visualization against black textured surface.</b> .....	28
<b>Figure 23: Sample 6: images taken with sample inside the T slot: (left) E1 plot for impacted surface and (right) E2 plot for back surface</b> .....	30
<b>Figure 24: Thermography (left) and X-ray CT (right) of T300/epoxy plate sample impacted at 10 J (Loyola et al., 2012)</b> .....	30
<b>Figure 25: Through-the-thickness Acoustic Microscopy image of T300/epoxy plate sample impacted at 20 J (La Saponara, 2018)</b> .....	31
<b>Figure 26: E1 for sample 2 impacted surface: (left) inside and (right) outside the T slot</b> .....	32
<b>Figure 27: E2 for sample 2 impacted surface: (left) inside and (right) outside the T slot</b> .....	32
<b>Figure 28: Sigma for sample 2 impacted surface: (left) inside and (right) outside the T slot</b> .....	33
<b>Figure 29: Static compression plot for sample 6</b> .....	34
<b>Figure 30: Acceptable failure modes LDM and LGM from ASTM D7137</b> .....	36
<b>Figure 31: Sample 3 front (left) and sample 7 back (right)</b> .....	36

<b>Table 1: Comparison of characteristics with NDT methods</b> .....	2
<b>Table 2: Dimensional Measurements of T300/epoxy samples</b> .....	11
<b>Table 3: Settings used for DIC Analysis</b> .....	19
<b>Table 4: Preliminary Pixel result statistics of Confidence Interval [Sigma]</b> .....	26
<b>Table 5: Pre-and post-impact thickness measurements</b> .....	27
<b>Table 6: Comparison of Inside and Outside Confidence Intervals</b> .....	31
<b>Table 7: Ultimate compressive strength of samples</b> .....	35

## ACRYONYMNS AND ABBREVIATIONS

AOI	Area of Interest
BVID	Barely Visible Impact Damage
CFRP	Carbon Fiber-Reinforced Polymer
DIC	Digital Image Correlation
FDM	Fused Deposition Modeling
NDT	Non-Destructive Testing
PETG	Polyethylene terephthalate glycol
VARTM	Vacuum Assisted Resin Transfer Molding

## ABSTRACT

Non-destructive testing methods often provide a key understanding of damage when examining carbon fiber-reinforced polymers (CFRP) without compromising their structural integrity. Yet the limitations of various accurate nondestructive testing (NDT) methods decrease the range of application within the commercial aerospace world due to the scale and complexity of parts post assembly. The study of this thesis investigated impact tests performed on T300 carbon fiber-reinforced polymer samples to understand if analysis by 2D digital image correlation (DIC) can be used to identify barely visible impact damage (BVID). The intent is that this process could allow monitoring of impact damage on an aircraft if baseline pre-impact images are available for those components. T300/epoxy plate samples were created through VARTM (Vacuum Assisted Resin Transfer Modeling), impacted following ASTM 7136 guidelines, and tested for residual compressive strength according to ASTM 7137 guidelines, to showcase the extent of damage. Strain of the pixels between images was calculated through DIC (Digital Image Correlation) from Correlated Solutions VIC 2D commercial software. A Lagrange tensor type was chosen for strain computation with a normalized squared differences criteria for correlation. The results provide a range of impact imagery via DIC on frontal (impacted) and posterior sides of the samples. By cross-referencing other NDT methods applied to impacted T300/epoxy at the same or similar energy levels and nearly identical manufacturing techniques, 2D DIC shows promising evidence that it could provide evaluation of damage from BVID on CFRPs.

# CHAPTER 1

## INTRODUCTION, LITERATURE REVIEW, AND PRELIMINARY WORK

### 1.1 Motivation

The aerospace industry is a major sector in the U.S. economy and carbon fiber reinforced polymers (CFRPs) are used in many structural applications, including critical components such as fuselages and wings. Various defects that occur overtime can cause critical failures. Because of the expensive nature of aerospace components, we need nondestructive testing methods to evaluate occurrence of damage as well as its severity which could produce hazards.

The research question of this study is if low-cost 2D Digital Image Correlation (DIC) with CFRPs can determine the presence of barely visible impact damage. It is commonly known that one considerable liability of composite structures is barely visible impact damage: an impacted surface may not exhibit visible proof of damage, but there may be substantial, visible damage on the opposite surface (in the form of matrix cracks and possibly even fiber damage). A standard inspection from a technician would most likely not find the defect and would require other NDT methods for confirmation. Even though a 3D DIC comes with a greater advantage, such as out-of-plane displacements and strains captured (Flores et al., 2017), more affordable 2D DIC may provide a suitable baseline of damage by comparison with other nondestructive testing methods such as X-Ray Tomography, Thermography and Acoustic Microscopy. See **Table 1** for a comparison of characteristics with these NDT methods. It is important to note that the cost of the setup does not include software.

**Table 1: Comparison of characteristics with NDT methods**

	Cost of Setup	Setup Complexity	Effort for Experimentation	Knowledge Required
2D DIC	Low	Low	Low	Medium
3D DIC	Medium	Medium	Medium	Medium
X-ray Tomography	High	High	High	High
Thermography	Medium	Medium	High	Medium
Acoustic Microscopy	Medium	High	High	High

In many cases of the commercial and defense sectors, rather outdated and non-consistent methods are used to investigate the structural integrity of CFRP aircraft parts. Currently, a commonly used NDT method is the “coin method” (Cawley and Adams, 1988), where a trained technician will use a coin or a digital hammer to lightly tap various panels on a plane's surface to detect defects. This is accomplished through listening for the distinction of acoustic resonance between the intervals of tapping. The process is said to be highly labor intensive in conjunction with the necessity of an experienced technician. The inaccuracy and inability associated with detecting various impacts, crushed honeycomb cores, delamination or other defects makes this methodology unreliable.

CRFPs have different damage types, such as delamination between layers, matrix, and fiber damage. It is well known that impact damage may not be visible on a CFRP-impacted surface (Schimmer et al., 2019). 2D DIC methods may assist in detecting this type of damage. A potential scenario for the application of 2D DIC could be along the lines of a pilot of a Boeing 787 report that birds were seen near the aircraft during take-off and a possible impact may have occurred. Investigation of whether a strike to the aircraft occurred could be carried out with an image of the aircraft before any flight and an image of the aircraft after landing at its destination. With input



from the pilot of where the impact may have occurred, a technician could examine if a) a strike had occurred and if so b) determine whether the strike imposed a greater amount of damage than what is deemed safe by a regulator agency, and c) document the strike and closely monitored to see if the damage is increasing and would be deemed unacceptable by the Maintenance, Repair and Operations (MRO) team in charge of the aircraft.

## 1.2 Carbon Fiber-reinforced Polymers

Carbon fiber-reinforced polymers (CFRPs) have enabled the advancement of various advanced aerospace structures due to their material properties in comparison to metallic materials, such as low weight, high stiffness, high strength, corrosion resistance, longer fatigue life, reduced maintenance, and retention of properties at high operating temperatures (Herakovich, 1998). In contrast to most metallic alloy materials based on aluminum, steel and titanium, CFRPs are not considered isotropic homogeneous materials. Instead, they are considered anisotropic heterogeneous viscoelastic materials whose properties also depend on manufacturing quality and processes, such as consistent fiber volume ratios, correct fiber orientation in ply layering, and human error that occur with the creation of the material (Elhajjar et al., 2019).

In addition, CFRPs exhibit different behaviors as a result of the direction of the fibers in comparison to the direction of loading. The stacking of individual fiber layers create a laminate and may vary with orientation, thickness and stacking sequence which is to influence an optimal direction of loading, thus strengthening the material. The examination of surface and internal composite damage cannot be executed in the same manner as conventional metallic materials: an example such as crack propagation is an instance where fiber-reinforced polymer materials behave

in a stark contrast to metals. Tough metallic materials resist crack formation and propagation by yielding, but cyclic loading or impacting will further propagate the crack within the structure. CFRPs may reduce crack propagation through a combined mechanism of woven fibers interfering with the crack propagation, and a polymer matrix that can yield and provide fracture toughness (Ritchie, 1988).

Aircraft structures typically contain laminates, with layers at varying fiber orientations and/or sandwich composites, with a thick core material (for example Kevlar honeycomb) between stiff skins, providing bending stiffness and impact resistance. An example of why different materials are used in composites would be that Kevlar provides excellent tensile properties at a lower cost than carbon fibers, but carbon fibers contain better compressive properties than Kevlar (Flores et al., 2017). Combining both into a composite attains the desired properties but is still economically viable with a large structure like an aircraft. Within this study we analyze just the monolithic laminate itself. Typically on an aircraft there would be composites with coatings such as paint or other additional layering materials.

### 1.3 Digital Image Correlation

Digital Image Correlation (DIC) is a precise, non-contact, and non-interferometric optical method used for measuring the displacement/deformation of a structural element/material subjected to external loading (Chu et al., 1985). The idea of the DIC method is based on the principles of continuum mechanics (rigid body mechanics), where a digital camera captures consecutive images of a structure's surface before and after the deformation of that structure. Once a series of photos are captured, they are analyzed through an in-house or commercial DIC software computer program. In the case of this study, a preliminary photo as well as a post impact photo would be compared to analyze deformation. An area of interest (AOI) is allocated to the DIC

program to analyze a specific portion of the comparative images, which in this case would be the impact site. To be able to correlation between the photos, the subset within the area of interest must contain distinctive features. These subsets of the images AOI are within a grid pattern comprised of square subsets to directly compare pixels. If the subset is large enough to include one grid intersection, the analysis can proceed without error. The user of the software can define selection criteria such as tensor type, image weighting, filter size of the subset and thresholds in acceptance of pixel matching confidence. In the case of this thesis, a commercial software, VIC-2D by Correlated Solutions was chosen from the previous utilization of the software within ARCES research laboratory. Typically, researchers will apply a unique pattern or random speckles / dots to the surface through fine mists of spray paint; this is done usually with a white background and black dots (Spencer et al., 2021; Chu et al., 1985). This is to increase the surface roughness as well as give an unambiguous start and end pixel for the AOI. In most cases, whether the material is metal, ceramic or composite, a glossy or satin paint under intense lighting would show reflections of the speckle patterns which aid the software in effective correlation. A speckle-free DIC method can also be used (Spencer et al., 2021), and was applied in the current thesis. Moreover, one paper (Niu et al., 2017) examined the DIC methodology using both a novel speckle-free pattern, and a traditional painted speckle pattern, to accurately identify differences on the material between stages of the photographs. It was found that, in their case, the speckle-free pattern had a similar accuracy as the conventional DIC method. In some regards, they found the speckle-free approach to be more accurate, because the traditional method would require layers of fine mist that would eventually build on the material and cause errors with image processing.

## 1.4 Preliminary Work

The research work started with the goal of applying DIC to 3D-printed samples made with a Fused Deposition Modeling (FDM) technique. The samples consisted of Polyethylene terephthalate glycol (PETG) polymer with chopped carbon fiber strands as reinforcement, to be studied with DIC in order to understand their bending and impact resistance. The reasoning behind this was that the literature considers this material combination as producing the highest tensile strength results for 3D-printed composites (Jiang et al., 2017; Mansour et al., 2018). The parameters regarding the print temperature, infill and pattern of print were adhered to as much as possible with the printer provided. The first samples were rectangular and approximately 200mm x 40mm x 6.5mm (LWH), and were subjected to four-point bending tests using ASTM D6272 on a hydraulic testing machine (MTS 810). Based on the user's testing choices and ASTM D6272, the material did not reach a significant deformation that could be easily identified by the DIC setup. Observing this issue created the motivation to see if plates made by this additively manufactured material would perform better under drop-weight impact and with barely visible damage, and whether DIC would be a useful technique. Multiple FDM samples of 95mm x 95mm x 5mm (LWH) were produced with various infill amounts and patterns that would in theory be able to absorb the energy of the drop-weight impact. It was quickly discovered that the carbon/PETG samples behaved in a brittle manner, shattering at energies as low as 5J, compared to composite samples made with traditional manufacturing methods. It is hypothesized that the chopped fibers, the potential lack of sufficient adhesion between fibers and polymer caused by the fast cure of an FDM composite, and the lower fiber volume ratio may all be reasons for the poor performance. To produce mechanically strong CFRP plates, they were manufactured with Vacuum Assisted Resin Transfer Molding instead of FDM, as described in the next Chapter.

## CHAPTER 2

### EXPERIMENTAL PROCEDURES

#### 2.1 Manufacturing of T300/epoxy plates by VARTM

CFRP samples were created using T300 carbon plain weave layers (with one layer having [0/90] orientation), and Proset 125/237 epoxy/hardener. **Figure 2** shows an overview of the VARTM (Vacuum Assisted Resin Transfer Modeling) process, a conventional out-of-autoclave manufacturing process for fiber-reinforced polymer composites, where a polymer (resin) infiltrates a laminate of dry fabric layers, and is driven across the laminate through vacuum pressure.

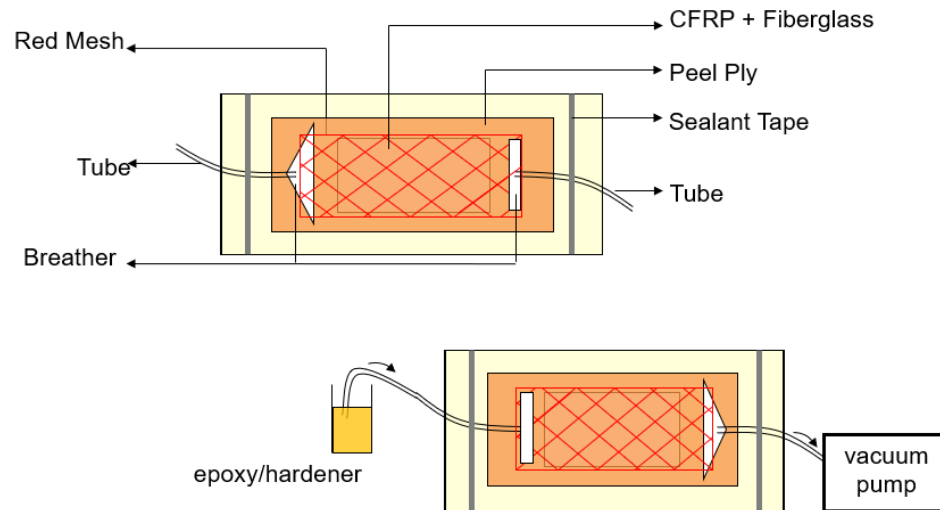


**Figure 1: Sketch of a typical VARTM setup (courtesy of Dr. La Saponara)**

The process requires several expendable supplies to remove voids from the panel, ease the flow process and ease the removal of the part from the mold. For this thesis, a total of 9 samples were created from a 356mm x 356mm layup with 10 layers of T300/epoxy. The process began by

cutting out ten 356mm x 356mm plain weave T300 fabric sheets from a roll. The next step was layering them in their original [0/90] orientation onto a flat metal square plate which was larger than the T300 sheets. This metal plate was the mold, the shape that the composite would assume upon curing. The plate would eventually be inserted into a vacuum bag during the VARTM process, and its corners were covered with duct tape to decrease the likelihood of rupturing the vacuum bag. It was decided to have a surface texture on the composite plate, based on the hypothesis that it could replace the speckle pattern typically applied to the surface for DIC analysis (**Figure 2**). The surface texture was provided by strips of T300 applied randomly onto Teflon-coated fiberglass.



**Figure 2: T300 fiber texturing during the preparation of the panel**

A 381mm x 381mm layer of Teflon-coated fiberglass layer prevents the sample from adhering to the vacuum bag after the resin has infiltrated the fabric and has fully cured. Two tubes were prepared on each end of the sample: one would allow the infiltration of the resin, the other the removal of air from the sample, which would also pull the resin across the entire sample.

The tubes were further wrapped by breather cloth, an airy polyester-based material that is used to ease removal of air from the panel. It also absorbs excess resin and acts as a filter against

unwanted inclusions from the epoxy/hardener container. Duct tape was used to hold the tubing in place. The last layer applied to the top of the panel was a 381mm x 381mm layer of red mesh: the red mesh aided the resin to better infiltrate the sample, by channeling it. The setup was finally completely by inserting everything into the vacuum bag and sealing it appropriately with temperature-resistant tape.

Testing of the sealant tape and the bag was a vital step in validating that the vacuum bag would work throughout the multi-hour VARTM process. This was tested by dry-running the vacuum without the presence of resin and using clamps to observe whether the pressure gauge attached to the vacuum pump had the expected reading.



**Figure 3: Initial VARTM bag setup and testing for leaks**

If a leak was noticed from the bag being refilled with air upon shutting off the vacuum pump, the sealant tape would be pressed down at locations thought to be the source of the leak from visual and audible indications. This process was repeated until the vacuum was maintained.

A mixture of 428 grams of resin and 122 grams of hardener were combined for a total of 550g of 125-237 LAM resin/hardener, according to the published ratio on the data sheet. This

amount was deemed to be sufficient for the volume of fabric to be infiltrated based on experience.

After the resin and hardener were combined and stirred into a mixing pot, the pot was placed in a small vacuum chamber to degas the mixture for approximately 25 minutes. By placing it in the chamber, the air in the mixture rises to the surface into a film that can be easily removed. This process is done to prevent bubbles from encroaching into the CFRP matrix and weakening the material. Degassing of the mixture was possible due to the published pot life (working time prior to gelation, where the mixture becomes too viscous to move through the part) of 7 hours at 25 °C . The entire VARTM process took nearly 3 hours with the pump running the entire time, see **Figure 4** for intermediate resin infiltration of the panel.

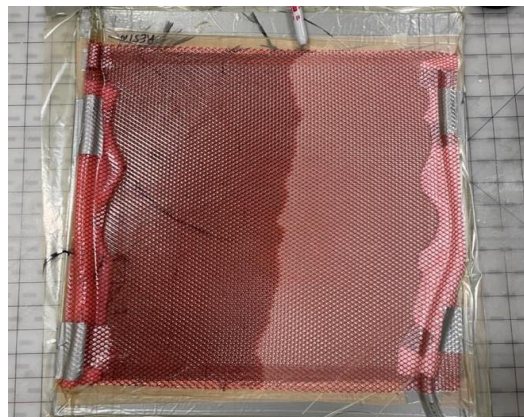


**Figure 4: Resin infiltrating the panel**

The tubes were clamped and the sample was moved to an oven (Yamato DKN-600 convection oven). The entire curing process was completed with a two-step cure, the first being a 14-hour cure time at 25°C and the second being an 8-hour cure time at 82°C. Once the sample completed its cure time, the bag was removed and the sample was checked for potential defects



and other imperfections such as voids which cause microcracks, delamination and fracturing (Dhimole, 2021).

A wet tile saw was used in order to cut the 9 samples used within the experiments. Even though a 356mm x 356mm sample was created, it was known that imperfections would occur around the outer perimeter of the sample (see **Figure 5**, with cured post-VARTM sample and the tile saw sample preparation, and **Table 2** for sample measurements).

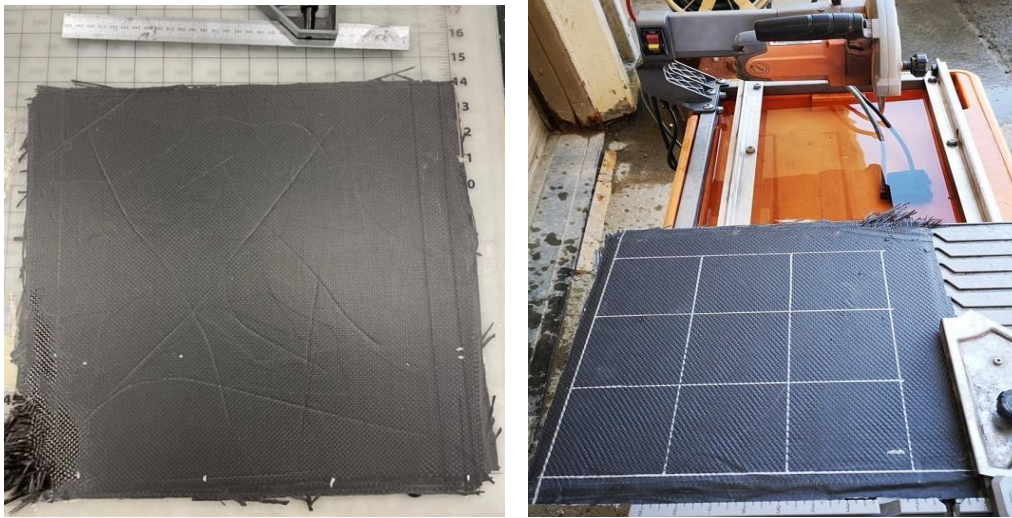


**Figure 5: As-manufactured T300/epoxy panel and preparation of the panel for tile saw cuts**

**Table 2: Dimensional Measurements of T300/epoxy samples**

Length [mm]	Width [mm]	Thickness [mm]
$96.01 \pm 0.77$	$95.98 \pm 0.49$	$2.27 \pm 0.00$

## 2.2 Impact testing

Impact testing of the T300/epoxy samples was accomplished using an instrumented impact tester (Instron 9250G). The ASTM D7136 standard was followed when performing the impacting of all samples. The machine was calibrated before testing. Once this was completed, the sample was placed into the fixture compatible with its geometry (see **Figure 6**). The first

round of impacts for 8 samples were done at a nominal impact energy equal to 10 J, with a 50.8mm hemispherical impactor (also named “head” in the plots), hitting the sample at the center of the sample. A second round of impacts was done for 4 of the samples, again at 10 J energy, but this time with a 25.4mm diameter cylindrical impactor. It was hypothesized that the second impact would show changes in the residual compression tests of the samples impacted twice, and could further highlights the benefits of DIC.

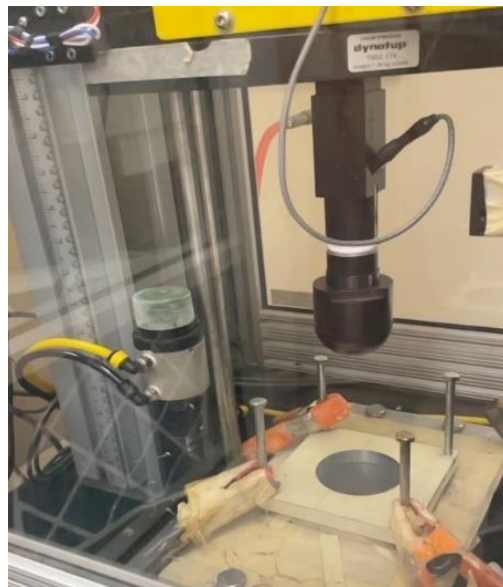


**Figure 6: Impact testing setup with the CFRP panel inside the fixture**

Other papers utilized various levels of energy (10J being the most common) with T300/polymer coupons or variations of T300, which produced both barely visible and visible impact damage, for example Symons, 2000, Loyola et al., 2012, Schimmer et al., 2019. With respect to these published works and this thesis, there were differences. The differences consisted of ply thickness or number of layers: 2mm in Loyola et al., 2012, Schimmer et al., 2019; 21 layers in Symons et al., 2000, versus this thesis (2.3mm thickness, 10 layers). In Schimmer et al., 2019, an impactor of 8mm diameter head is used, instead of the 26mm and 51mm impactors used in the

experiments of this thesis. Finally, Loyola et al. (2012) used Proset 117LV/237 resin instead of Proset 125/237 (Loyola is a former graduate student of Dr. La Saponara's and many of the techniques and equipment were the same). These sources show that a 10 J nominal impact energy produced barely visible impact damage, while also preventing noise within the data with respect to the load cell capacity of the impactor. With this equipment and its nominal energy capacity of 180 J, data acquired for impact energies lower than 10 J appear to be noisy. **Figure 7** shows impact load and energy curves for the first preliminary sample tested. The peak of the energy curve is the actual impact energy experienced by the sample, while the steady-state value is the energy absorbed by the sample.

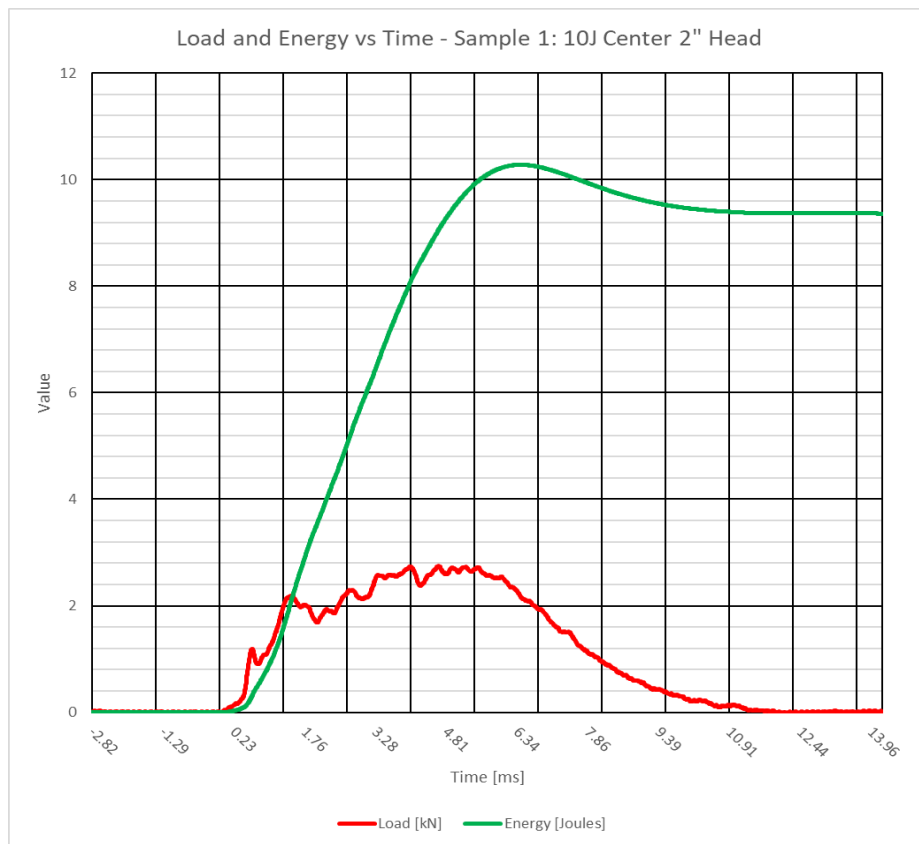


**Figure 7: Impact load and energy curves of sample 1**

### 2.3 Digital Image Correlation Setup

The DIC equipment consisted of a Mako G-503B, a 1/2.5-inch monochromatic 5-megapixel CMOS sensor camera equipped with an Edmund Optics 25mm fixed focal length lens to capture 16-bit TIFF type images via ethernet cable to the selected image software (Vimba Viewer by Allied Vision). The camera was attached to an orthogonal mounting setup which clamped to a table and connected to the camera (mounted vertically) through a universal adapter mounting bracket. Two T slot aluminum rails were used as a guide to where to place each plate sample as seen in **Figure 8**. They were mounted together with a 90° bracket and were mounted to the table with a C clamp. On the larger of the two T slot aluminum rails was a ruler to provide a scale in the photos. Next to the camera was a 150 W halogen light source which was clamped to large aluminum blocks to prevent any movement. The light source incorporated two alligator arm style attachments which were aimed in a manner to prevent any shadows from forming during the image capturing. This consideration was made because the greyscale pattern that the DIC software uses is extremely sensitive to changes in light, shadows, etc.

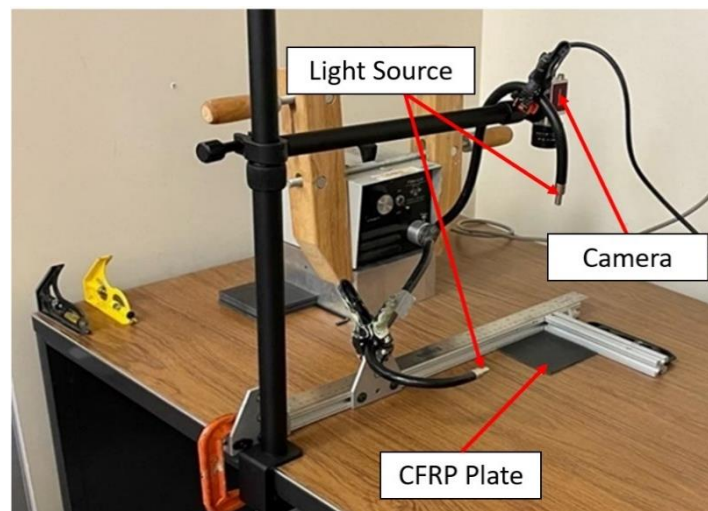


**Figure 8: Experimental setup to acquire Digital Image Correlation**

It was important to replicate the location of baseline and post-impact photos with the highest accuracy possible to remove the error of rigid body translation and rotation. This was achieved through mounting the setup further with various clamps and weights to mitigate apparatus movement between the photos. The setup was isolated and bare to reduce the likelihood of human error of contact with the apparatus. The VIC-2D software can remove some rigid body motion in cases where photos are within an acceptable margin. The image correlation from the pixel grayscale pattern requires photos to be within a small margin. The rigid body removal feature was tested (on samples 1-4 and preliminary sample), but did not affect the post-processing strain computation enough to be considered significant within the data captured with the variables discussed with Section 2.2. Within this study rigid body rotation was not used for the CFRP plates as an additional feature with the DIC analysis as it did not provide any improvement in detecting BVID.

#### 2.4 Digital Image Correlation (DIC) Capturing and Processing

Pictures were captured in two different manners for the DIC setup, see **Figure 9**. The first type was taking photography using the sample placed on the table while against the 90° portion of the T slot 90°, while the second was placing the sample within the 90° portion of the T slot. This was done for the photos of both the front as well as back impacted samples. For a comparison between baseline and post-impact photos, there is a total of 8 photos: 4 pre-impact and 4 post-impact photos.



**Figure 9: Capturing images with sample outside (right) and inside (left) the T slot fixture**



**Figure 10: Post impact image capturing outside with front side (right) and back side (left)**

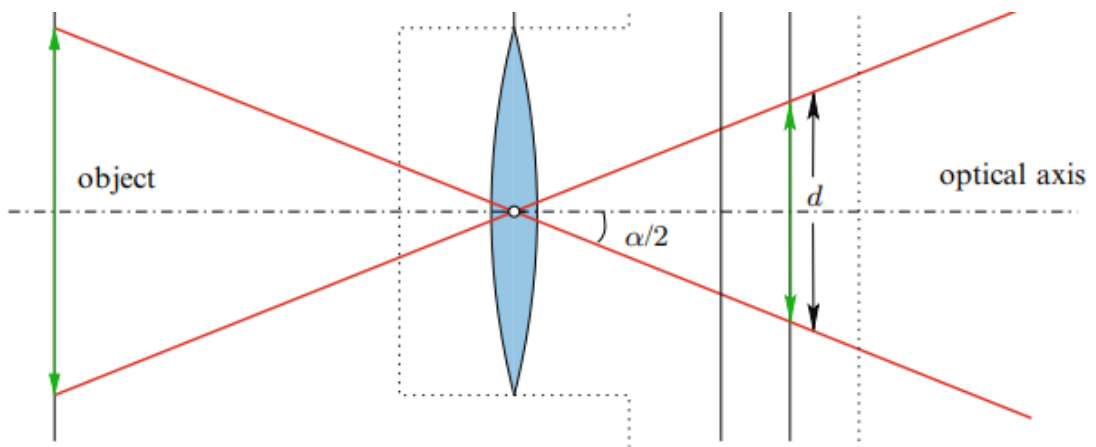


**Figure 11: Focal plane of an object (plate) (Sutton, 2009)**

The reason for placing the sample both on the table and the insert of the T slot is to offset any displacement from the impact. While a sample that is placed on the bottom of the T slot (flat

on the table) may change the focal plane from photo to photo (see **Figure 10** and **Figure 11**) from an impact in the form of a mound shape, placing the sample inside the T slot allows for the focal plane to remain the same. Impacting a sample would create a mound shape deformation which, when capturing the post impact photo, would change the field of depth for that specific photo. When testing preliminary samples, it was found out that placing the sample on a flat surface after impacting resulted in tilting of the sample because of this deformation. Since the area of interest with impacting would not reside near the edges of the impact, placing the sample in the T slot accomplished fixing two problems that would regularly cause errors or appear less accurate: the first is that the original focal plane of impact would not be changed; the second is that by inserting the sample into the T slot, the sample would essentially be floating except for two edges, thus eliminating the tilting of the sample as observed when the sample was placed flat on the table after impact. Both types of photos (inside and outside) were captured to confirm these assumptions as only the preliminary sample provided insight to this matter. Utilizing only 1 sample was not sufficient enough (in terms of population size) to confirm the result of the observation.

Because the square specimens are built from plain weave, with quasi-isotropic properties, it can be justified that within the strain equations seen for composites, the stiffness in the two directions is the same, i.e.,  $E_{xx} = E_{yy}$ , allowing for a simplification of the in-plane strain analysis to be the same as metallic material (Herakovich, 1998). Through the program, a set of displacement maps for the surface are created and strain fields can be evaluated from the pictures (Sutton et al, 2009; Sierakowski et al, 2011). A Lagrange tensor type was selected to calculate the strain fields, to allow for potentially large strains caused by impact (Sutton et al, 2009). The selection criteria for the correlation of images was the normalized sum of squares differences method. This was chosen because this criterion is unaffected by scale in lighting (intensity, reflectivity, and



brightness of lighting) which provided more flexibility in lighting errors within photo capturing; other methods such as squared differences and zero-normalized squared differences are both effected by lighting manipulations. Additionally, a Gaussian distribution provides a compromise between spatial and displacement resolution. (Sutton et al, 2009).

$$1. C = F^T F$$

$$2. E = \frac{1}{2}(C - I)$$

$$3. \chi_{\text{NSSD}}^2 = \sum w(x) \left( \frac{\sum H_i G_i}{\sum G_i^2} G_i - H \right)^2$$

where

Eq1 - F is the deformation gradient tensor

Eq 2 - E is the (baseline) strain tensor

Eq 3 - G is the reference image post-impact (pixels)

Eq 3 - H is the reference image pre-impact (pixels)

Eq 2 - E is the (baseline) strain tensor

Eq 3 -  $\chi_{\text{NSSD}}^2$  is the Normalized Sum of Squares Differences

Eq 3 - w(x) is the weighted Gaussian subset

Moreover

$$4. E_1 = \frac{E_{xx} + E_{yy}}{2} + \sqrt{\left(\frac{E_{xx} - E_{yy}}{2}\right)^2 + \left(\frac{E_{xy}}{2}\right)^2}$$

$$5. E_2 = \frac{E_{xx} + E_{yy}}{2} - \sqrt{\left(\frac{E_{xx} - E_{yy}}{2}\right)^2 + \left(\frac{E_{xy}}{2}\right)^2}$$

where:

Eq 4 - E1 is the major principal strain



Eq 4 and 5 -  $E_{xx}$  is the strain in the x direction

Eq 4 and 5 -  $E_{yy}$  is the strain in the y direction

Eq 4 and 5 -  $E_{xy}$  is the shear strain

Eq 5 -  $E_2$  is the minor principal strain

Processing the image on the VIC 2D program included choosing an AOI that would conservatively cover where the impact had occurred on the sample (see **Figure 12**): the red highlight over the specified area is considered the AOI, with the yellow grid being the subset of the image examined. Other image processing options included choosing various local filter sizes, a maximum of confidence margin, consistency threshold and matchability threshold.

**Table 3: Settings used for DIC Analysis**

	Local Filter Size [pixels]	Maximum of confidence margin	Consistency threshold	Matchability Threshold.
Values	15	0.05	0.02	0.1

The local filter enabled the calculated strains to be smoothed, to produce a clear strain field that is both accurate as well as void of noise from insignificant errors. Other variables are optimized to create a statistical confidence region, which was produced through the covariance matrix of the correlation; if the data exceeded the threshold, insignificant subsets would be removed.

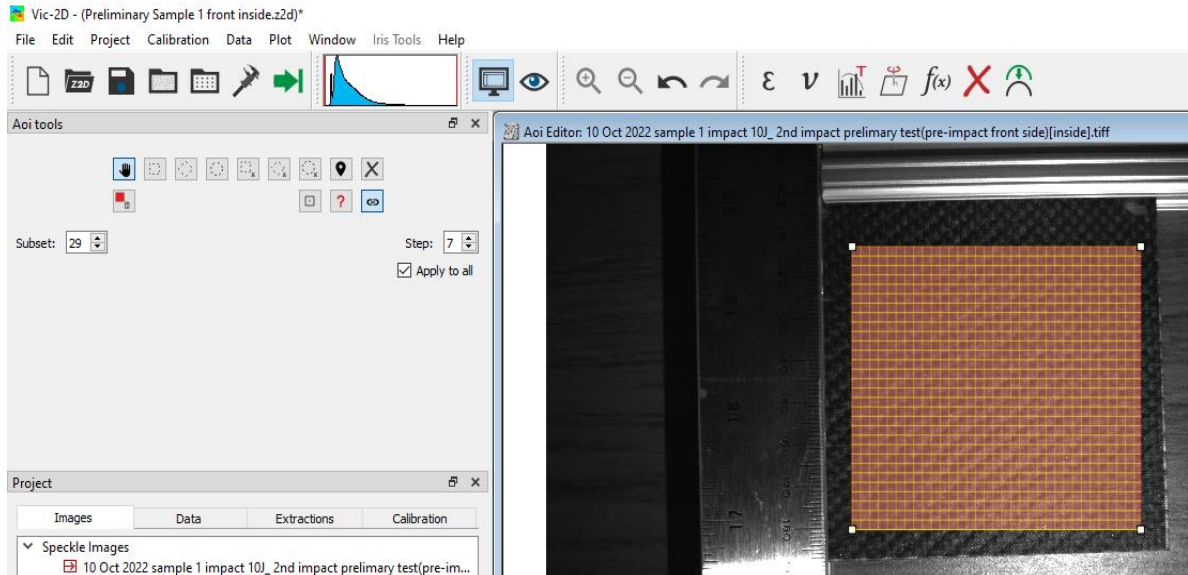


**Figure 12: Digital Image Correlation AOI and Grid layout**

## 2.5 Residual Compression Testing Setup

The ASTM standard D7137/D 7137M standard describes an uniaxial residual compression test, which is performed on symmetric (evenly distributed ply layers) laminated plates, which have been previously damaged through out-of-plane loading indentation or drop-weight impact using ASTM D7136/D7136M. The purpose of these tests was to show a correspondence between the DIC results and the compressive residual strengths of the impacted samples. This is done by vertically loading the top of the fixture onto the top of the sample, while the rest of the fixture holds the sample in place. Residual compression testing must be done until a failure point is met by the sample or else it is considered unusable for data.

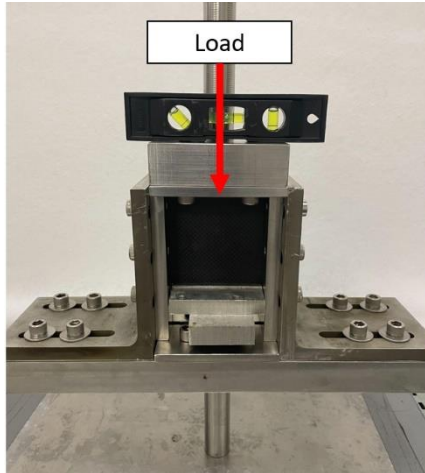


**Figure 13: Residual compression fixture with sample (sample is 95mm x 95mm)**

The sample was secured into the fixture shown in **Figure 13**. Bolts around the fixture were securely fastened with an Allen wrench. Only one side of the fixture was loosened to allow the insertion of a new sample between compression tests to minimize the variation between samples. Within the lower portion of the fixture, metal slats were placed for the sample to be sufficiently secure. The fixture was then gripped into a hydraulic testing machine (MTS 810). The sample was then compressed to its failure point at the selected displacement rate. When the sample was removed, it was marked along the site of failure to determine the mode of failure described through the ASTM standard.

Not knowing what the point of failure would be, sample 2 was used for preliminary tests, to gauge the appropriate maximum load setting on the MTS for the samples. It was at this stage where the estimation of failure was thought to be approximately 30kN of force or less. The rest of the samples were compressed at the rate 1mm per minute. After the residual compression testing, the samples were measured with calipers to determine how much the sample had deformed in 5 locations.

## CHAPTER 3

### RESULTS AND DISCUSSION

#### 3.1 Preliminary Testing of CFRP Panels

After the creation of the CFRP samples, preliminary testing with the DIC setup and the impact tester were performed to validate whether the surface texture would require the addition of a speckle pattern for the DIC analysis. The preliminary testing of one individual CFRP sample showed that the surface roughness of the material was sufficient to use in actual testing without the need of a speckle pattern. The DIC highlighted the presence of damage on the surface opposite of the impacted surface. The images depict strain of the pixels in the x- [ $E_{xx}$ ] (**Figure 14**) and y- axes [ $E_{yy}$ ] (**Figure 15**), while the shear strain [ $E_{xy}$ ] is in **Figure 16**. Other images include the first [ $E_1$ ] (**Figure 17**) and second principal strain [ $E_2$ ] (**Figure 18****Error! Reference source not found.**), and the principal strain angle [ $\Gamma$ ] (**Figure 19**). The preliminary DIC results indicated that a confidence interval [ $\Sigma$ ] of at least 95% was achieved for the correlation of the pixels from before and after images of the impact test as shown in **Figure 20** and statistics of [ $\Sigma$ ] in **Table 4**. This confirmed that the digital image correlation was successful with this apparatus. It should be noted that the highest values of [ $\Sigma$ ] were the points (red as indicated by color scale) where the analysis was least confident in its correlation between images. These higher uncertainty areas were around the impact site, and resulted in barely visible impact damage on the back of the plate sample.

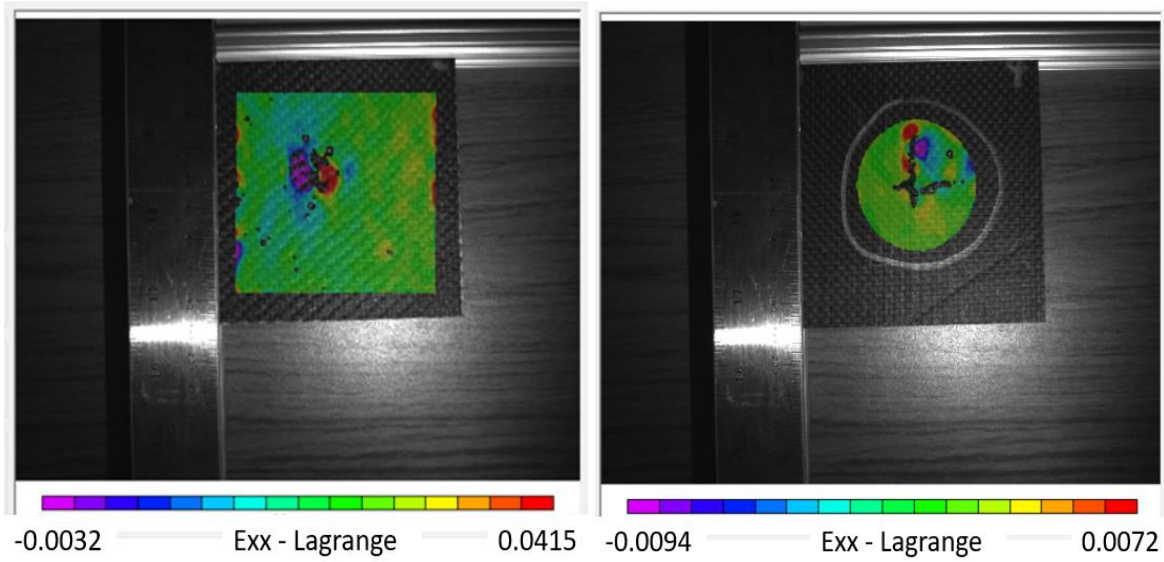


**Figure 14: Preliminary strain results Exx for impacted/ front (left side) and back (right side) surface.**

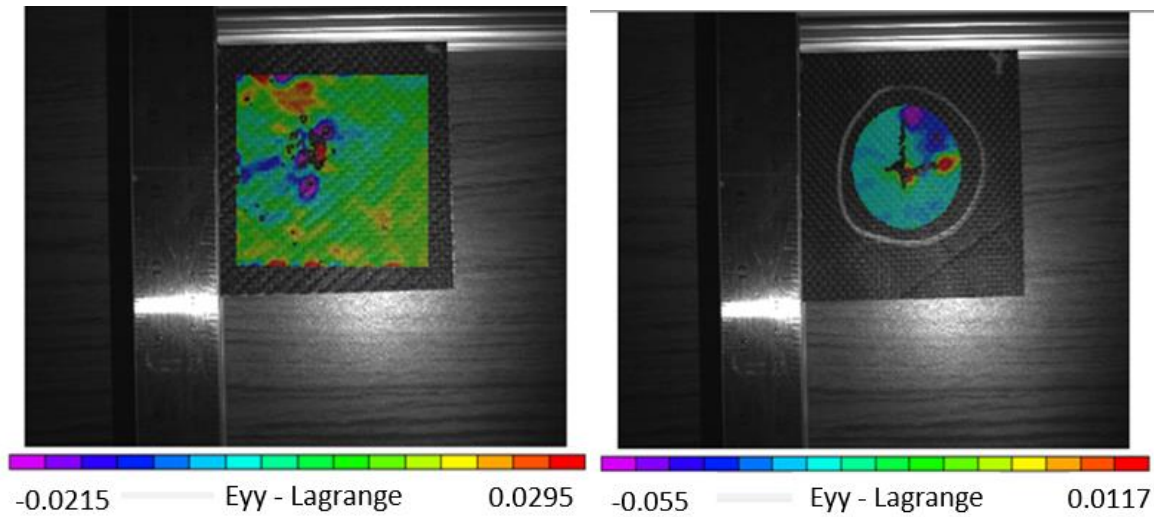


**Figure 15: Preliminary Eyy results for front (left side) and back (right side) surfaces**

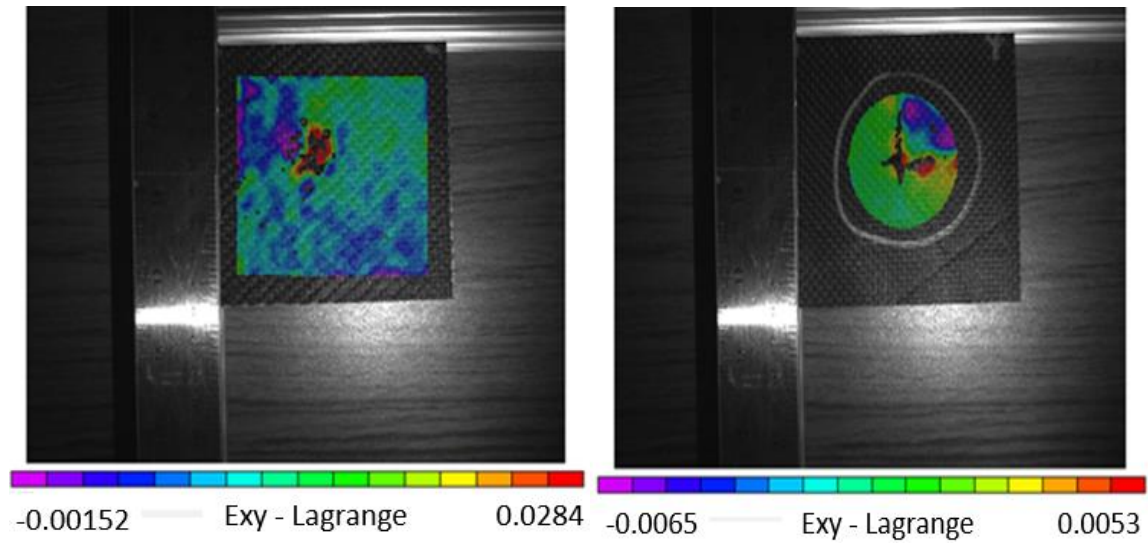


**Figure 16: Preliminary Exy results for front (left side) and back (right side) surfaces**

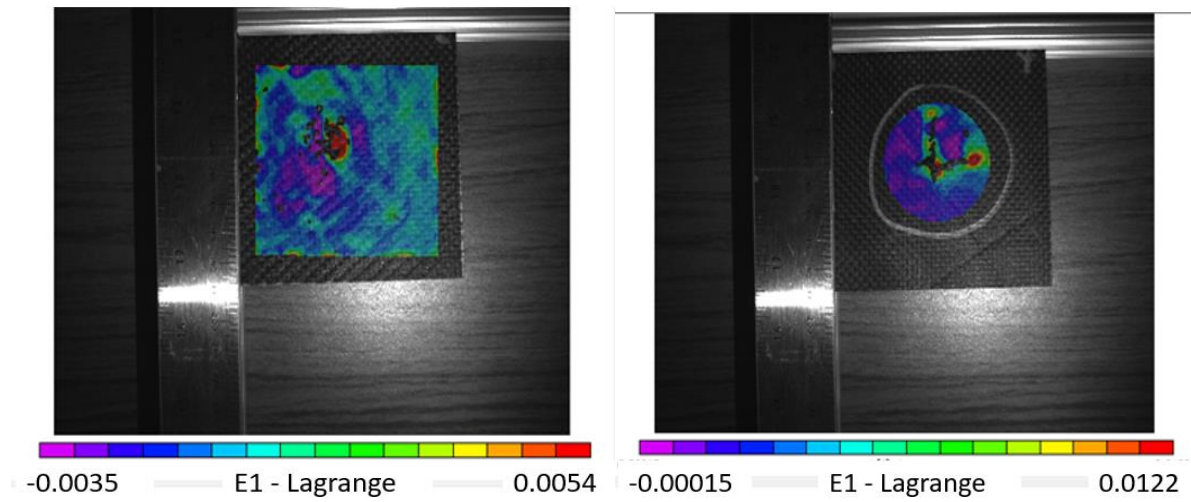


**Figure 17: Preliminary first principal strain (E1) results for front (left side) and back (right side) surfaces**

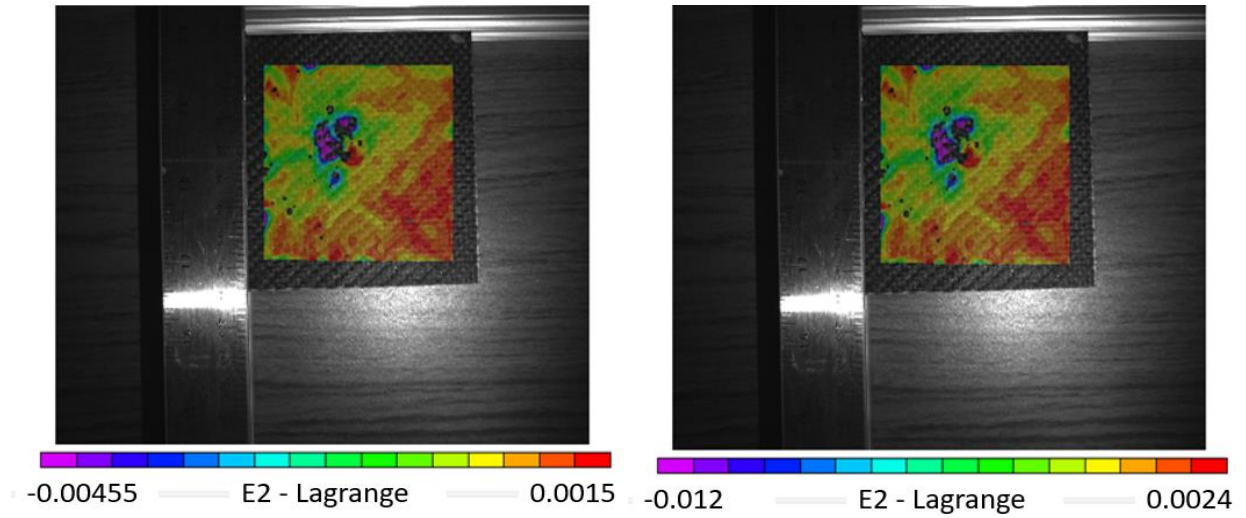


**Figure 18: Preliminary second principal strain [E2] results for front (left side) and back (right side) surfaces**

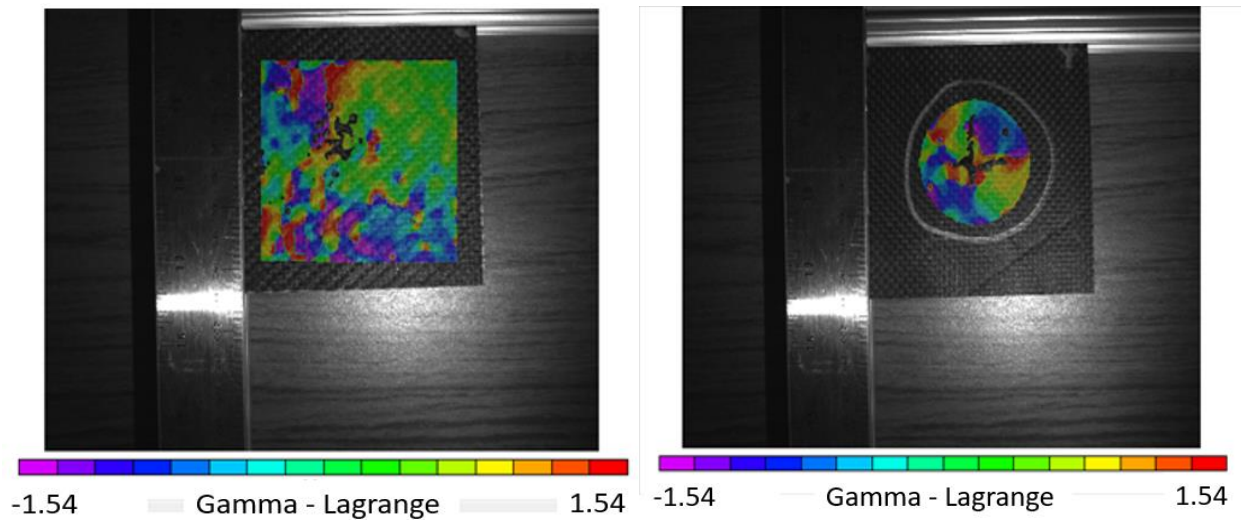


**Figure 19: Preliminary strain angle [Gamma] results for front (left side) and back (right side) surfaces**



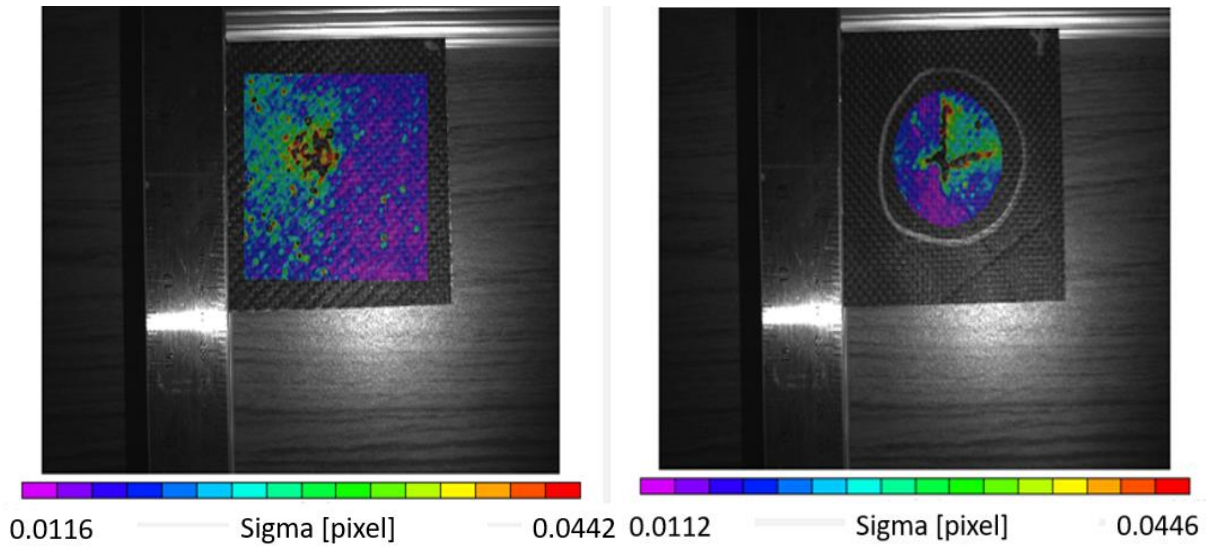


**Figure 20: Preliminary Sigma results for front (left side) and back (right side) surfaces**

For the back side of the preliminary sample (see **Figure 14-Figure 20**), a circular AOI was required because of the highlighting from a grey marker between impacting the sample and capturing the image post-impact. The AOI should not contain anything unknown (such as this highlight) within the analyzing stage. From this point forward highlighting was only utilized to mark sample numbers and corners at the top border before the sample was impacted to avoid the issue of a limited AOI size.

**Table 4: Preliminary Pixel result statistics of Confidence Interval [Sigma]**

	Front side impact	Back side impact
Max [Sigma]	4.99e-02	4.97e-02
Average [Sigma]	2.00e-02 ± 6.50e-03	2.16e-02 ± 7.71e-03

### 3.2 Impact Damage

Impacting occurred at the sites shown in **Figure 21**. All 8 plate samples (as well as the preliminary one) were impacted once at the center of the plate (red circle) at an energy level of 10J with a 51mm head. Plate samples 5 and 6 were impacted a second time with the smaller diameter 26mm diameter head, and off center (blue site in **Figure 21**). Finally, plate samples 7



and 8 were impacted a second time as well with the smaller diameter head, but this time at the green site (**Figure 21**). All impacts were at the same nominal energy level, 10 J. Sample thickness measurements were taken with calipers at 5 different locations post impact within **Figure 21** and shown within **Table 5**.

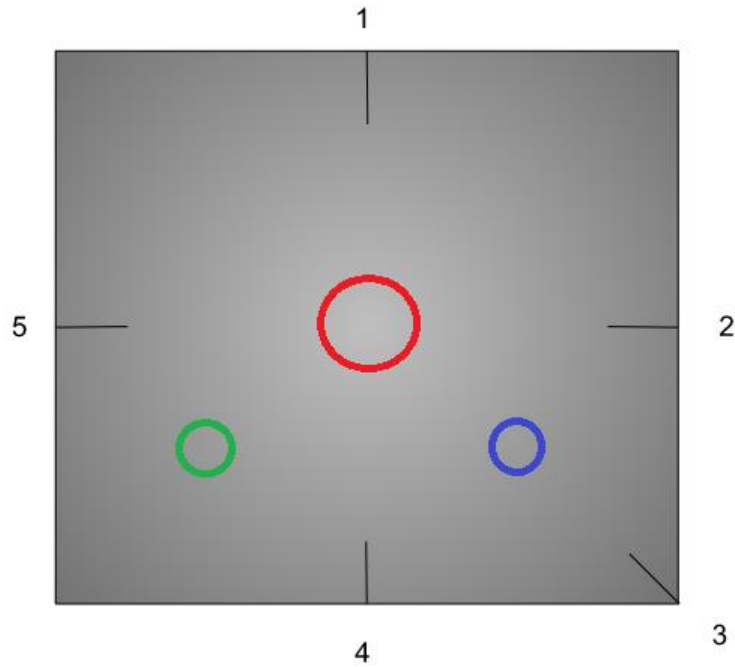


**Figure 21: Impact locations (not to scale) and post-impact thickness measurement locations**

**Table 5: Pre-and post-impact thickness measurements**

	Post-Impact Thickness 1 [mm]	Post-Impact Thickness [mm]	Post-Impact Thickness 3 [mm]	Post-Impact Thickness 4 [mm]	Post-Impact Thickness 5 [mm]
Samples 1-8 first impact	$2.56 \pm 0.09$	$2.51 \pm 0.09$	$2.34 \pm 0.07$	$2.52 \pm 0.05$	$2.55 \pm 0.05$
Samples 4-8 second impact	$2.60 \pm 0.13$	$2.72 \pm 0.17$	$2.72 \pm 0.28$	$2.71 \pm 0.14$	$2.59 \pm 0.10$

**Table 5** shows that the post impact thickness was increased between the first and second impact. This is also true between the preliminary average thickness (2.27mm) of all samples in **Table 2**.

All 9 tested samples showed BVID on both the impacted surface and posterior side, but with BVID on the back side being more pronounced with a visible cross shape that is further identified in **Figure 22** with grey highlight. The “T” shaped cross was expected as the with the [0/90] orientation of the ply layup within the laminate would fail along the fibers and not in the 45°- or 60°-degree orientation (Schimmer,.F. et al,2019) (Ge et al, 2022) (Grabi et al, 2022) .

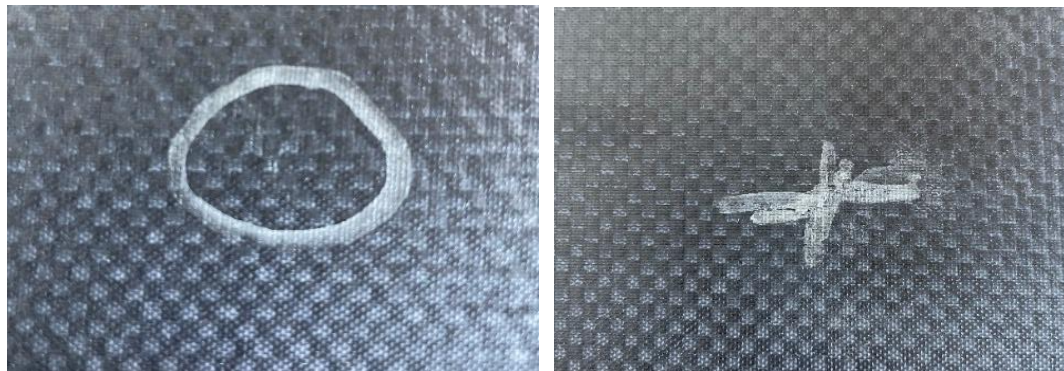


**Figure 22: Close-up of sample 1 impacted surface (left) and back surface (right): the silver marker was added post impact to aid visualization against black textured surface.**

Further impacting samples with a smaller diameter head on the second round of testing produced a larger “T” shaped cross. This could be the result of the impact from a more concentrated impact area, further delamination or other damage modes accrued from the previous impact.

### 3.3 DIC Analysis

All post-processing of the plate samples (preliminary sample, and eight test samples) produced a confidence interval of greater than 95%, meaning that the correlation of all images was reasonably correct and the strain estimated through VIC-2D was statistically acceptable. The DIC processing results showed that a link between the damage observed on the surface of the studied material could indeed be detected using DIC within this study. A paper (Loyola et al., 2012) with a T300/epoxy plate sample with the same impact energy 10 J, similar thickness (2mm in comparison to the 2.3mm within this study) and the same manufacturing technique produced a damage feature with both X-ray CT and thermography that is similar to the images produced by DIC in this thesis. One difference is the type of epoxy resin, a low-viscosity polymer, Proset 117LV instead of the available Proset 125 of this study. The hardener is the same, Proset 237. The published mechanical properties appear higher (up to 15%) for the 117LV/237 combination. This could mean that the T300 plates with Proset 125/237 epoxy could have lower impact resistance with respect to the T300 plates with Proset 117LV/237 epoxy. With the 10 J impacts, Loyola et al. (2012) observed in their X-ray CT scan a “T” cross , which was also visible on the thermography images. The DIC analysis produces a similar shape (see **Figure 23** and **Figure 24**).

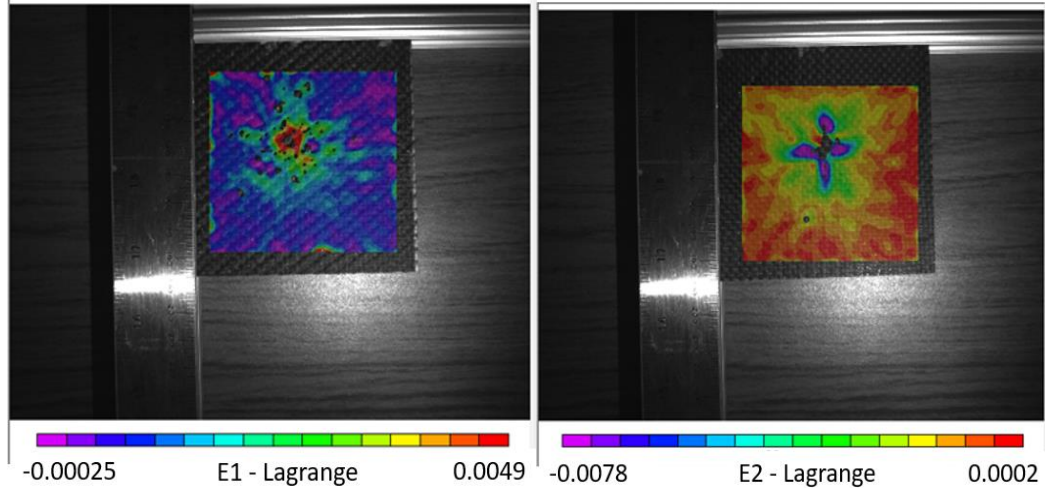


**Figure 23: Sample 6: images taken with sample inside the T slot: (left) E1 plot for impacted surface and (right) E2 plot for back surface**

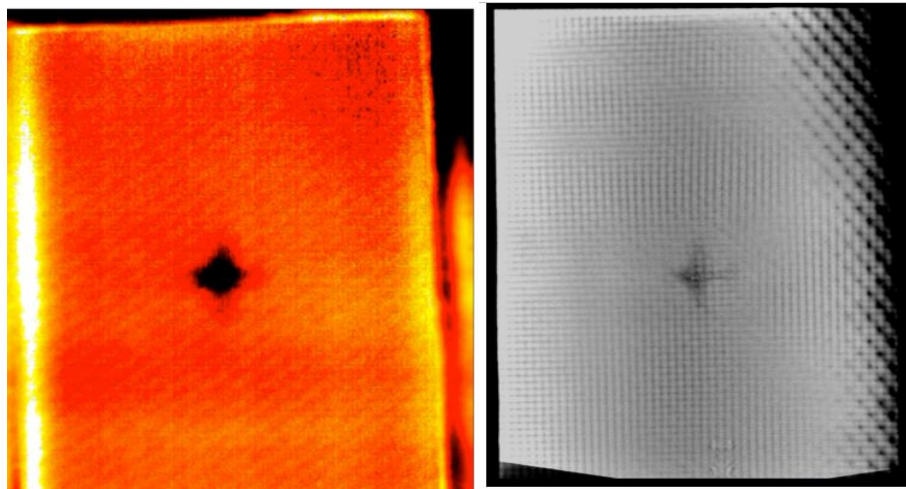


**Figure 24: Thermography (left) and X-ray CT (right) of T300/epoxy plate sample impacted at 10 J (Loyola et al., 2012)**

Indication of impact location was best observed to be the plot of the first principal engineering strain (E1) for the impacted surface, and the plot of the second principal engineering strain (E2) for the back side (see **Figure 23**), when the sample is positioned inside the T slot. This “T” shaped cross observation is also demonstrated by acoustic microscopy (also known as C-scan) of T300 carbon/epoxy plates (La Saponara, 2018) as shown in **Figure 25**.

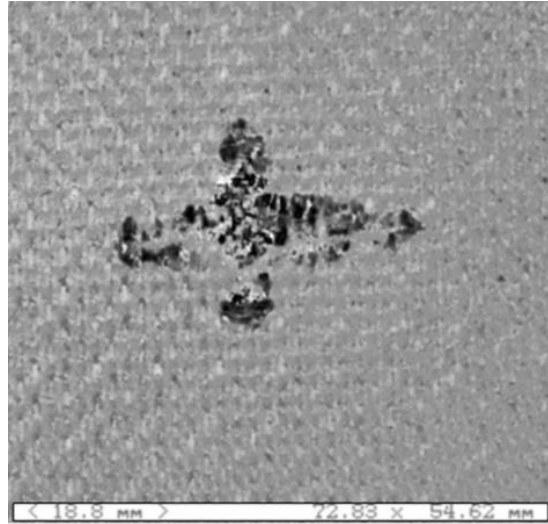


**Figure 25: Through-the-thickness Acoustic Microscopy image of T300/epoxy plate sample impacted at 20 J (La Saponara, 2018)**

More often than not, the DIC analysis when the sample was located outside the T slot (“outside” images) was shown to be less accurate in terms of providing a clear visual indication of the impacted site than the DIC images when the sample is located inside the T slot (“inside” images). It can also be observed that “outside” photos typically had a lower statistical confidence interval than their “inside” counterparts (see **Table 6.** )

**Table 6: Comparison of Inside and Outside Confidence Intervals**

	Inside Images [Sigma]	Outside Images [Sigma]
Averages	$0.022 \pm 0.01$	$0.027 \pm 0.01$

As stated with the preliminary results, it would most likely be due to the focal plane being undisturbed between pre- and post-impact captured images. Clear examples of this can be seen such as first (E1) and second principal strain (E2) as well as the confidence interval (sigma) for sample 2 (see **Figure 26**, **Figure 27**, and **Figure 28**). The focal plane being aligned between both images allows the correlation to properly depict what is expected from impacting.

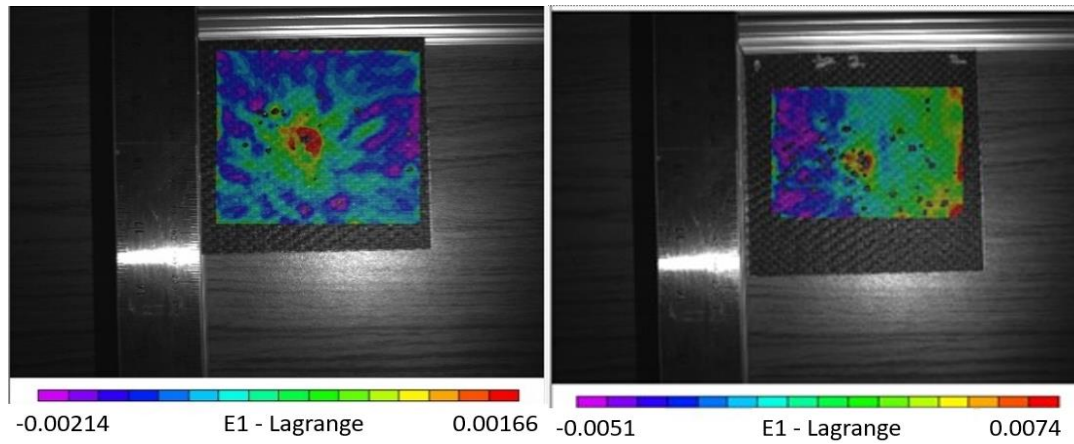


**Figure 26: E1 for sample 2 impacted surface: (left) inside and (right) outside the T slot**

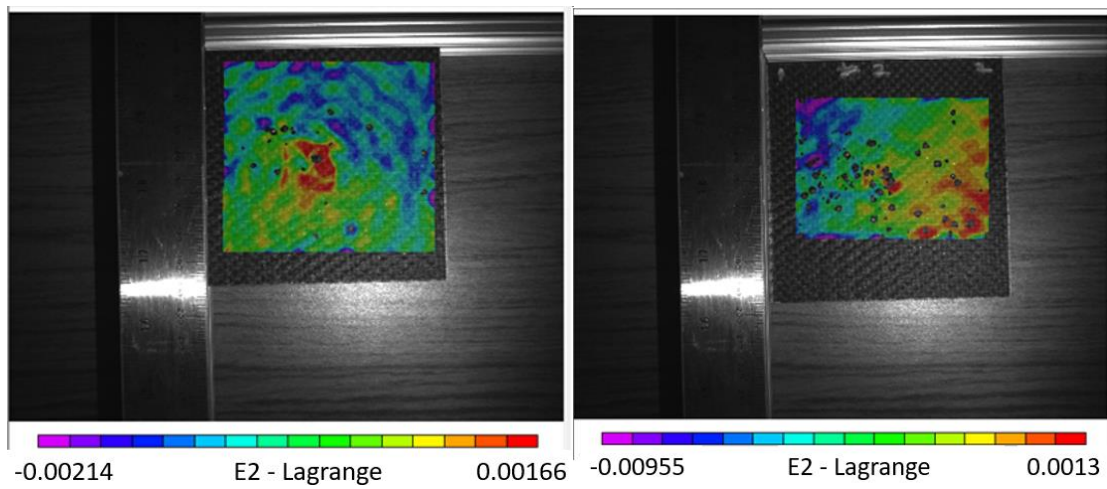


**Figure 27: E2 for sample 2 impacted surface: (left) inside and (right) outside the T slot**

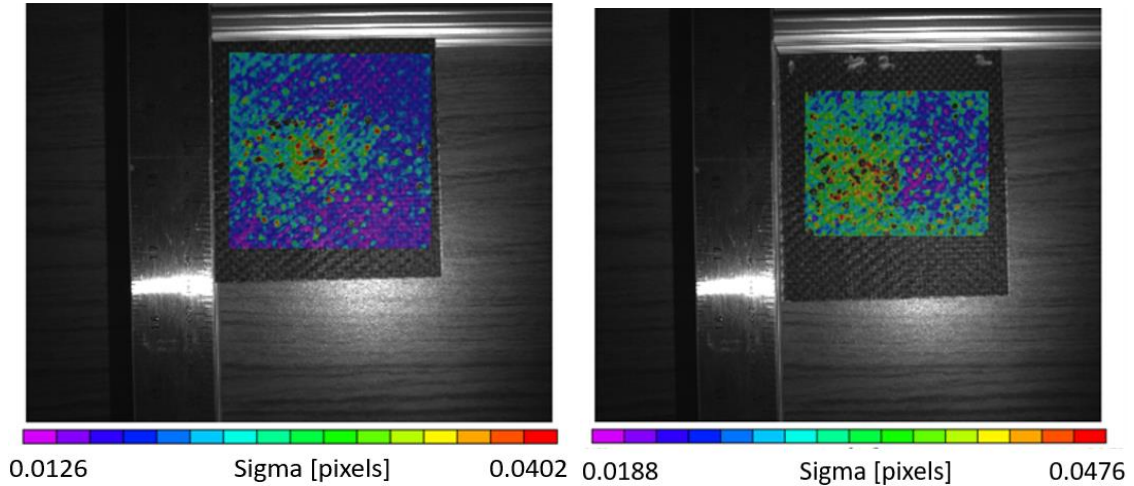


**Figure 28: Sigma for sample 2 impacted surface: (left) inside and (right) outside the T slot**

After the second impact of samples 5, 7 and 8, the visual results were not as clear with respect to those of samples impacted in the center. All samples with this second impact still came within the 95% confidence interval to show correlation. It is thought that this deviation could result from the further warpage of the sample from the initial impact (whether it be a front or back side images), and this would create a less accurate comparison for the DIC analysis (see **Appendix C**). The further warpage could be caused from delamination or other failure modes.

The attempt was to create the largest AOI possible but in some cases, smaller sizing of AOI was needed because of the settings and thresholds that were assigned. The difference of the AOI sizes were observed within the size of the data captured.

### 3.4 Testing of Residual Compressive Strength

The residual compressive strength testing showed that the extent of the damage within the carbon fiber between impacts did not completely compromise the integrity of the structure. This can be observed through the maximum load of sample 5 (which was impacted twice) being



able to take the highest load of all the samples, including those who were impacted only once. Compression testing can be shown through static compression plots as seen with **Figure 29**.

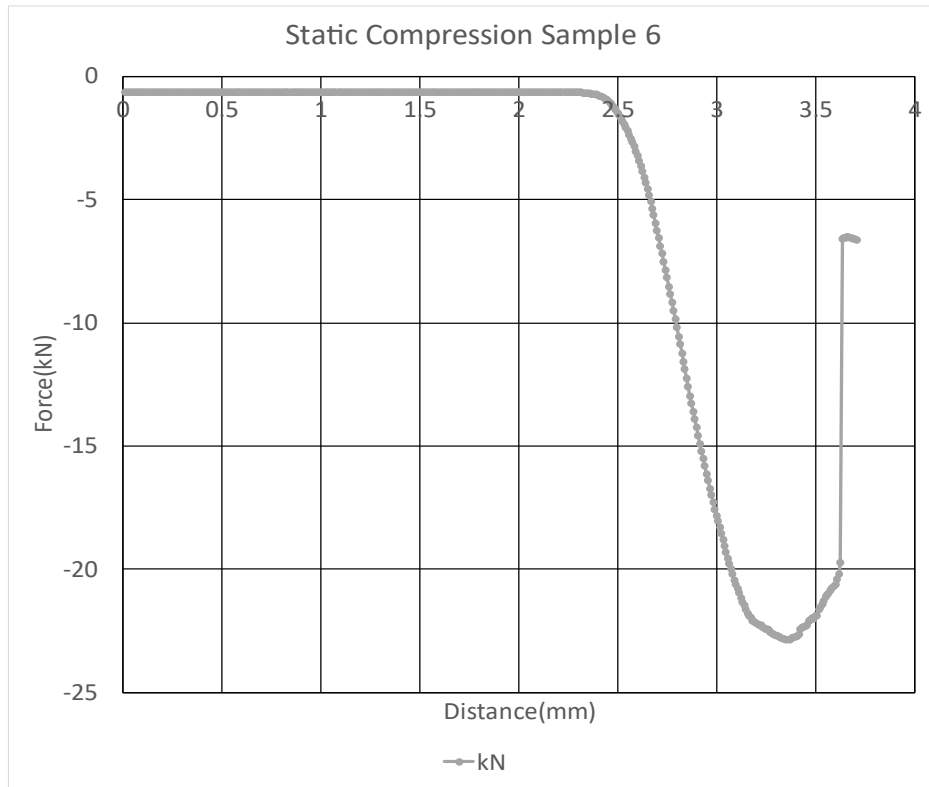


**Figure 29: Static compression plot for sample 6**

The after-impact compressive strength was calculated as  $F^{CAI} = \frac{P_{Max}}{A}$  according to ASTM D7137. Three out of four samples which took a second impact (5, 6, and 7) were observed to have a higher ultimate strength than samples 1, 3, and 4. Sample 2 was removed from the analysis because the failure point was not reached on first compression of the plate, meaning that the sample could not adhere to the standard. This aspect is important because the strain impact in this case was not as detrimental to the structure but could still be identified through DIC analysis. During manufacturing, local defects such as resin pockets, voids or changes in fiber waviness during the infiltration process could be possible, leading to particular samples being stronger,



and to data scatter. On the other hand, the data in **Table 4** has a coefficient of variation COV equal to 10%, which is deemed an acceptable engineering error.

**Table 7: Ultimate compressive strength of samples.**

**Sample 2 is removed as explained in the text.**

Sample	Ultimate Strength (MPa)
1	-2.31
3	-2.41
4	-2.45
5	-2.79
6	-2.46
7	-2.57
8	-2.00

All of the samples fractured within the required time of 1-10 min at the crosshead displacement rate of 1mm/min, as per ASTM D7137 standard. Within the setup of the residual compressive strength test, it was noticed that most of the samples failed due to “LGM” mode (shown in **Figure 30** and **Figure 30**). Sample 7 was the only sample to fail in “LDM” mode and along the second impact site (see **Figure 30** and **Figure 30**).

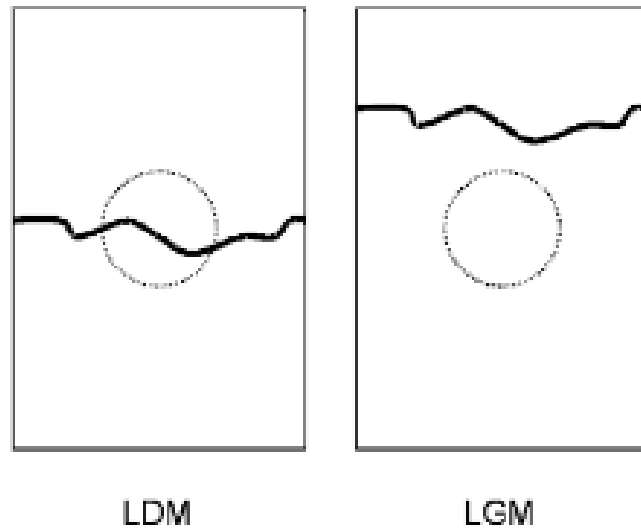


**Figure 30: Acceptable failure modes LDM and LGM from ASTM D7137**

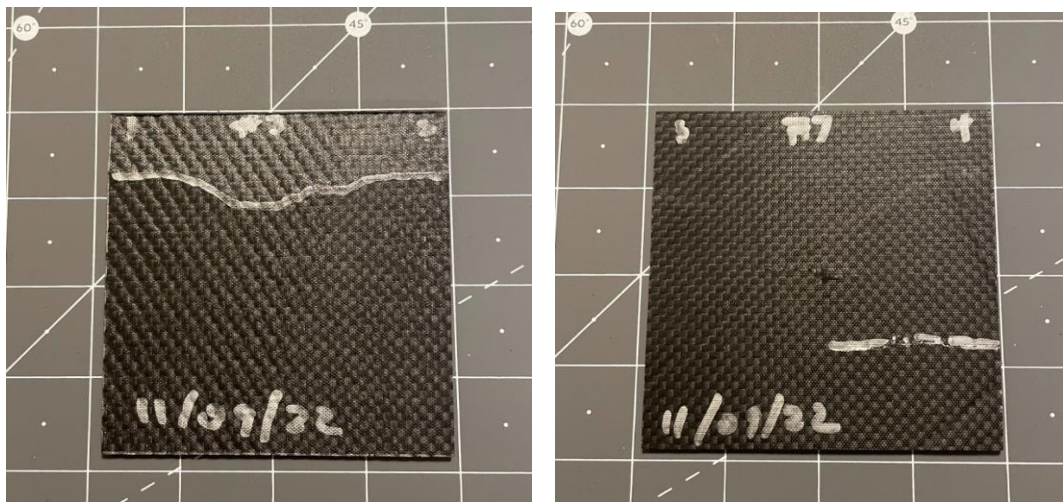


**Figure 31: Sample 3 front (left) and sample 7 back (right)**

A baseline for unimpacted samples was unfortunately not available due to the limited number of CFRP samples produced, which were prioritized for DIC work. The second round of impacting and image capturing was able to quantify the presence of damage between impacts as well as confirm that DIC was able to detect off-center impacts. Even though the indications were not as clear (in a visual sense and not a statistical), the DIC technique was still able to accomplish impact detection. An improved experimental setup would be to perform all of the

testing with a larger quantity of samples, understanding that VARTM is labor intensive and variations in samples from the same lot may occur. Nonetheless, the number of impacting samples used was deemed acceptable by ASTM D7136. This thesis work could not find a clear connection between residual compressive strength values after a 10 J impact (seen with the BVID on the samples) and DIC image.

## CHAPTER 4

### CONCLUSIONS AND FUTURE WORK

We provided a proof-of-concept that the applied 2D DIC setup could identify the presence of barely visible impact damage in CFRP structures with reasonable accuracy, as the correlation between images achieved the 95% confidence interval between pre- and post-impact photography for the 10J impact energy level. The DIC analysis in comparison with X-ray CT, Thermography and Acoustic Microscopy produced comparable results on very similar samples (Loyola et al., 2012). While it may be debated whether the extent of the damage could be captured with 2D DIC, this experimental work also confirmed that the low-cost 2D DIC apparatus utilized was able to capture damage from barely-visible impacted samples without the use of speckle patterns.

While this 2D methodology shows promise of determination of impact, future work is needed to evaluate the extent of damage at a direct comparison with the NDT methodologies instead of cross comparison with similar studies. This would allow a more comprehensive approach to detect variations between the methodologies instead of trying to account for deviations with engineering judgement. Another aspect for future work would be assessing the DIC results with impacts of CFRP plates at different energy levels. This could determine if the damage seen within the analysis is replicated with NDT at higher energy levels which produce visible impact damage.

A limitation with the study was the inability to modify image scales and replicate the size of the AOI among all samples. This would aid future studies to numerically compare and

quantify extent of damage. Another limitation was the amount of data that could be exported, this required the data to be averaged from sets of 5 pixels in both the x and y directions.

## References

- Bataxi, Chen, X., Yu, Z., Wang, H., Bil, C. (2015). Strain monitoring on damaged composite laminates using digital image correlation. *Procedia Engineering*, 99, 353–360. <https://doi.org/10.1016/j.proeng.2014.12.547>
- Bathias, C. (1991). Fracture and fatigue of high performance composite materials: Mechanisms and prediction. *Engineering Fracture Mechanics*, 40(4-5), 757–783. [https://doi.org/10.1016/0013-7944\(91\)90234-r](https://doi.org/10.1016/0013-7944(91)90234-r)
- Briggs, T. M., Loyola, B. R., Loh, K. J., La Saponara, V., Chen, J. C. (2012). Comparative Study of Non-destructive Damage Evaluation Methodologies for CFRP Low Velocity Impact Damage. *Proceedings of SAMPE Technical Conference | OSTI.GOV*. Retrieved March 8, 2023, from <https://www.osti.gov/biblio/1117164>
- Camirero, M. A., Lopez-Pedrosa, M., Pinna, C., Soutis, C. (2013). Damage assessment of composite structures using digital image correlation. *Applied Composite Materials*, 21(1), 91–106. <https://doi.org/10.1007/s10443-013-9352-5>
- Cantwell, W. J., Morton, J. (1991). The impact resistance of Composite Materials — a review. *Composites*, 22(5), 347–362. [https://doi.org/10.1016/0010-4361\(91\)90549-v](https://doi.org/10.1016/0010-4361(91)90549-v)
- Caputo, F., De Luca, A., Lamanna, G., Borrelli, R., & Mercurio, U. (2014). Numerical Study for the structural analysis of composite laminates subjected to low velocity impact. *Composites Part B: Engineering*, 67, 296–302. <https://doi.org/10.1016/j.compositesb.2014.07.011>
- Cawley, P., Adams, R. D. (1988). The mechanics of the coin-tap method of non-destructive testing. *Journal of Sound and Vibration*, 122(2), 299–316. [https://doi.org/10.1016/s0022-460x\(88\)80356-0](https://doi.org/10.1016/s0022-460x(88)80356-0)
- Cerbu, C., Xu, D., Wang, H., Roşca, I. C. (2018). The use of digital image correlation in determining the mechanical properties of materials. *IOP Conference Series: Materials Science and Engineering*, 399, 012007. <https://doi.org/10.1088/1757-899x/399/1/012007>
- Chu, T.C., Ranson, W.F., Sutton, M.A., Peters, W.H. (1985) Application of digital-image-correlation techniques to experimental mechanics. *Experimental Mechanics*, 25:232–244. doi: 10.1007/BF02325092
- Dhimole, V. K., Serrao, P., Cho, C. (2021). Review and suggestion of failure theories in voids scenario for VARTM processed composite materials. *Polymers*, 13(6), 969, <https://doi.org/10.3390/polym13060969>

- Elhajjar, R., Grant, P., Ashforth, C. (2019). *Composite Structures: Effects of Defects*. Wiley.
- Felipe-Sesé, L., Díaz, F. A. (2018). Damage methodology approach on a composite panel based on a combination of fringe projection and 2D digital image correlation. *Mechanical Systems and Signal Processing*, 101, 467–479. <https://doi.org/10.1016/j.ymssp.2017.09.002>
- Flores, M., Mollenhauer, D., Runatunga, V., Beberniss, T., Rapping, D., Pankow, M. (2017). High-speed 3D digital image correlation of low-velocity impacts on composite plates. *Composites Part B: Engineering*, 131, 153–164, <https://doi.org/10.1016/j.compositesb.2017.07.078>
- Ge, X., Zhang, P., Zhao, F., Liu, M., Liu, J., Cheng, Y. (2022). Experimental and numerical investigations on the dynamic response of woven carbon fiber reinforced thick composite laminates under low-velocity impact. *Composite Structures*, 279, 114792, <https://doi.org/10.1016/j.compstruct.2021.114792>
- Gholizadeh, S., (2022). Impact behaviours and non-destructive testing (NDT) methods in carbon fiber composites in aerospace industry: A Review. Pre-print, available under <https://doi.org/10.37473/dac/10.22541/au.164502808.88072147/v1>
- Grabi, M., Chellil, A., Habibi, M., Grabi, H., Laperriere, L. (2022). Characterization of low-velocity impact and post-impact damage of Luffa MAT composite using acoustic emission and digital image correlation. *Journal of Composite Materials*, 56(11), 1651–1665. <https://doi.org/10.1177/00219983221083733>
- Herakovich, C. T. (1998). *Mechanics of fibrous composites*, Wiley.
- Hill, E. v. K., Geiselman, N. L. (2014). Prediction of Ultimate Compression after Impact Loads in Graphite-Epoxy Coupons from Ultrasonic C-Scan Images Using Neural Networks. In *Smart Composites: Mechanics and Design*, edited by R. Elhajjar, V. La Saponara and A. Muliana, CRC Press.
- Janeliukstis, R., Chen, X. (2021). Review of Digital Image Correlation Application to large-scale composite structure testing. *Composite Structures*, 271, 114143, <https://doi.org/10.1016/j.compstruct.2021.114143>
- Jiang, D., Smith, D. (2017). Anisotropic mechanical properties of oriented carbon fiber filled polymer composites produced with fused filament fabrication. *Additive Manufacturing*, 18:84–94. doi: 10.1016/j.addma.2017.08.006
- Kammers, A. D., Daly, S. (2011). Small-scale patterning methods for digital image correlation under scanning electron microscopy. *Measurement Science and Technology*, 22(12), 125501. <https://doi.org/10.1088/0957-0233/22/12/125501>

Koohbor, B., Mallon, S., Kidane, A., Sutton, M. A. (2014). A DIC-based study of in-plane mechanical response and fracture of orthotropic carbon fiber reinforced composite. *Composites Part B: Engineering*, 66, 388–399. <https://doi.org/10.1016/j.compositesb.2014.05.022>

La Saponara, V., (2018). An Overview of Wave Propagation Techniques in Fiber-Reinforced Polymer Composite Plates, pp. 490-501, in *Comprehensive Composites II*, vol. 1, P. Beaumont and C. Zweben editors, Elsevier, ISBN: 9780081005330

Laurin, F., Charrier, J.-S., Lévêque, D., Maire, J.-F., Mavel, A., Nuñez, P. (2012). Determination of the properties of composite materials thanks to Digital Image Correlation Measurements. *Procedia IUTAM*, 4, 106–115. <https://doi.org/10.1016/j.piutam.2012.05.012>

Lobanov, D., Strungar, E. (2020). Mathematical data processing according to Digital Image Correlation Method for polymer composites. *Frattura Ed Integrità Strutturale*, 14(54), 56–65. <https://doi.org/10.3221/igf-esis.54.04>

Madhu, S., Balasubramanian, M., Kannan, S. (2020). [PDF] surface roughness assessment based on digital image texture analysis of CFRP composites machined by swirling abrasives: Semantic scholar Retrieved from: <https://www.semanticscholar.org/paper/SURFACE-ROUGHNESS-ASSESSMENT-BASED-ON-DIGITAL-IMAGE-Madhu-Balasubramanian/65cfb61fe6a1f7a357b7fafd838b856ebfe6c3f0>

Mansour, M., Tsongas, K., Tzetzis, D., Antoniadis, A. (2018). Mechanical and Dynamic Behavior of Fused Filament Fabrication 3D Printed Polyethylene Terephthalate Glycol Reinforced with Carbon Fibers. *Polymer-Plastics Technology and Engineering*, 2018;57:1715–1725. doi: 10.1080/03602559.2017.1419490

Naresh, K., Shankar, K., Velmurugan, R., Gupta, N. K. (2020). High strain rate studies for different laminate configurations of bi-directional glass/epoxy and carbon/epoxy composites using DIC. *Structures*, 27, 2451–2465. <https://doi.org/10.1016/j.istruc.2020.05.022>

Niu, Y., Shao, S., Park, S.B., Kao, C. (2017) A novel speckle-free digital image correlation method for in situ warpage characterization. *IEEE Transactions on Components, Packaging and Manufacturing Technologies*, 7:276–284. doi: 10.1109/TCPMT.2016.2635581

Ritchie, R. O. (1988). Mechanisms of fatigue crack propagation in metals, ceramics and composites: Role of crack tip shielding. *Materials Science and Engineering: A*, 103(1), 15–28, [https://doi.org/10.1016/0025-5416\(88\)90547-2](https://doi.org/10.1016/0025-5416(88)90547-2)

Runarsson, T., Jonsson, M., Unnthorsson, R. (2016). NDT methods for evaluating carbon fiber composites. *Academia.edu*. Retrieved from [https://www.academia.edu/28448949/NDT\\_Methods\\_for\\_Evaluating\\_Carbon\\_Fiber\\_Composites](https://www.academia.edu/28448949/NDT_Methods_for_Evaluating_Carbon_Fiber_Composites)



Sarma, P. M. M. S., Karunamoorthy, L., Palanikumar, K. (2008). Surface roughness parameters evaluation in machining GFRP composites by PCD tool using digital image processing. *Journal of Reinforced Plastics and Composites*, 28(13), 1567–1585, <https://doi.org/10.1177/0731684408089858>

Schimmer, F., Ladewig, S., Motsch, N., Hausmann, J. M., Ehrlich, I. (2019). Comparison of low-velocity impact damage behavior of unidirectional carbon fiber-reinforced thermoset and thermoplastic composites. *Key Engineering Materials*, 809, 9–14, <https://doi.org/10.4028/www.scientific.net/kem.809.9>

Sierakowski, R., Kujawińska, M., Malesa, M., Malowany, K., Piekarczyk, A., Tymińska-Widmer, L., Targowski, P. (2011). Digital image correlation method: A versatile tool for engineering and art structures investigations. In: Rodriguez-Vera R., Diaz-Urbe R., editors. *Proceedings of the SPIE Volume 8011, the 22nd Congress of the International Commission for Optics: Light for the Development of the World; Puebla, Mexico. 15–19 August 2011*; p. 80119RL, Newaz GM. *Damage tolerance in advanced composites*. Technomic, 1995

Spencer, R., Hassen, A. A., Baba, J., Lindahl, J., Love, L., Kunc, V., Babu, S., Vaidya, U. (2021). An innovative digital image correlation technique for in-situ process monitoring of composite structures in large scale additive manufacturing. *Composite Structures*, 276, 114545. <https://doi.org/10.1016/j.compstruct.2021.114545>

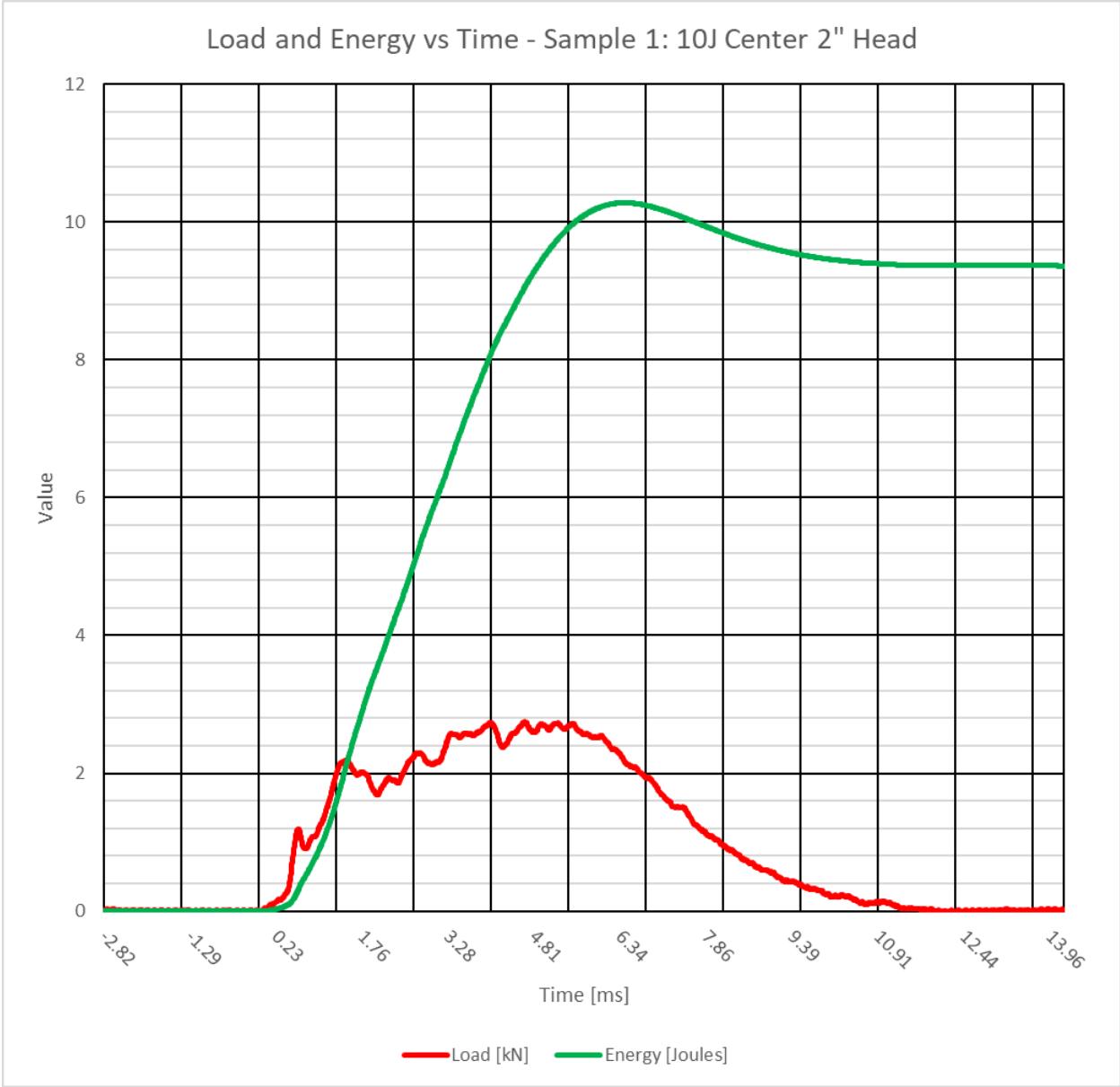
Sutton, M. A., Orteu Jean-José, Schreier, H. W. (2009). *Image correlation for shape, motion and deformation measurements: Basic concepts, theory and applications*, Springer.

Symons, D. D., Davis, G. (2000). Fatigue testing of impact-damaged T300/914 carbon-fibre-reinforced plastic. *Composites Science and Technology*, 60(3), 379–389. [https://doi.org/10.1016/s0266-3538\(99\)00138-4](https://doi.org/10.1016/s0266-3538(99)00138-4)

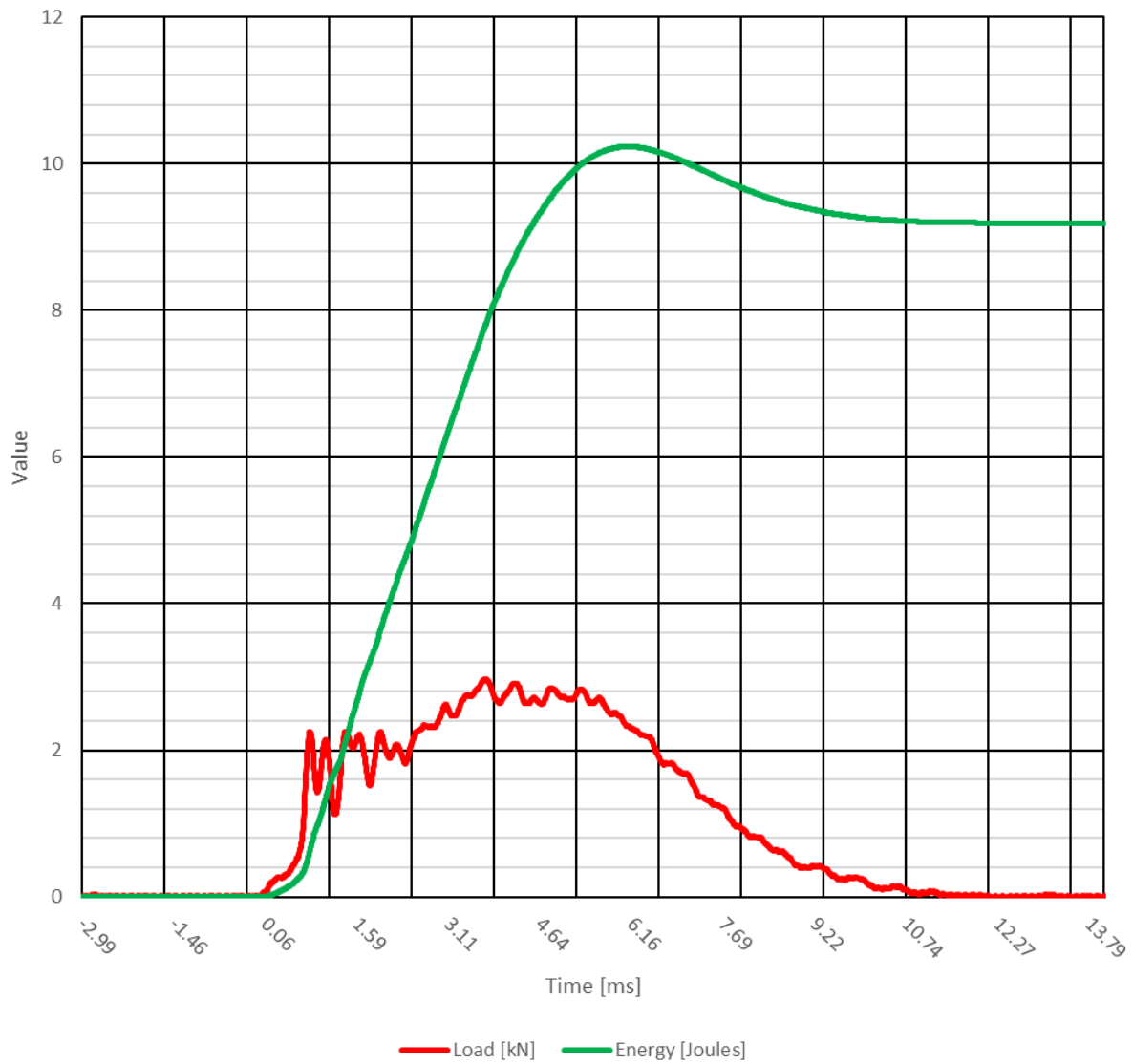
Vavilov, V. P. (2014). Modeling and characterizing impact damage in carbon fiber composites by thermal/infrared non-destructive testing. *Composites Part B: Engineering*, 61, 1–10, <https://doi.org/10.1016/j.compositesb.2014.01.034>

# Appendix A – Impact Testing Results

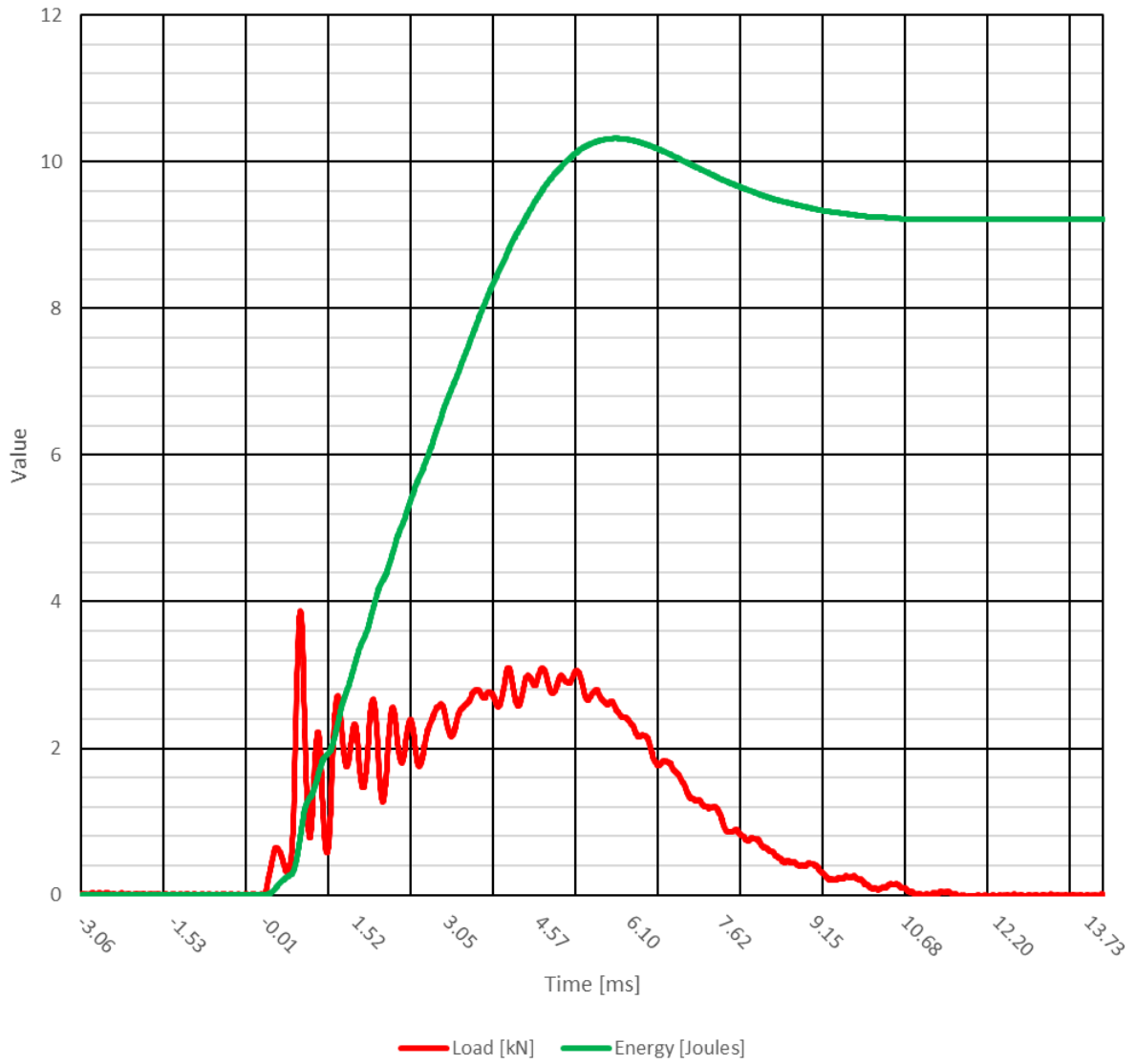
## First Round of Impacting



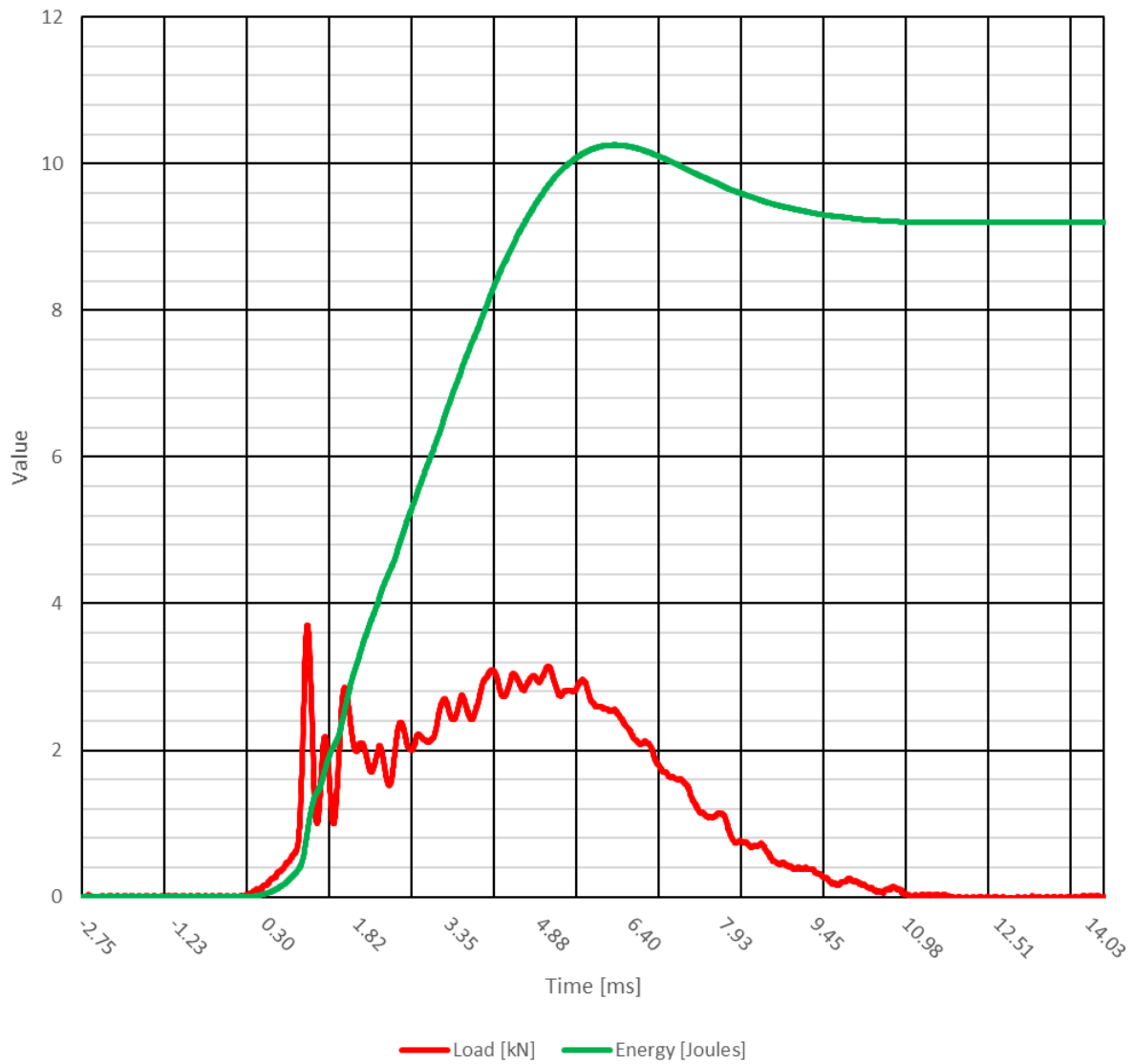
Load and Energy vs Time - Sample 2: 10J Center 2" Head



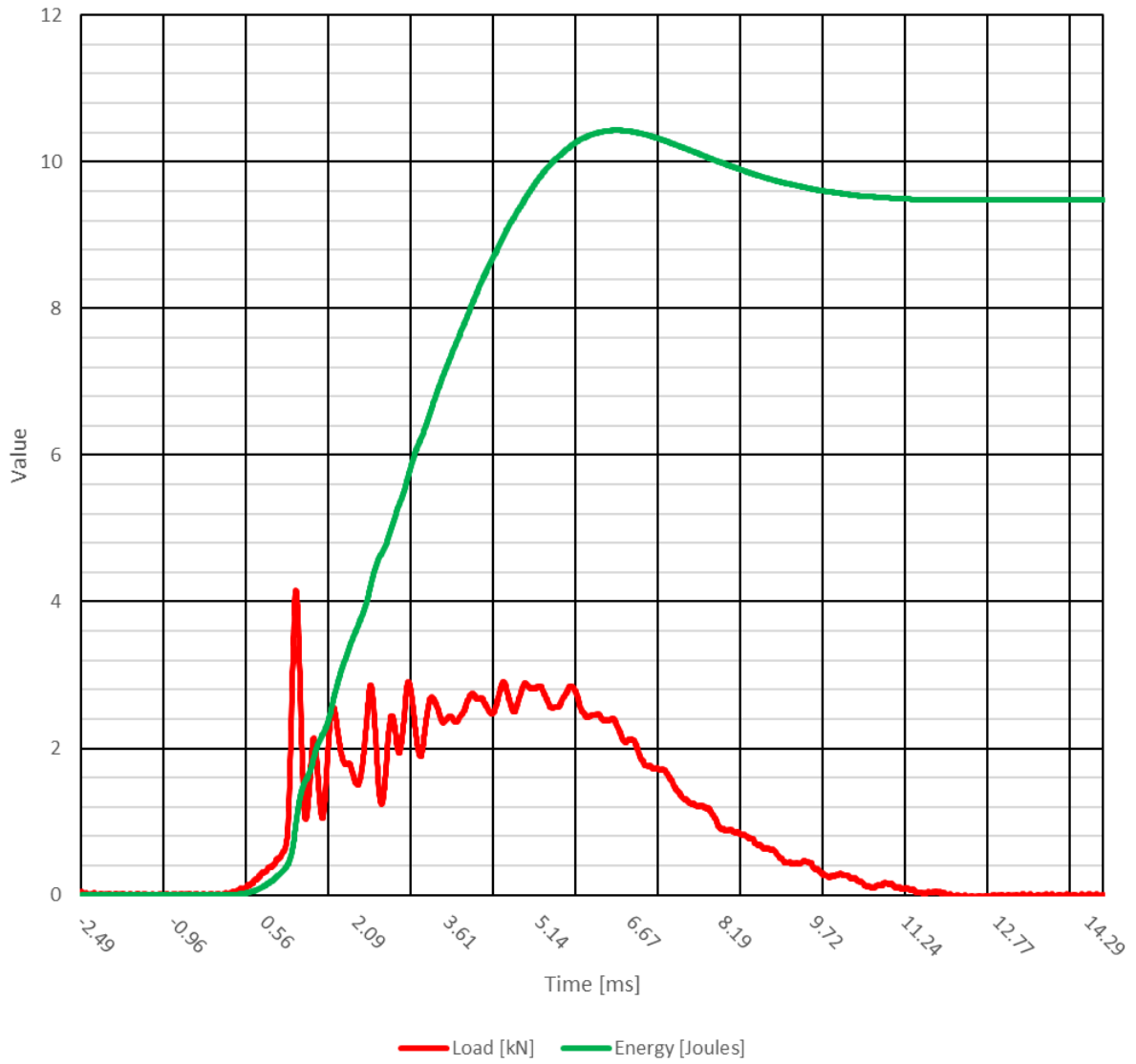
Load and Energy vs Time - Sample 3: 10J Center 2" Head



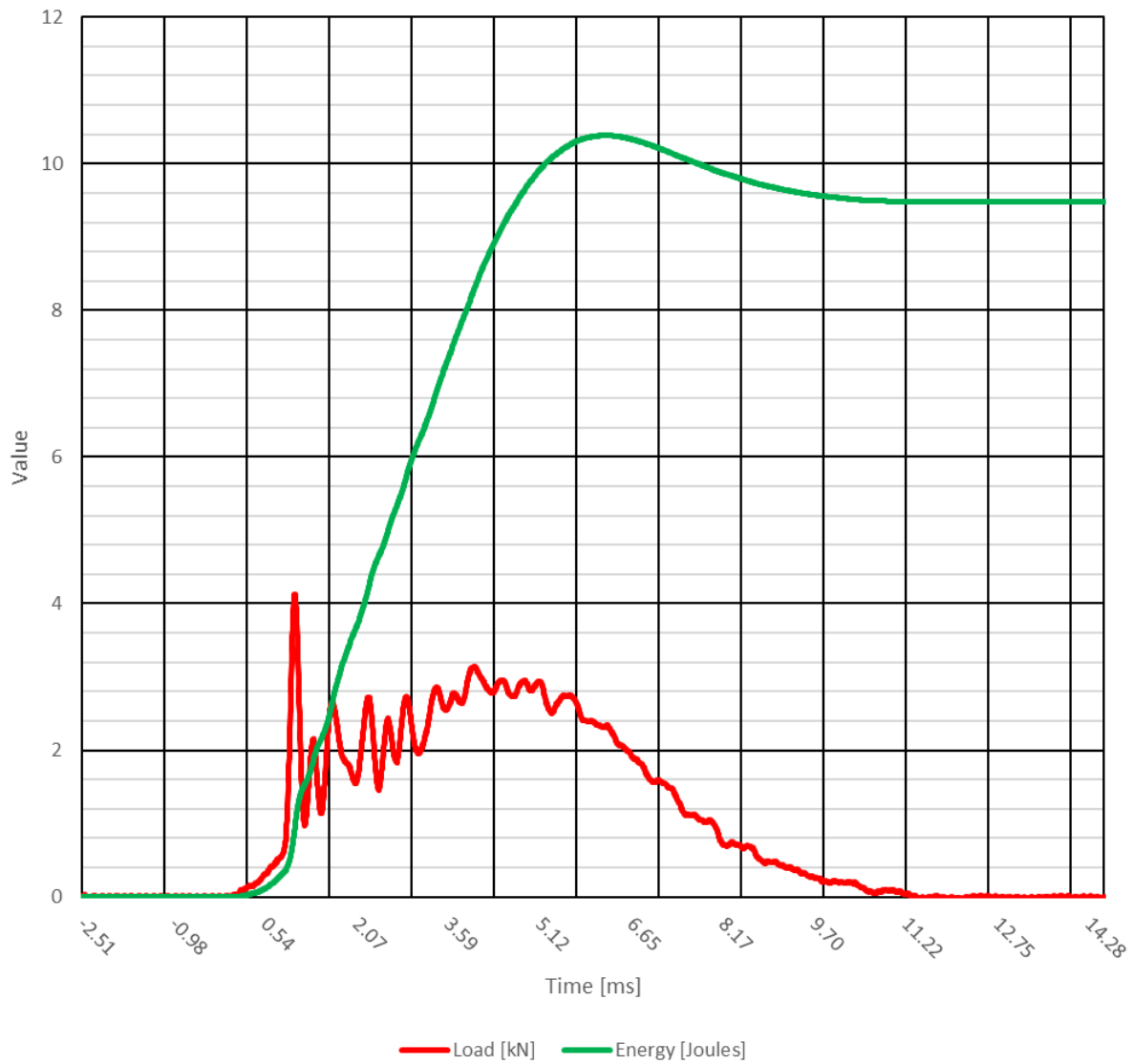
Load and Energy vs Time - Sample 4: 10J Center 2" Head



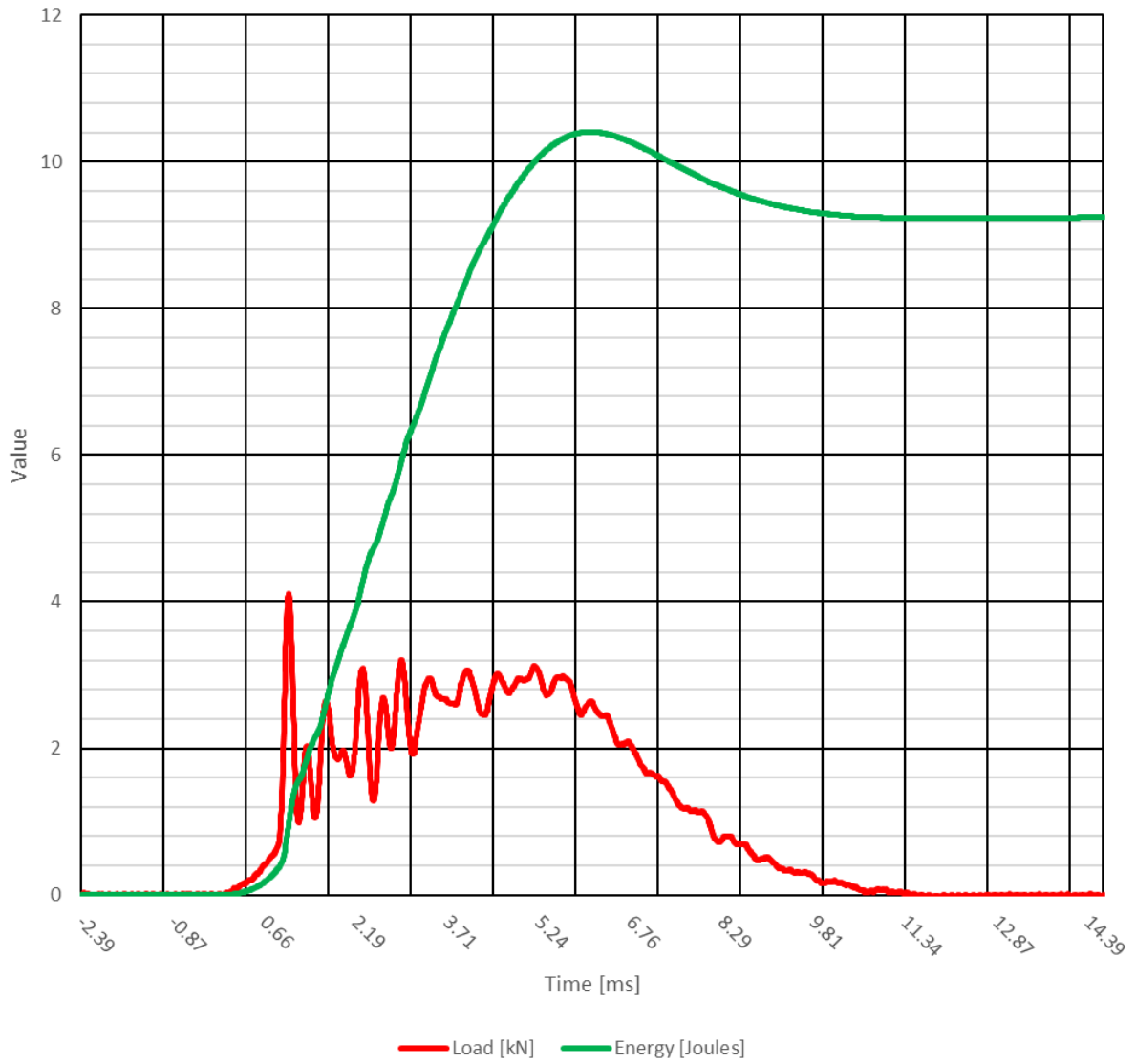
Load and Energy vs Time - Sample 5: 10J Center 2" Head



Load and Energy vs Time - Sample 6: 10J Center 2" Head

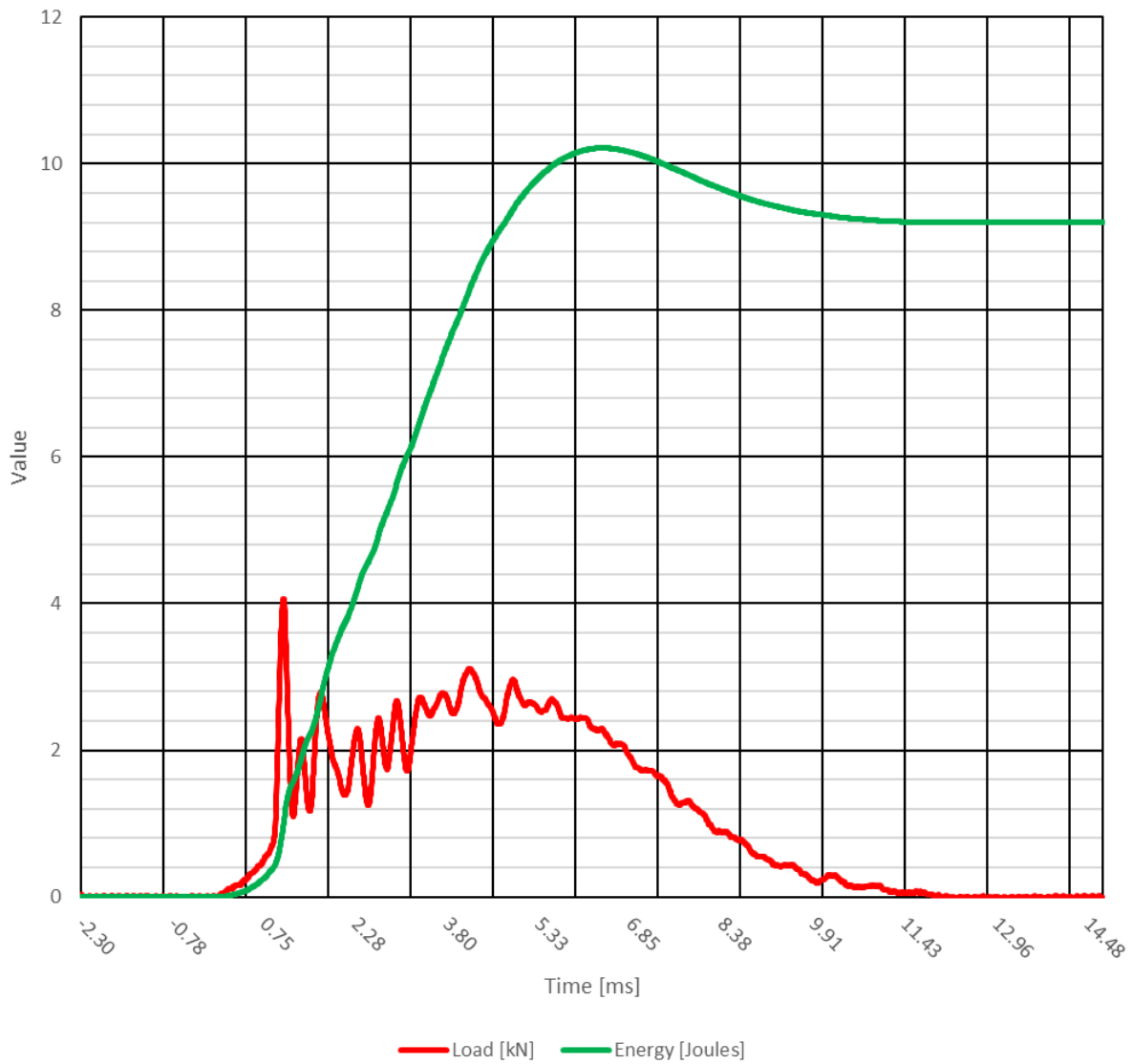


Load and Energy vs Time - Sample 7: 10J Center 2" Head

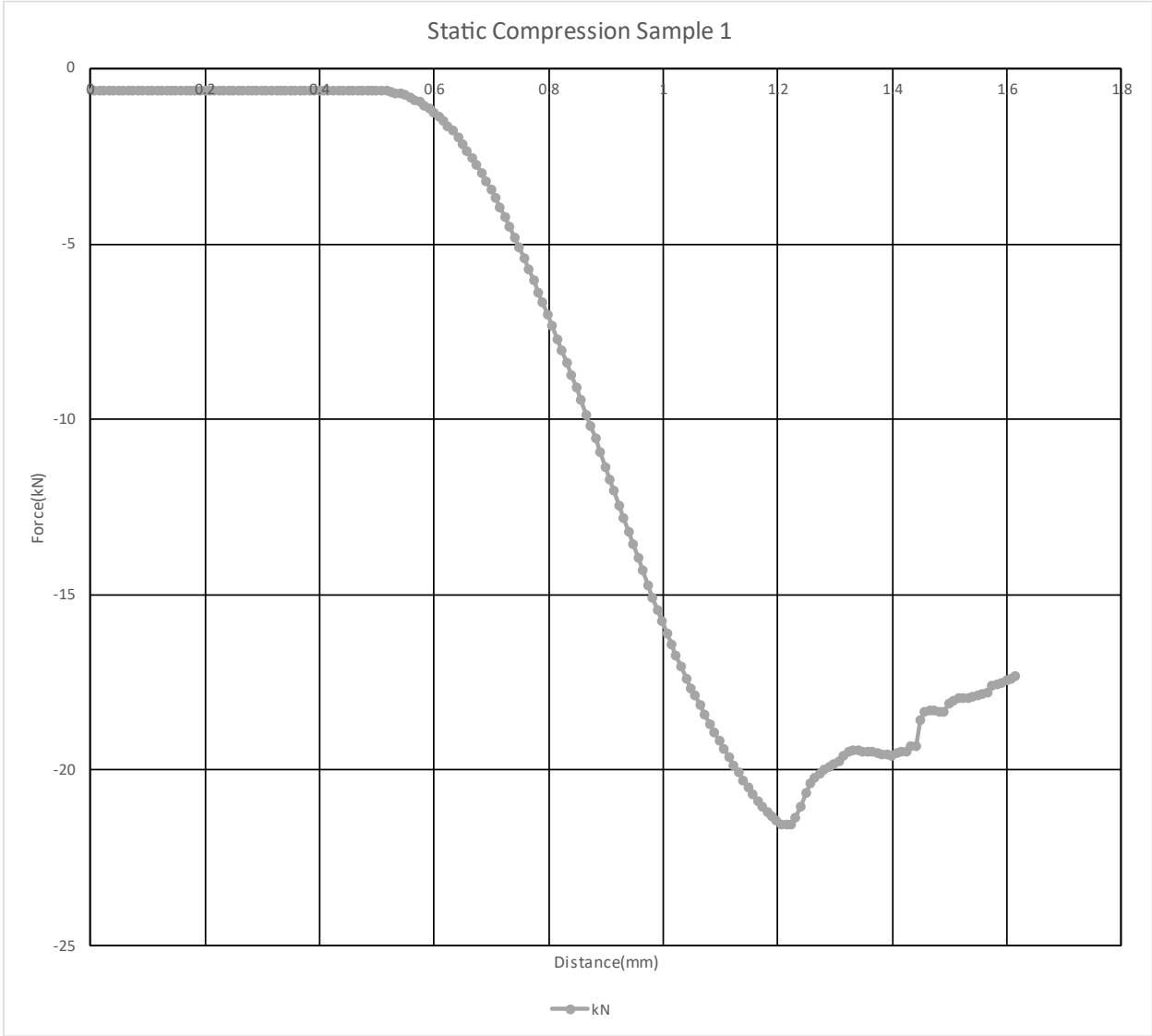


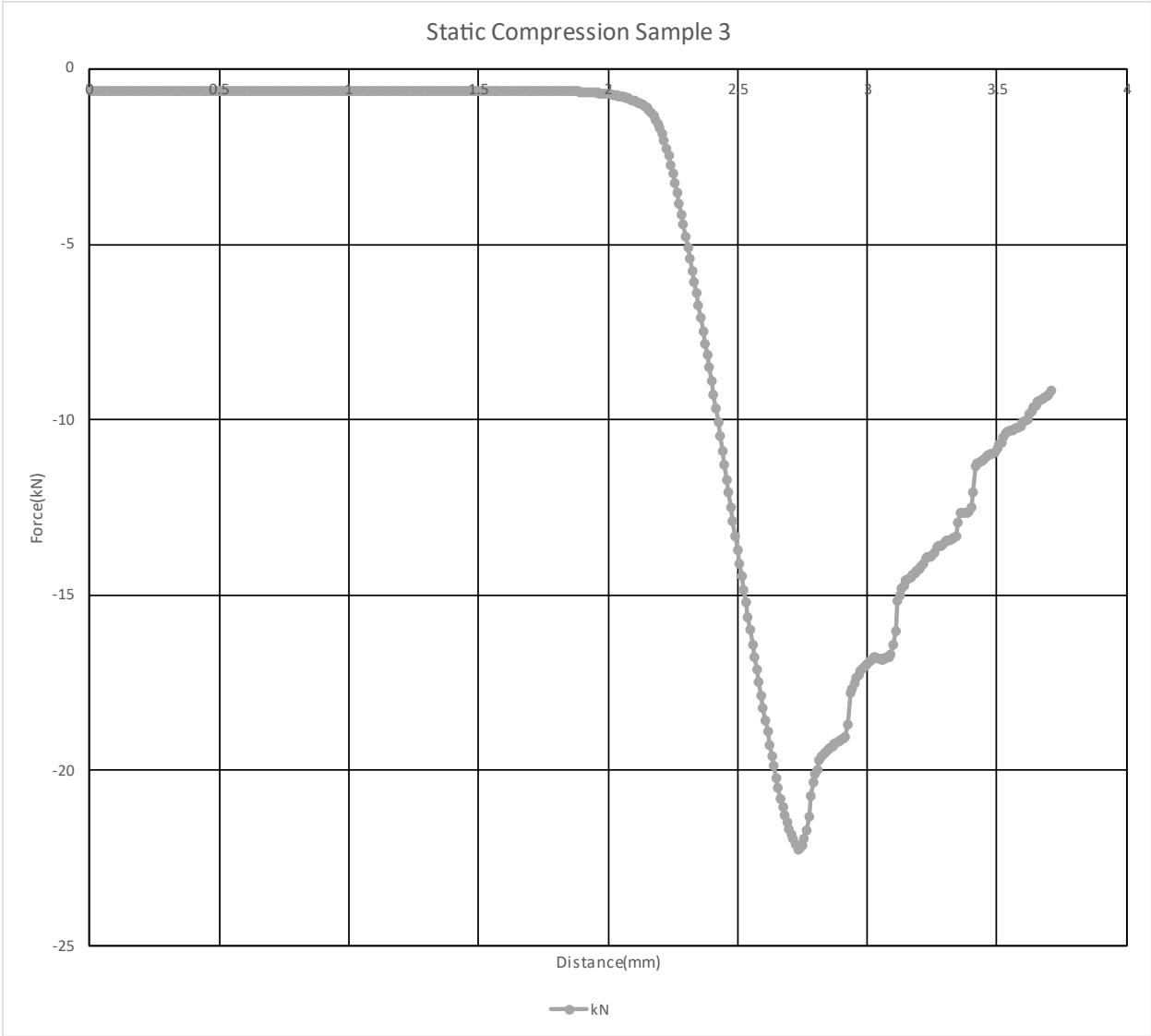


Load and Energy vs Time - Sample 8: 10J Center 2" Head

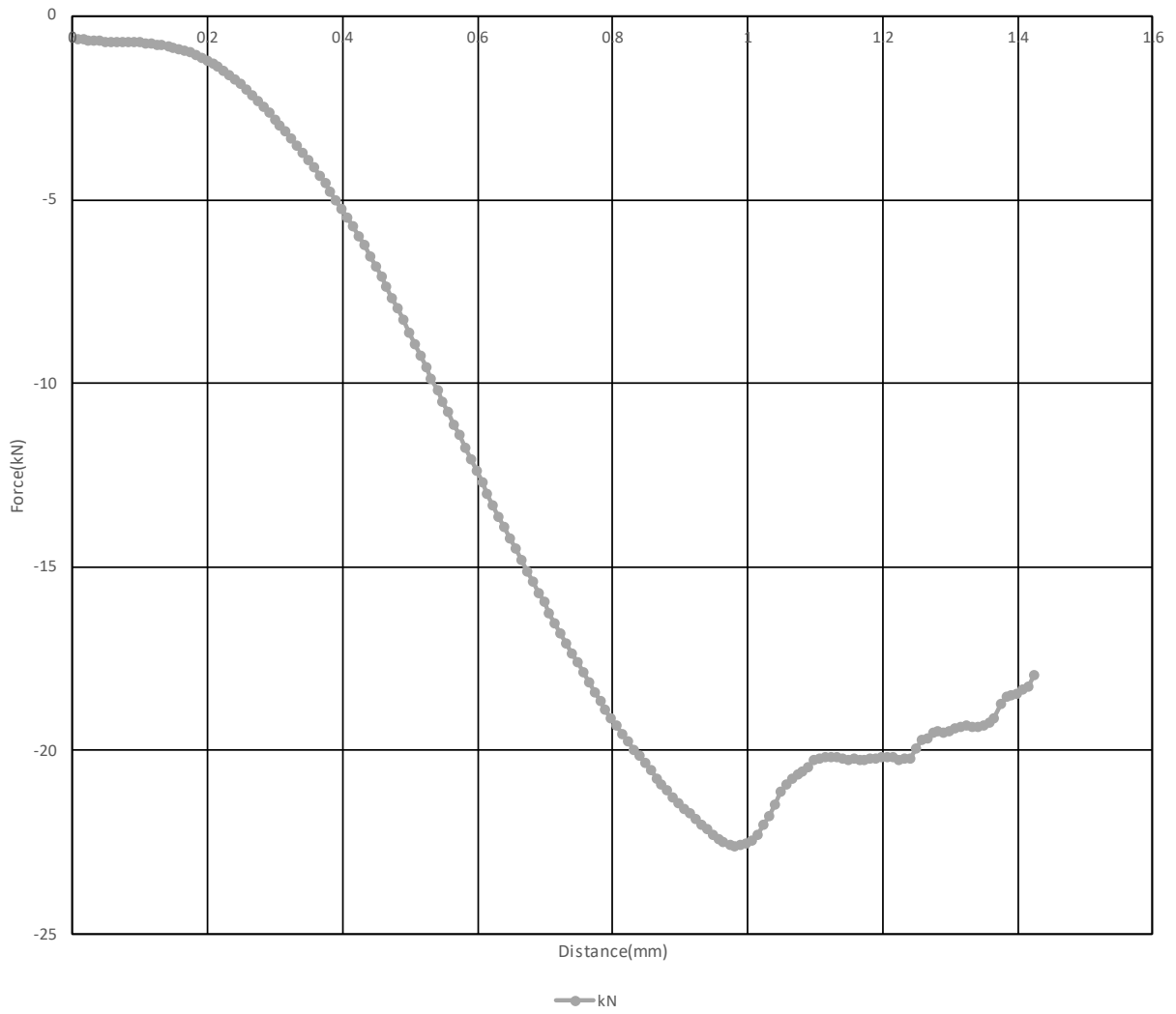


# Appendix B – Residual Compressive Results

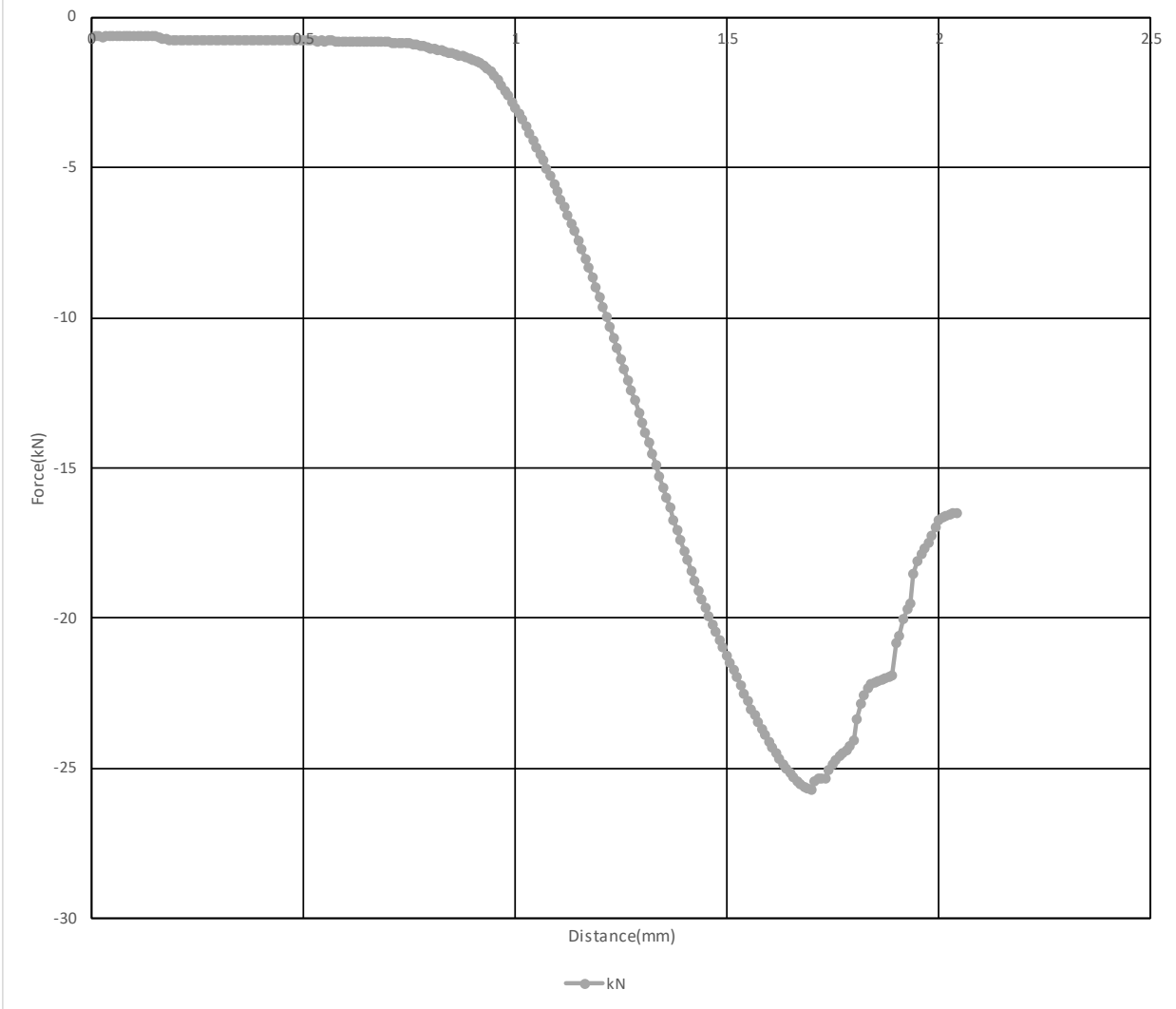


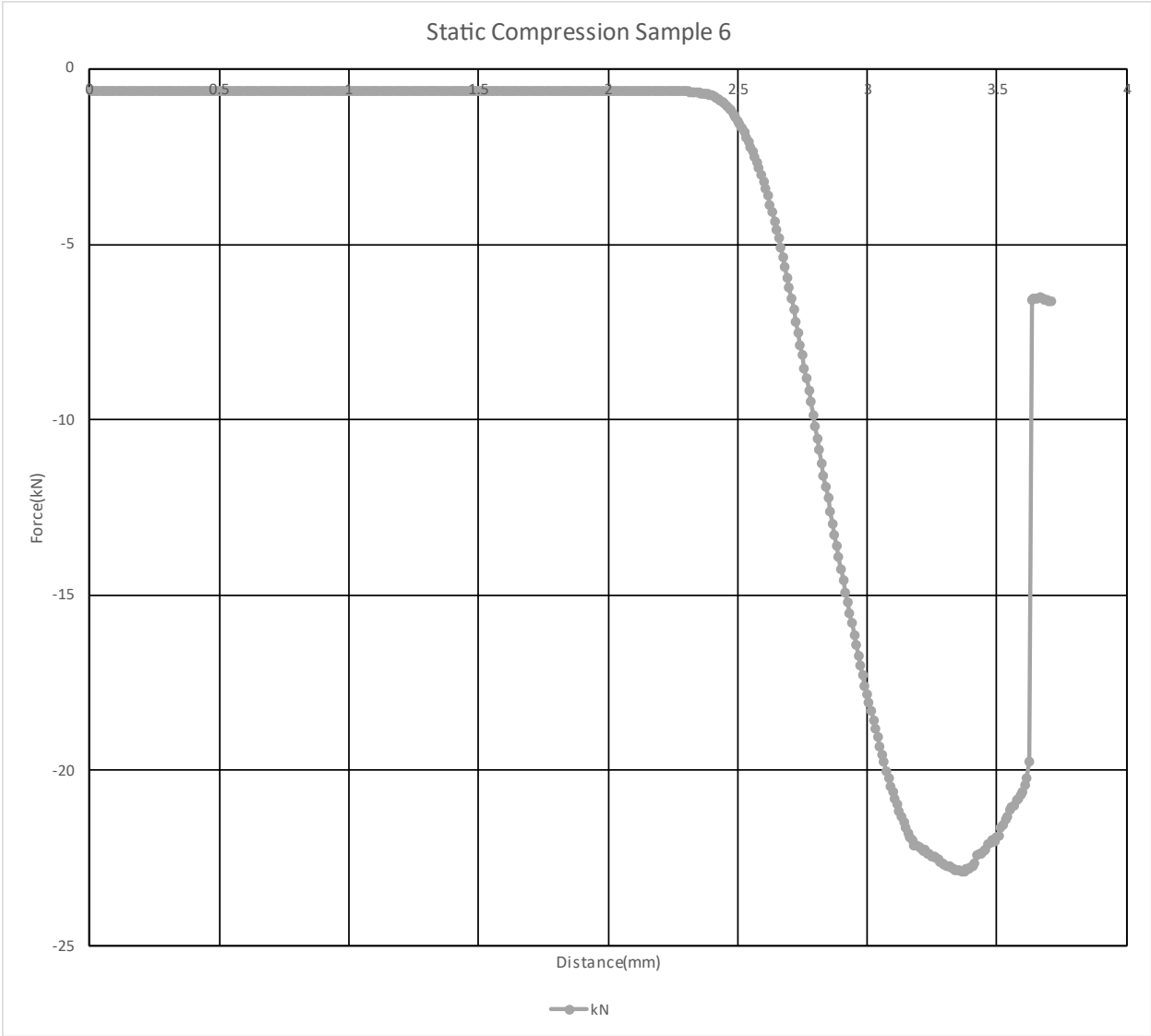


Static Compression Sample 4

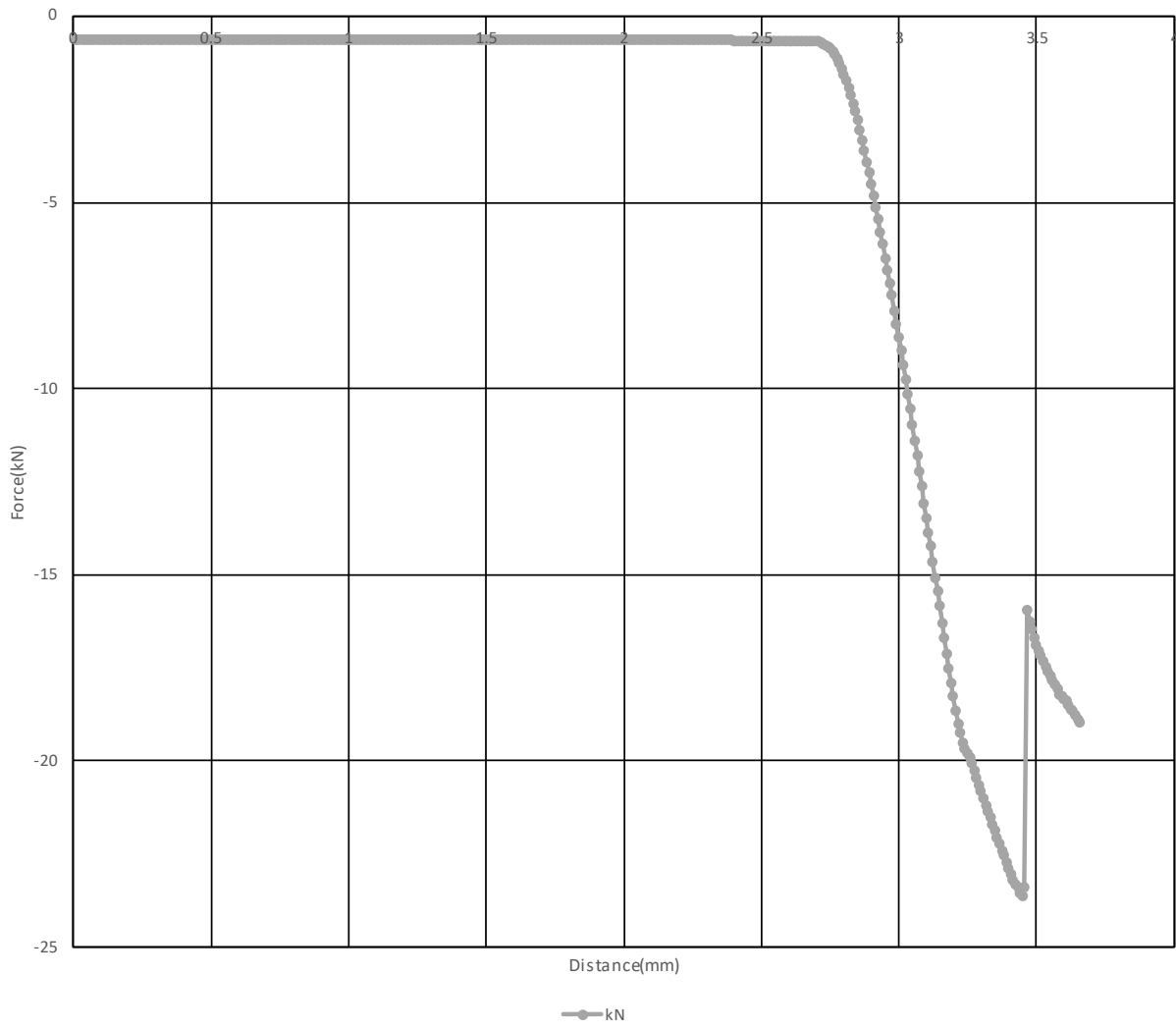


Static Compression Sample 5

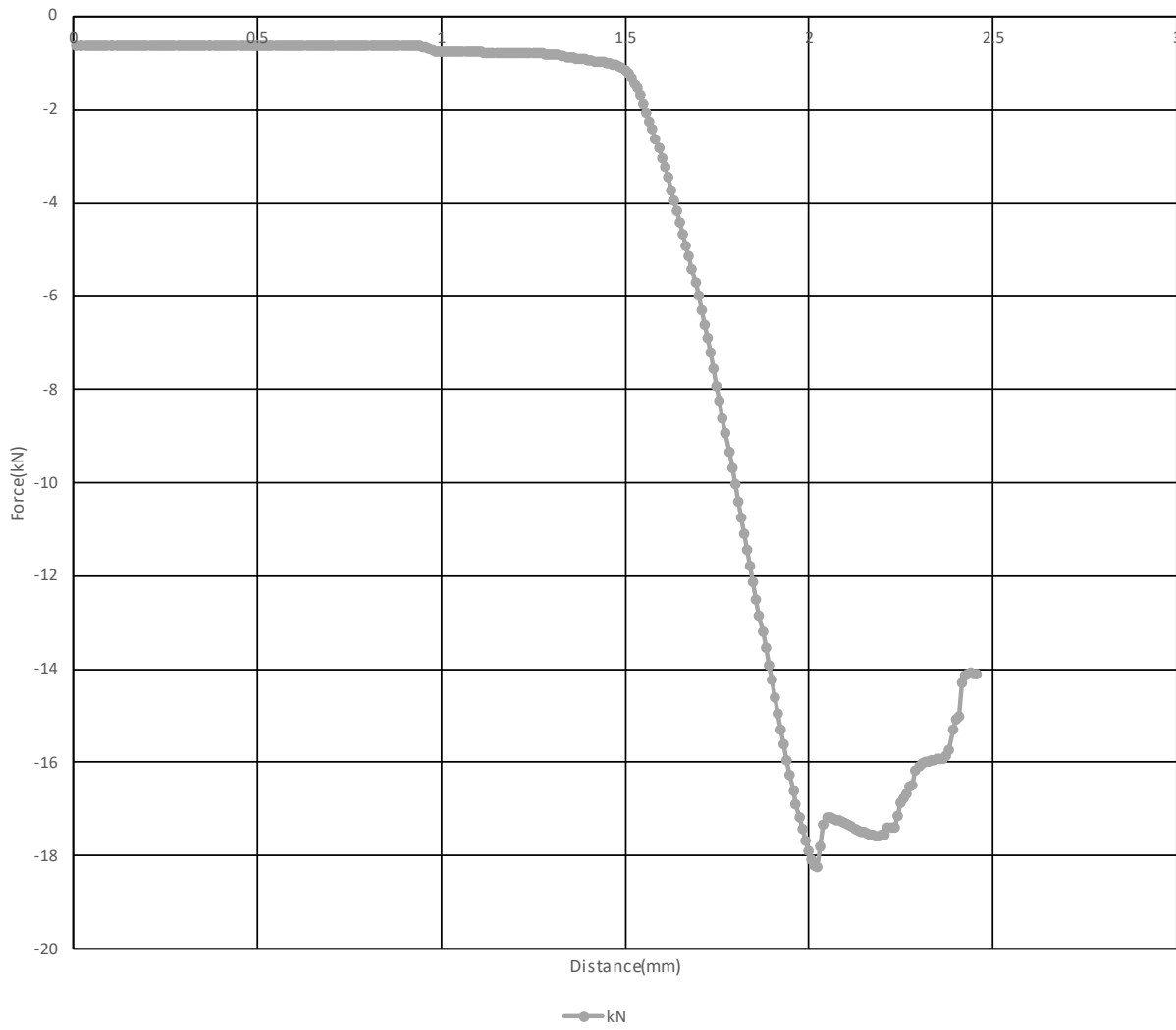




Static Compression Sample 7



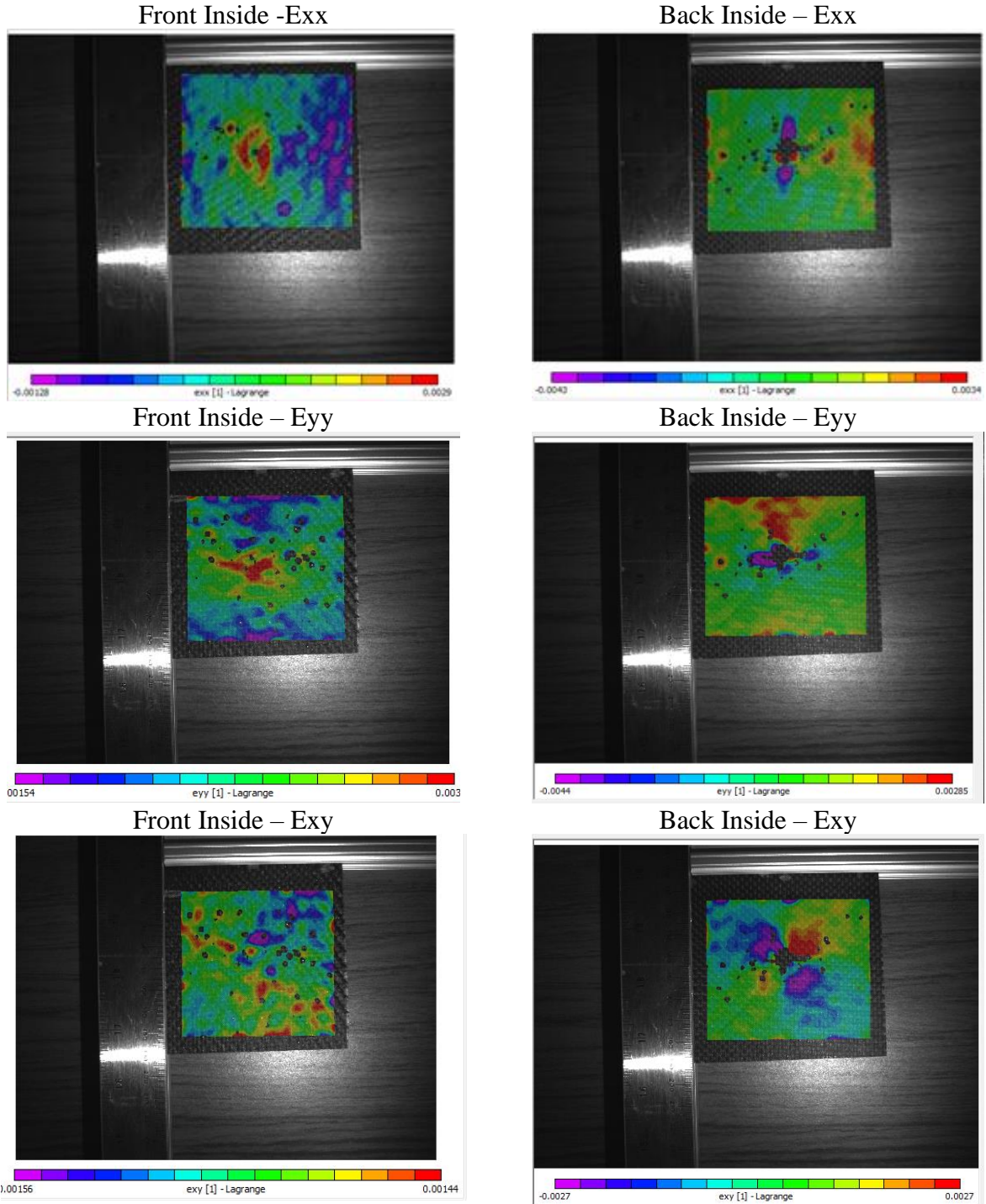
Static Compression Sample 8



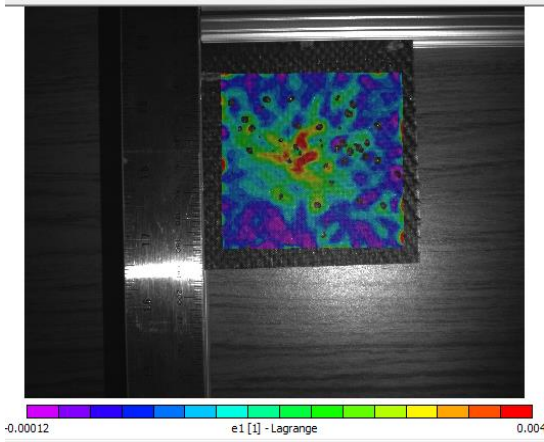


## Appendix C – Digital Correlation Results

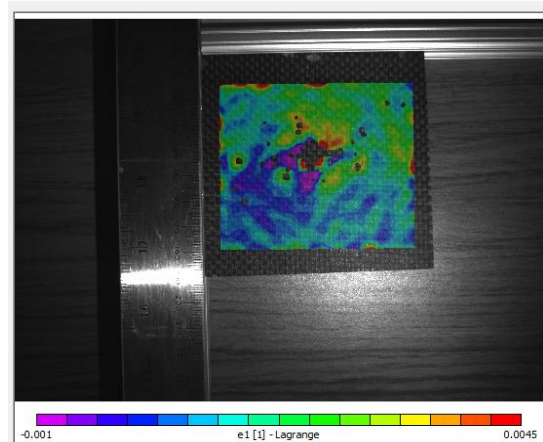
Sample 1 – First Impact 10J – 2 in diameter head with center impact



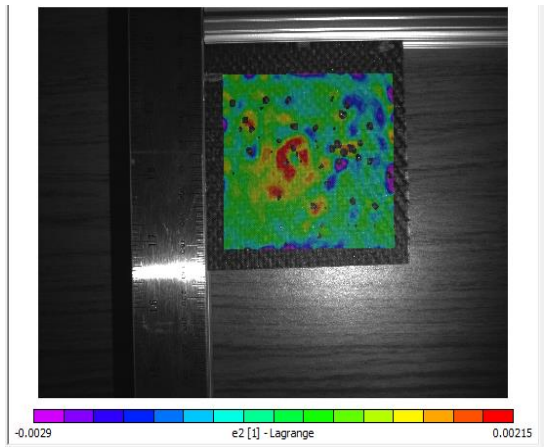
Front Inside – E1



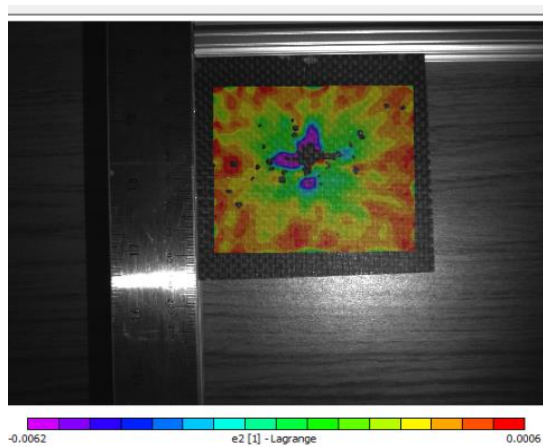
Back Inside – E1



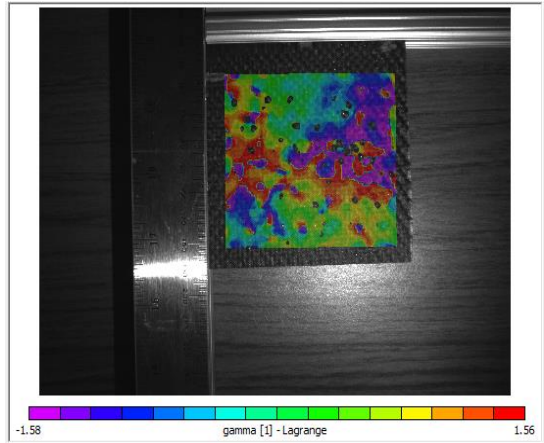
Front Inside – E2



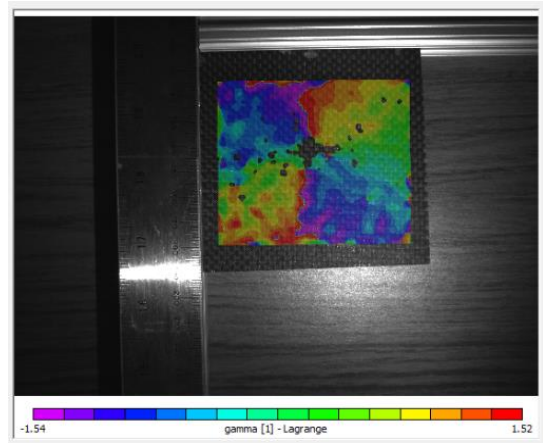
Back Inside – E2



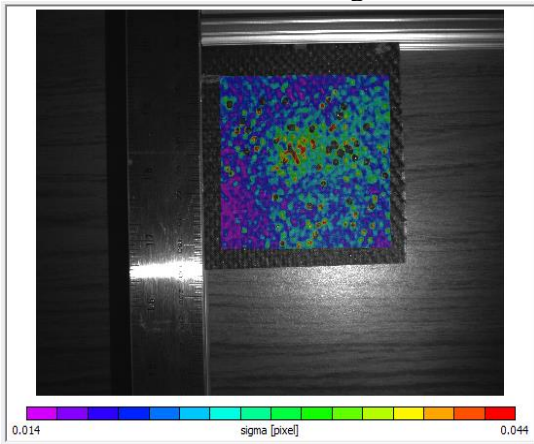
Front Inside – Gamma



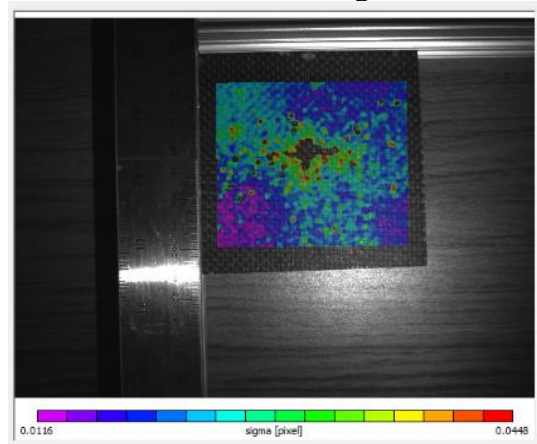
Back Inside – Gamma



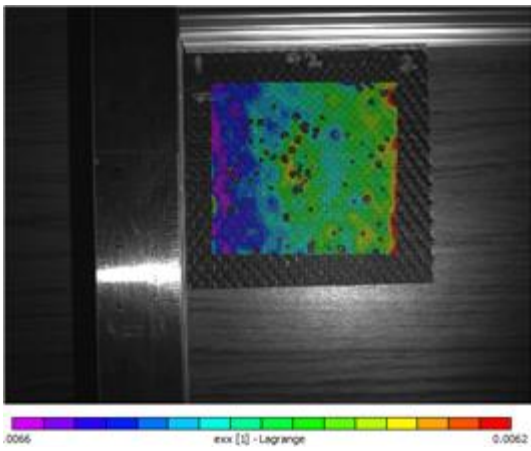
Front Inside – Sigma



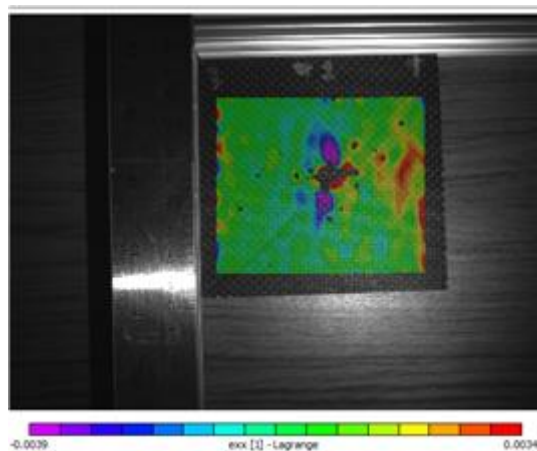
Back Inside – Sigma



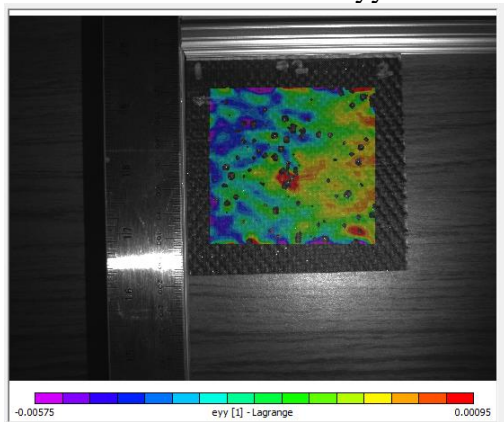
Front Outside -Exx



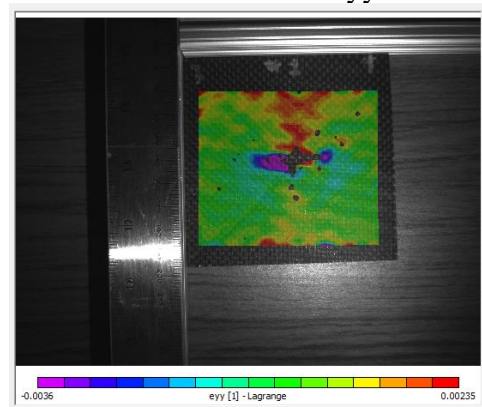
Back Outside – Exx



Front Outside – Eyy

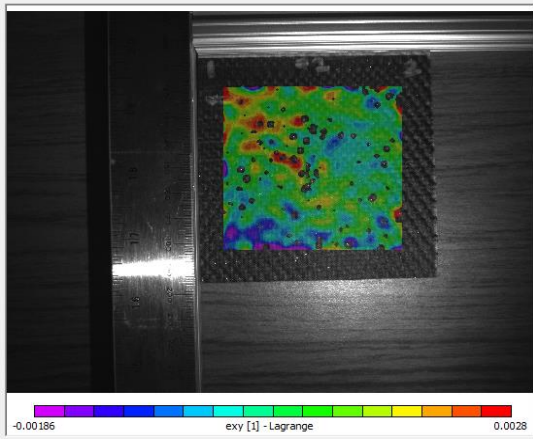


Back Outside – Eyy

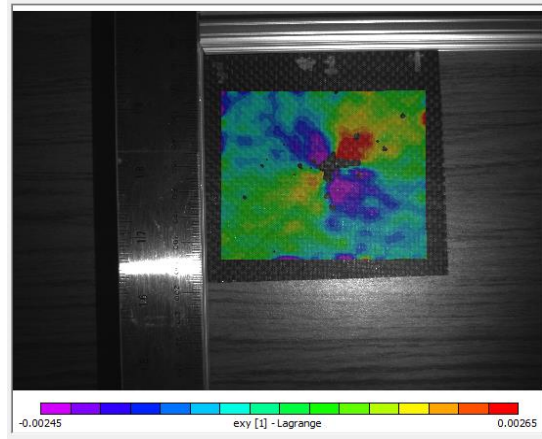




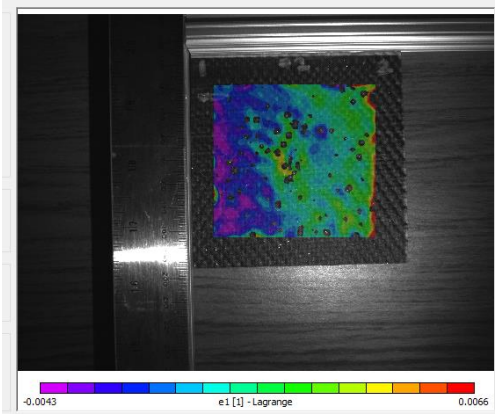
Front Outside – Exy



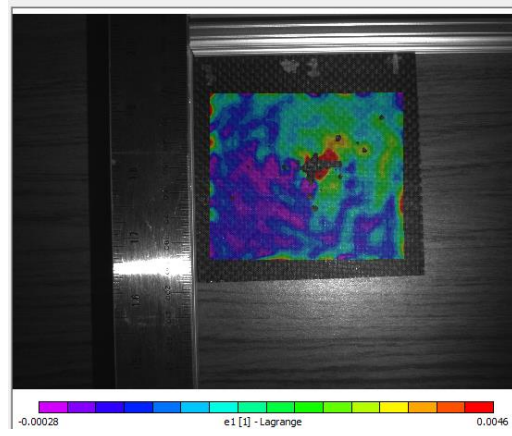
Back Outside – Exy



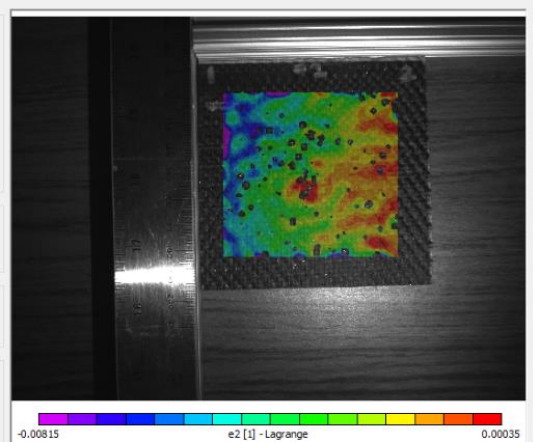
Front Outside – E1



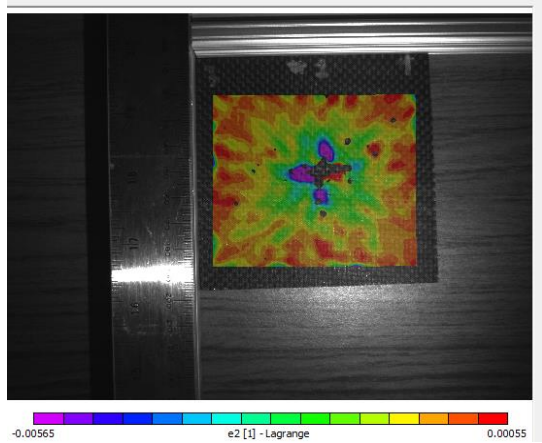
Back Outside – E1



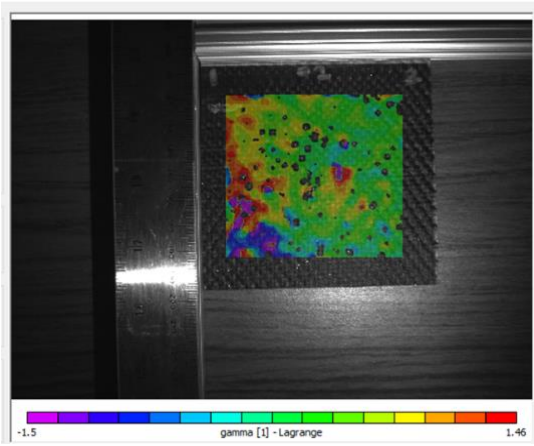
Front Outside – E2



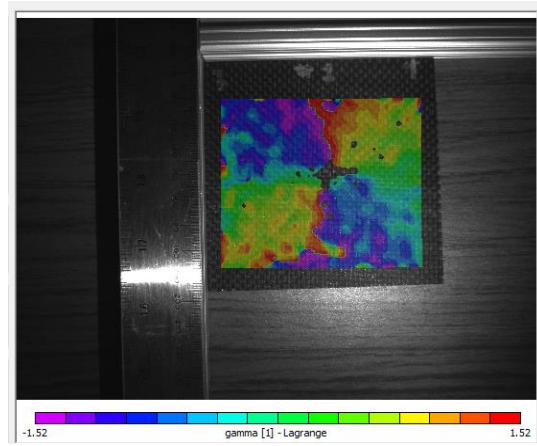
Back Outside – E2



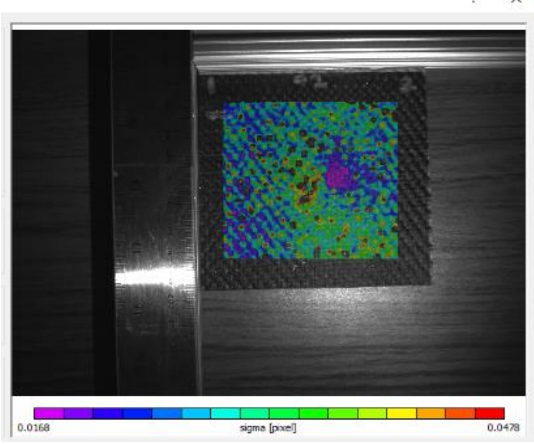
Front Outside – Gamma



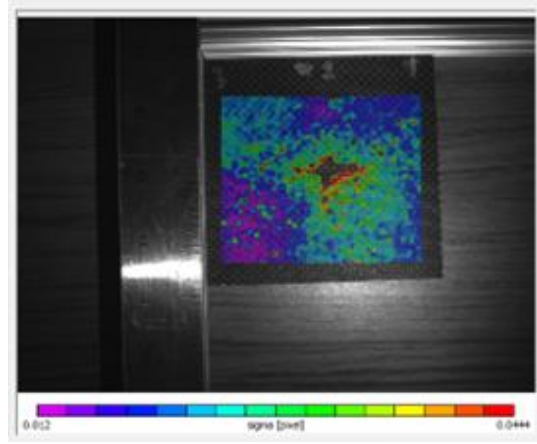
Back Outside – Gamma



Front Outside – Sigma

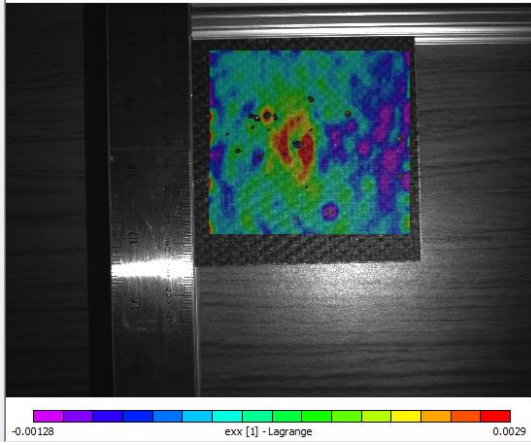


Back Outside – Sigma

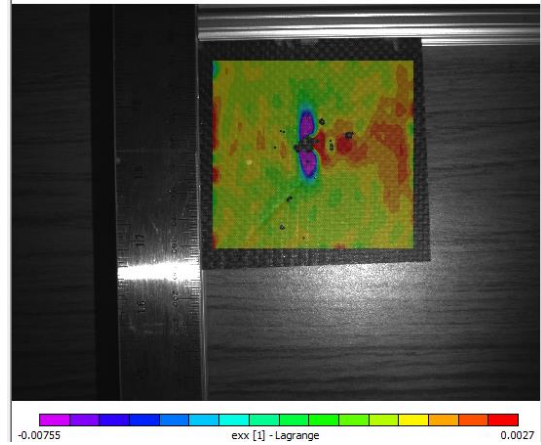


Sample 2 – First Impact 10J – 2 in diameter head with center impact

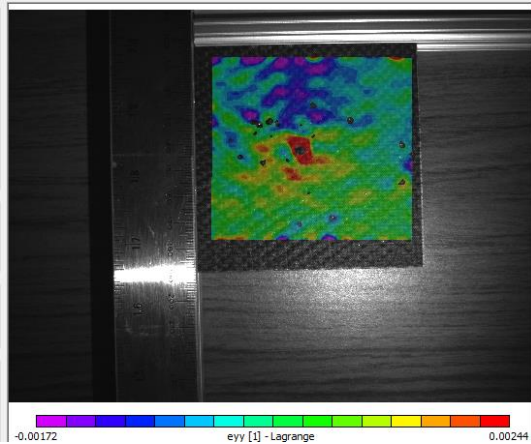
Front Inside – Exx



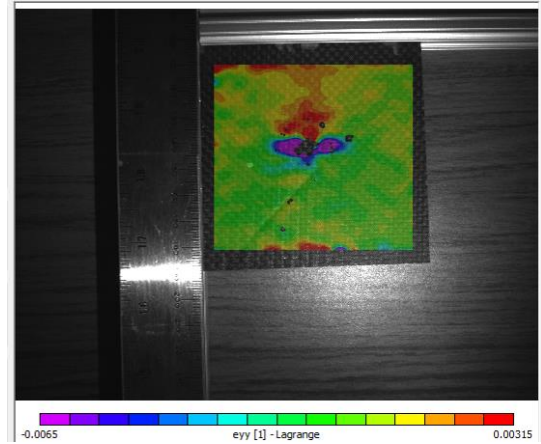
Back Inside – Exx



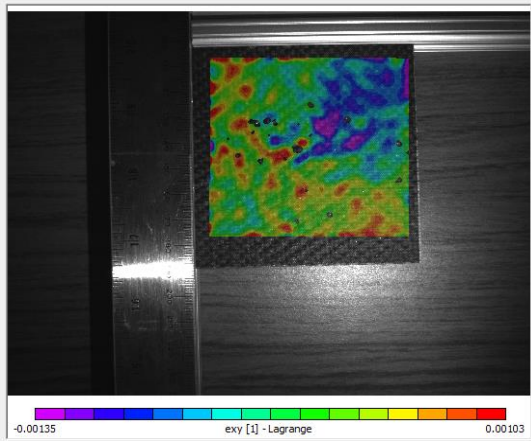
Front Inside – Eyy



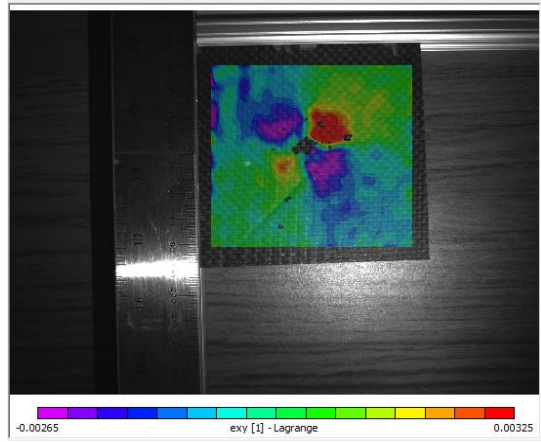
Back Inside – Eyy



Front Inside – Exy

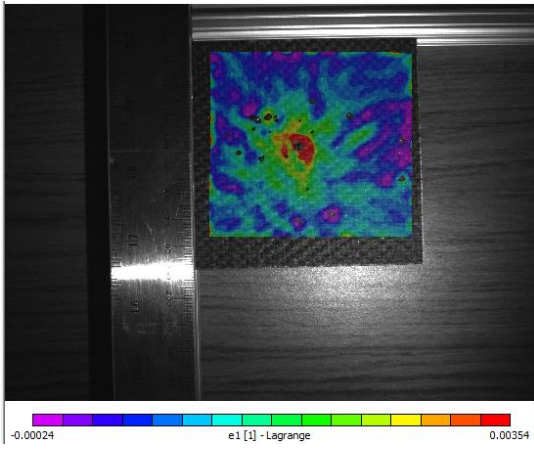


Back Inside – Exy

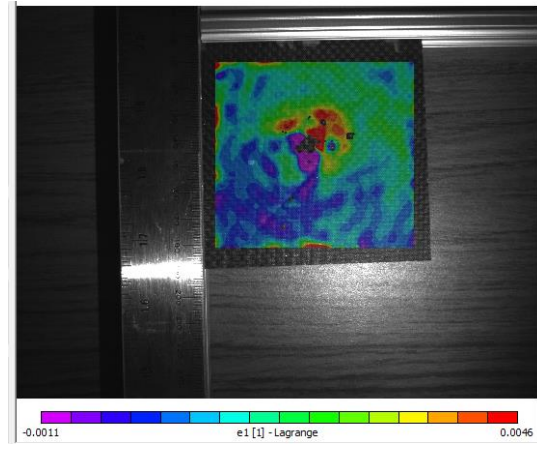




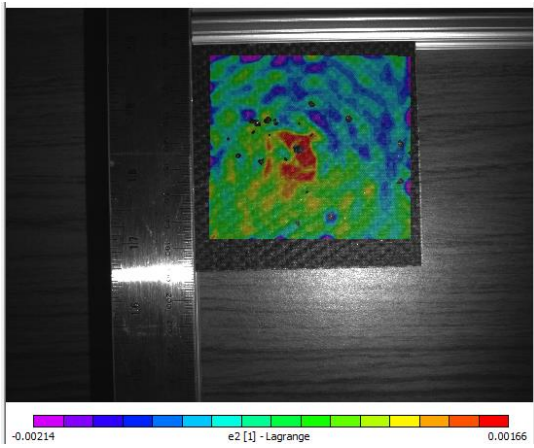
Front Inside – E1



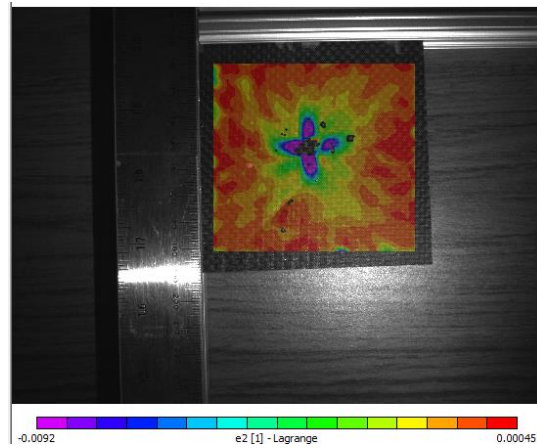
Back Inside – E1



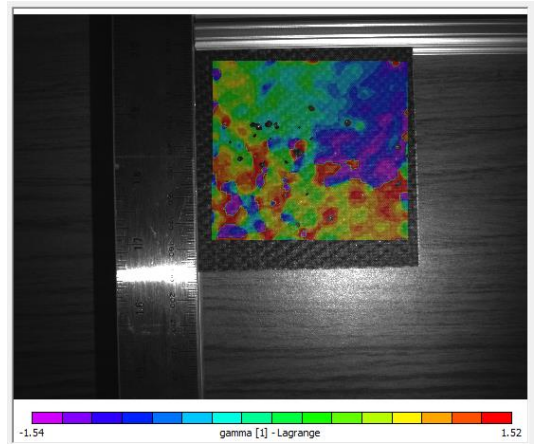
Front Inside – E2



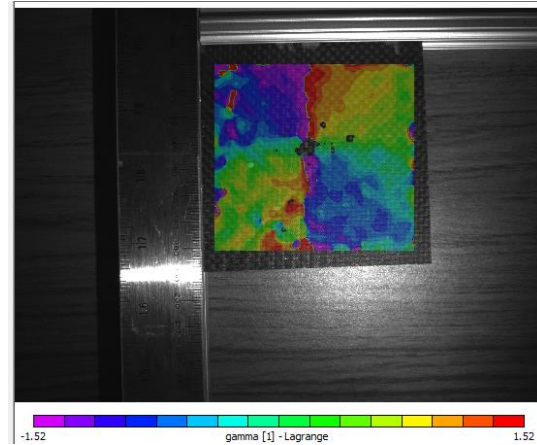
Back Inside – E2



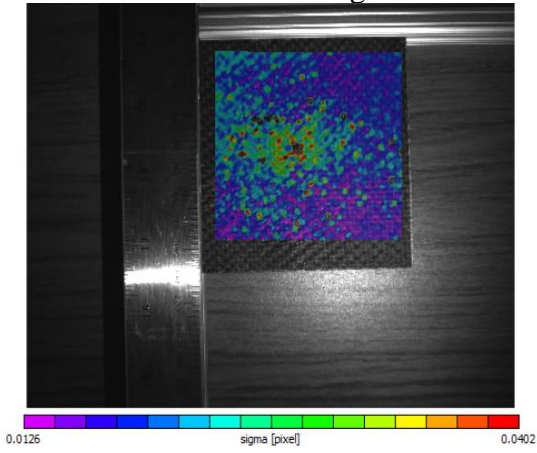
Front Inside – Gamma



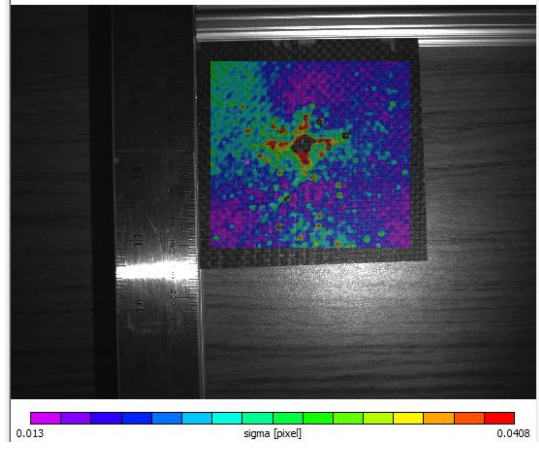
Back Inside – Gamma



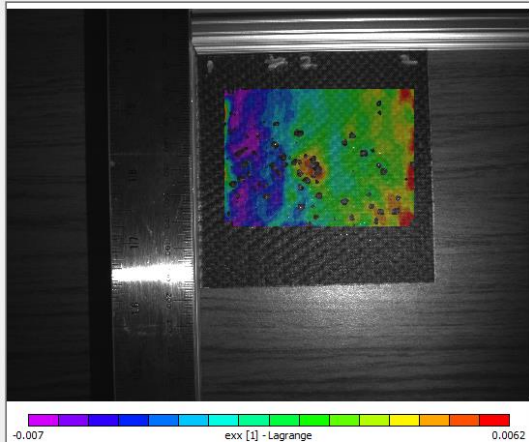
Front Inside – Sigma



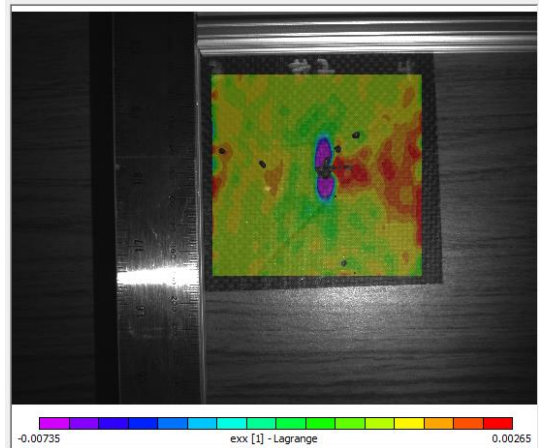
Back Inside – Sigma



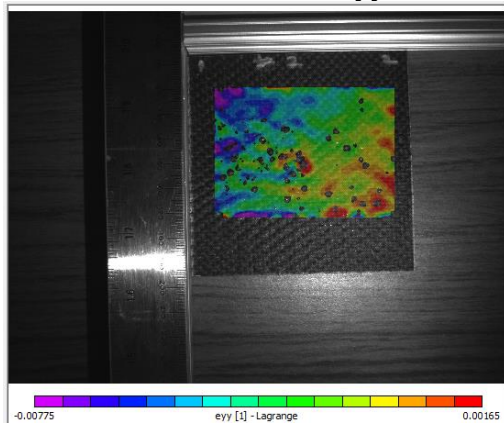
Front Outside -Exx



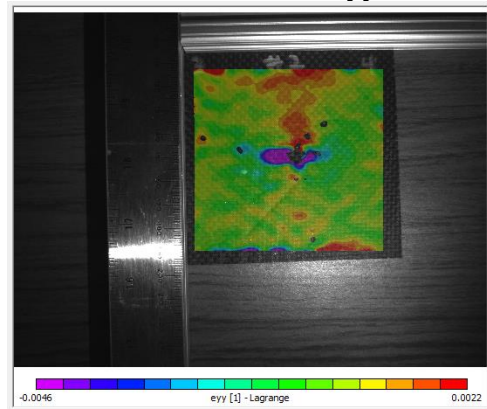
Back Outside – Exx



Front Outside – Eyy

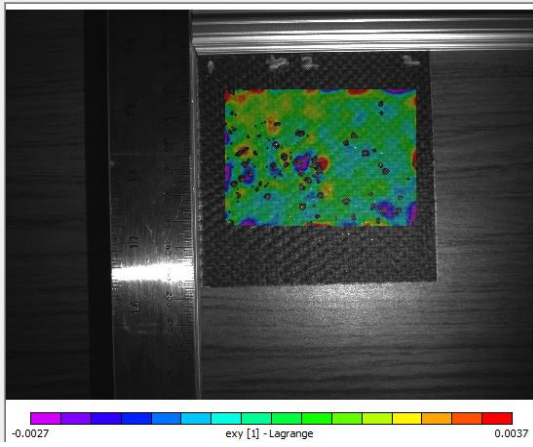


Back Outside – Eyy

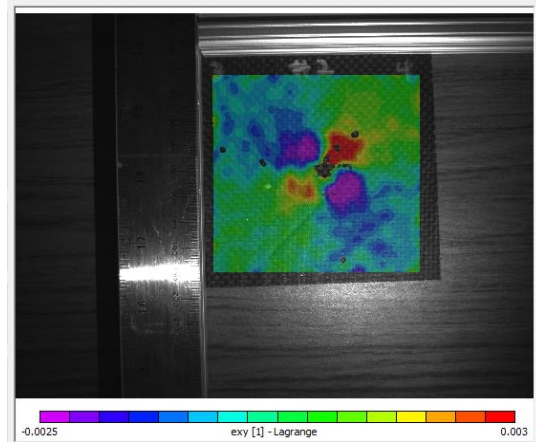




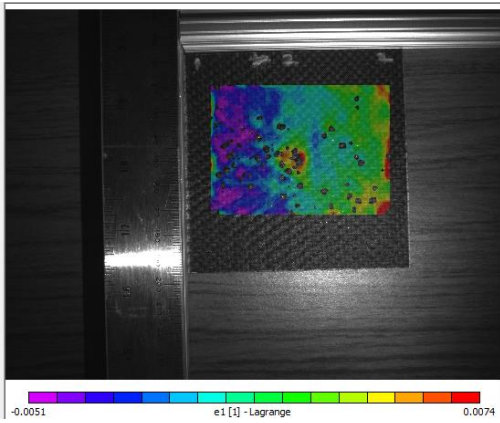
Front Outside – Exy



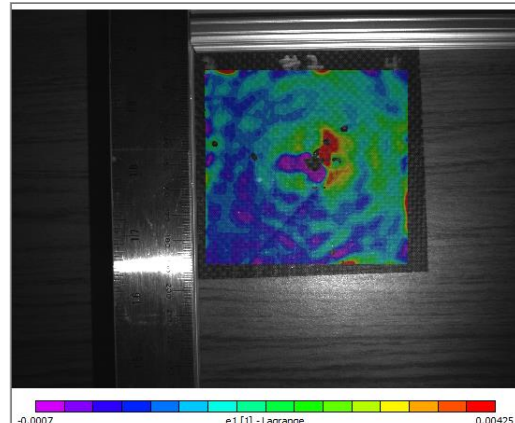
Back Outside – Exy



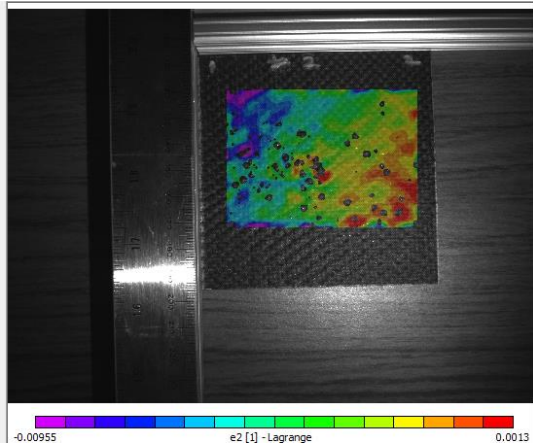
Front Outside – E1



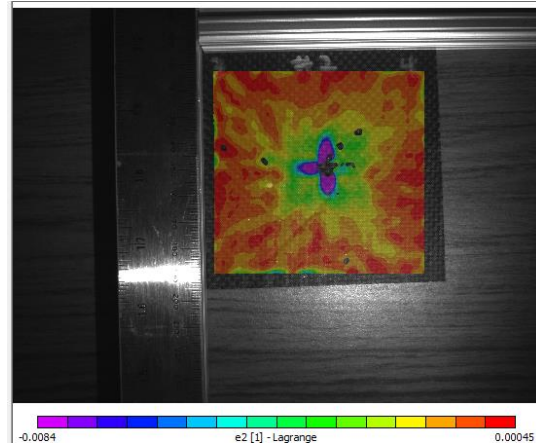
Back Outside – E1



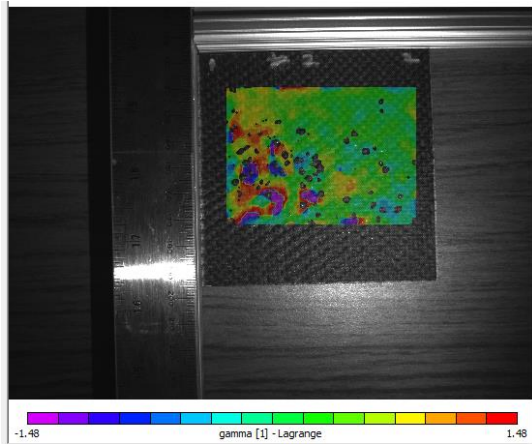
Front Outside – E2



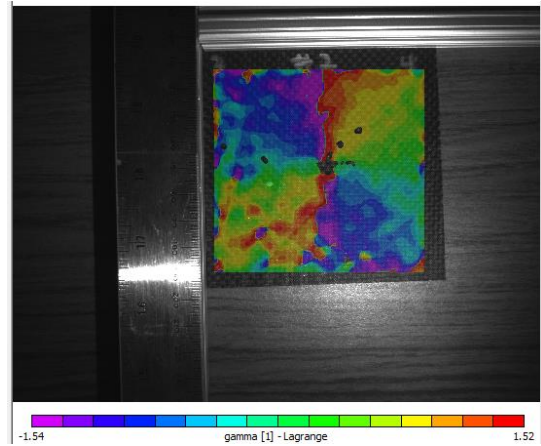
Back Outside – E2



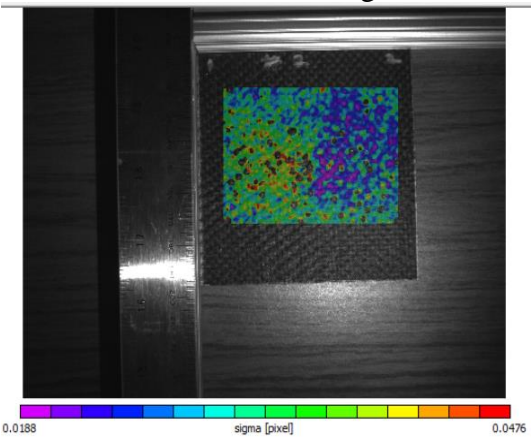
Front Outside – Gamma



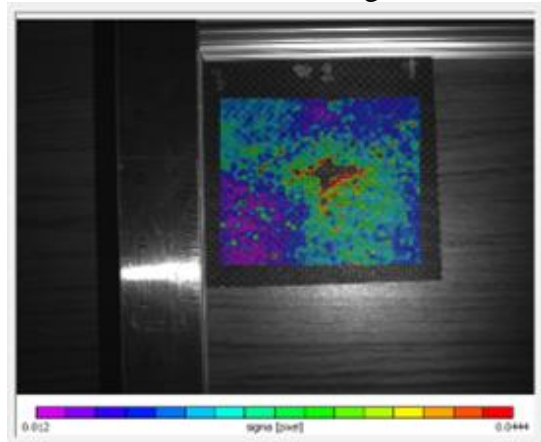
Back Outside – Gamma



Front Outside – Sigma

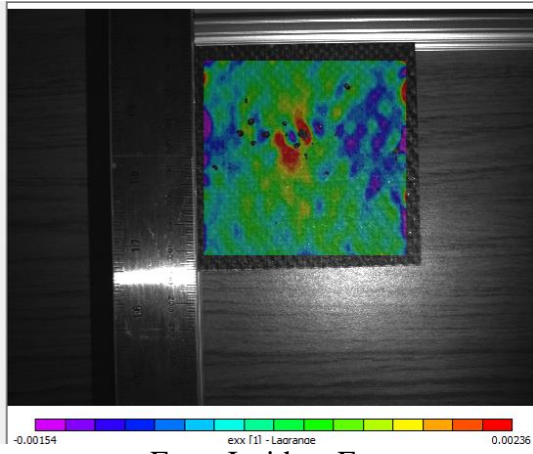


Back Outside – Sigma

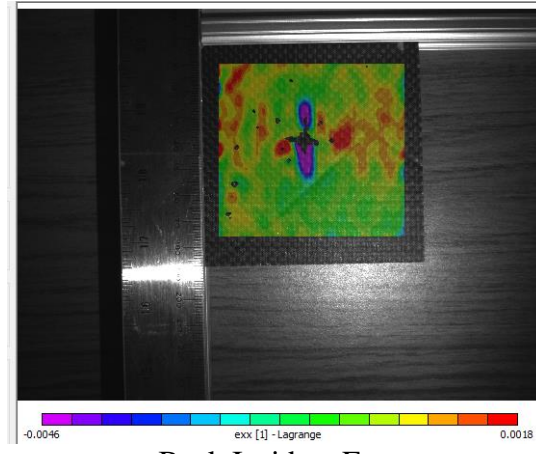


Sample 3– First Impact 10J – 2 in diameter head with center impact

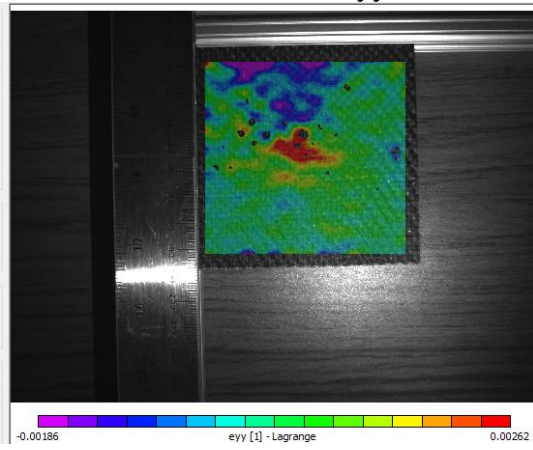
Front Inside – Exx



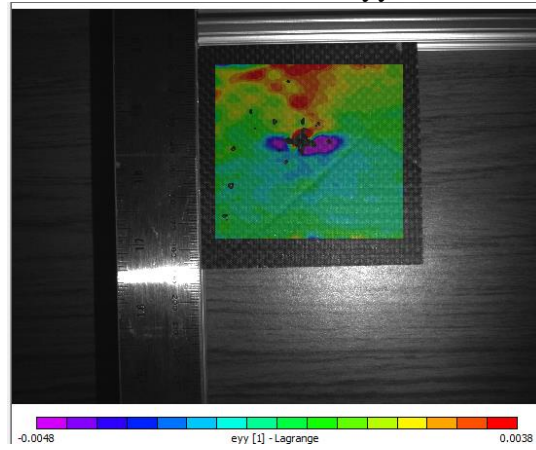
Back Inside – Exx



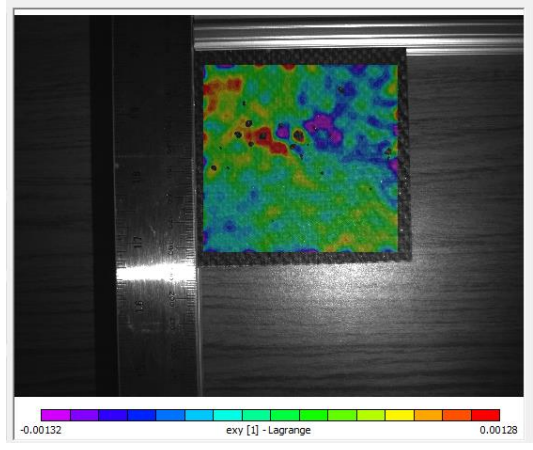
Front Inside – Eyy



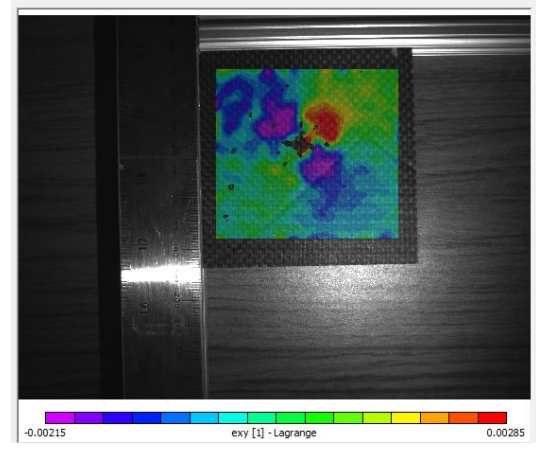
Back Inside – Eyy



Front Inside – Exy

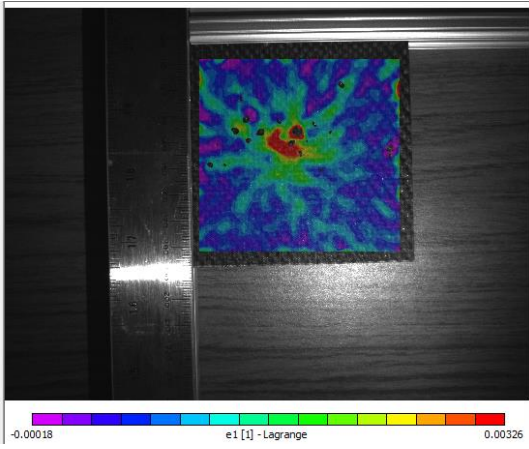


Back Inside – Exy

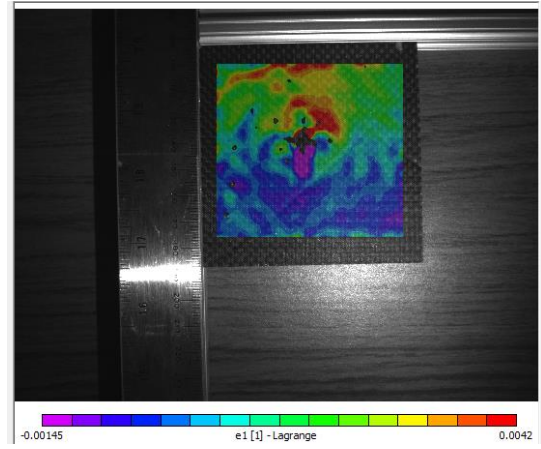




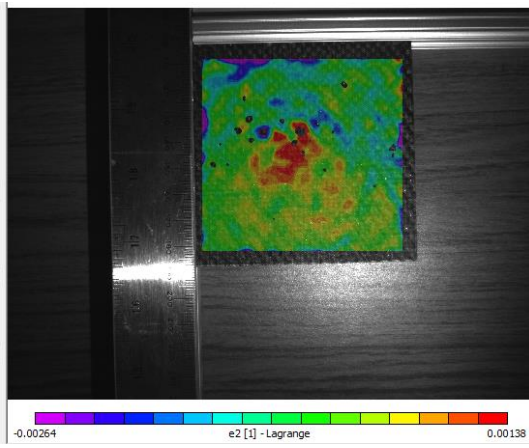
Front Inside – E1



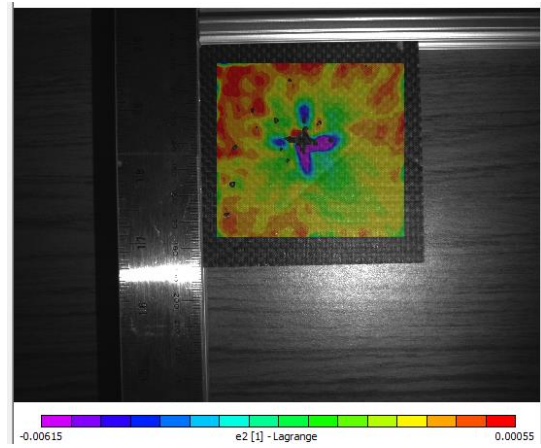
Back Inside – E1



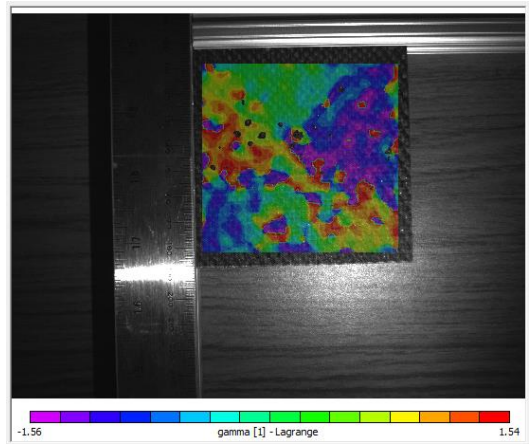
Front Inside – E2



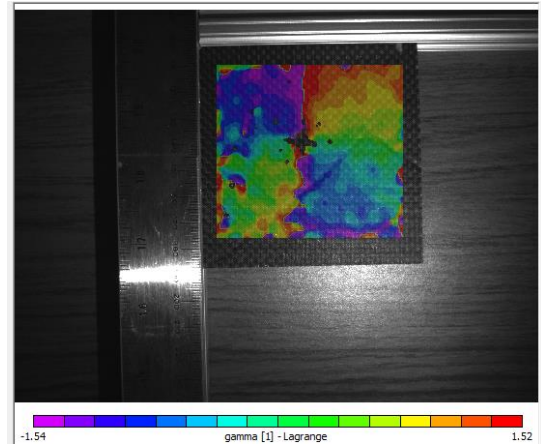
Back Inside – E2



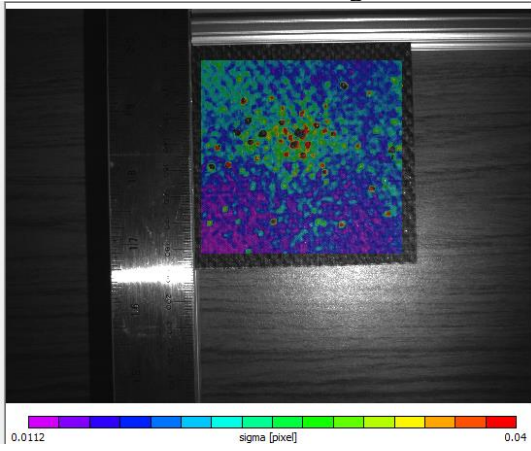
Front Inside – Gamma



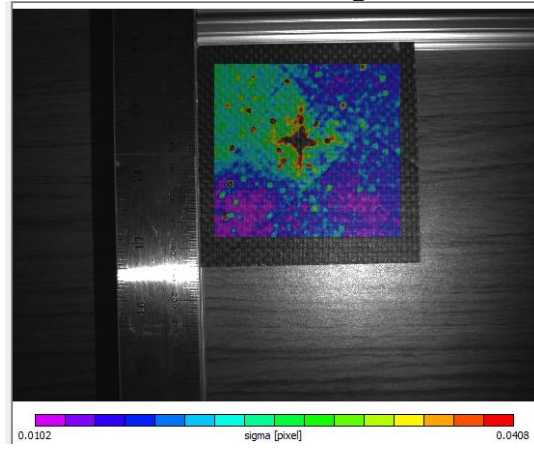
Back Inside – Gamma



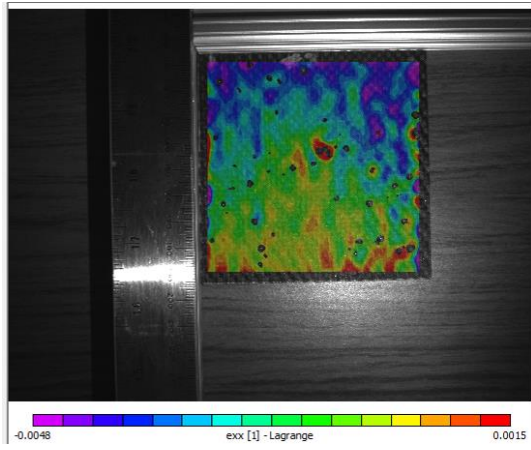
Front Inside – Sigma



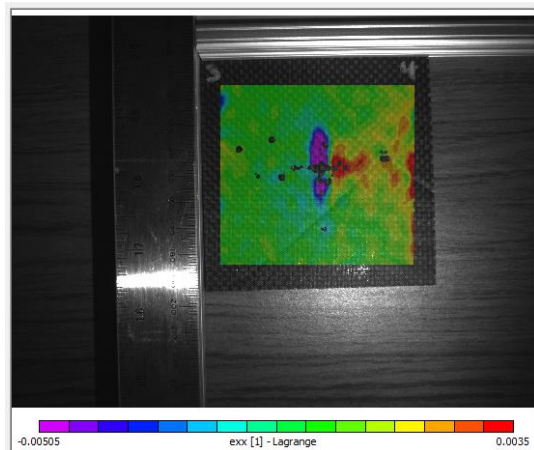
Back Inside – Sigma



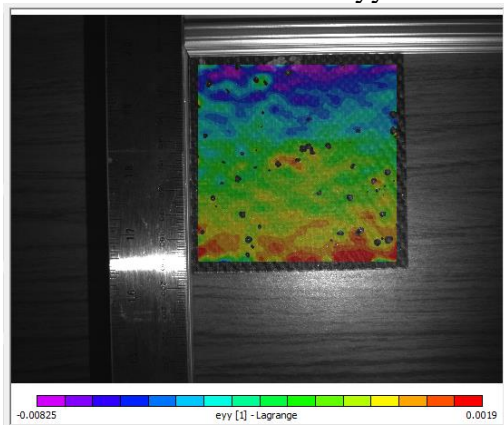
Front Outside -Exx



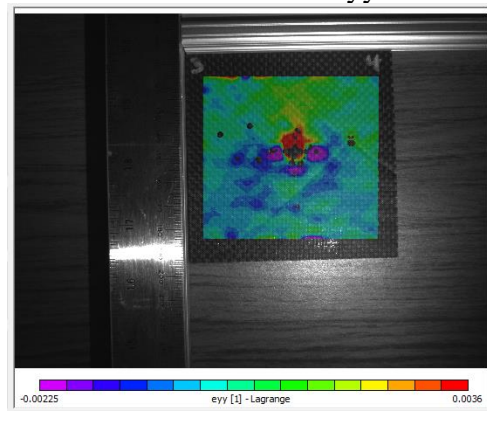
Back Outside – Exx



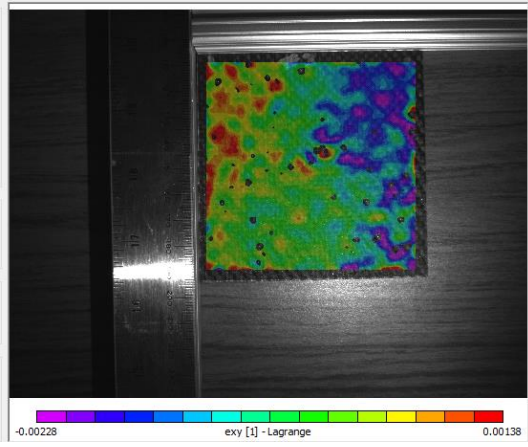
Front Outside – Eyy



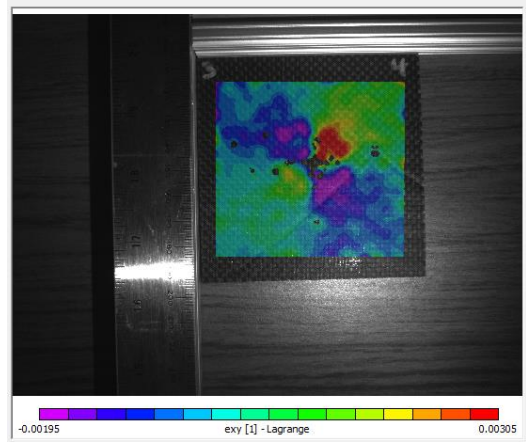
Back Outside – Eyy



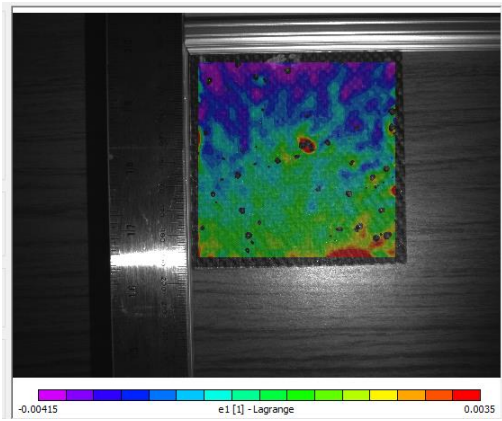
Front Outside – Exy



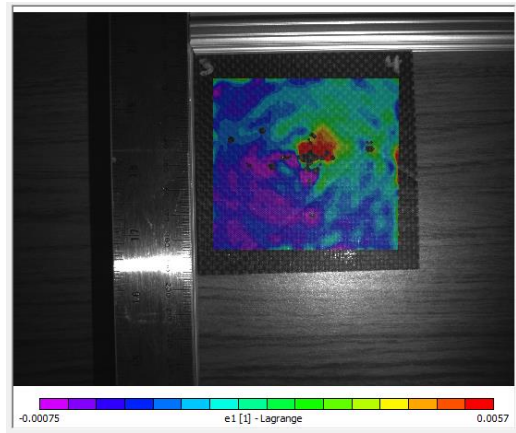
Back Outside – Exy



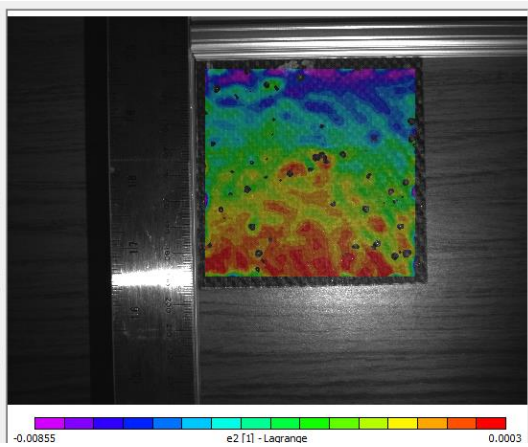
Front Outside – E1



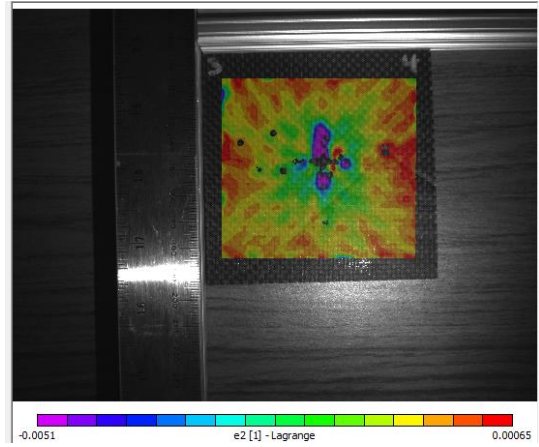
Back Outside – E1



Front Outside – E2

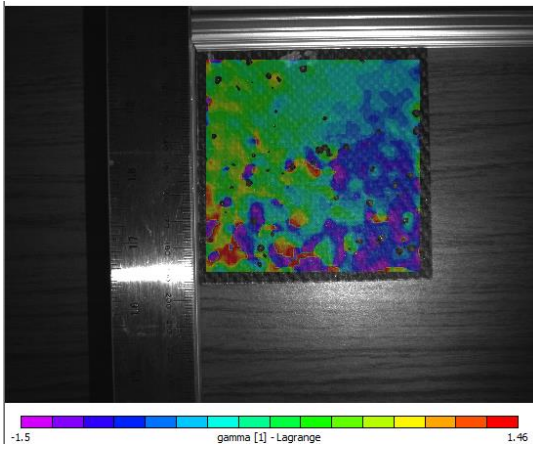


Back Outside – E2

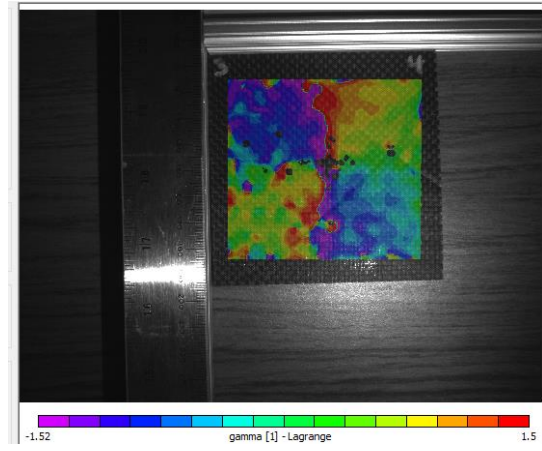




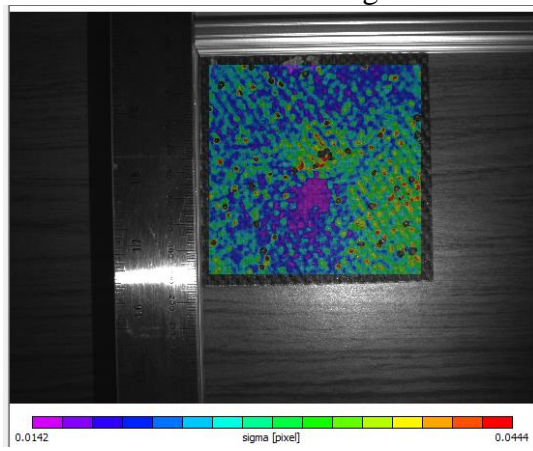
Front Outside – Gamma



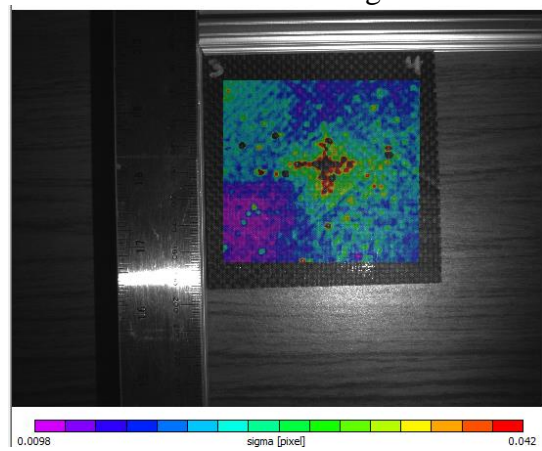
Back Outside – Gamma



Front Outside – Sigma

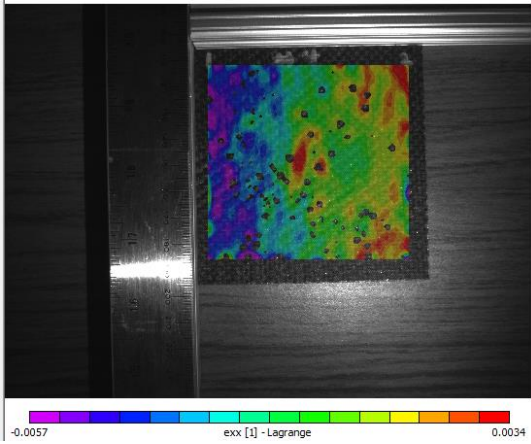


Back Outside – Sigma

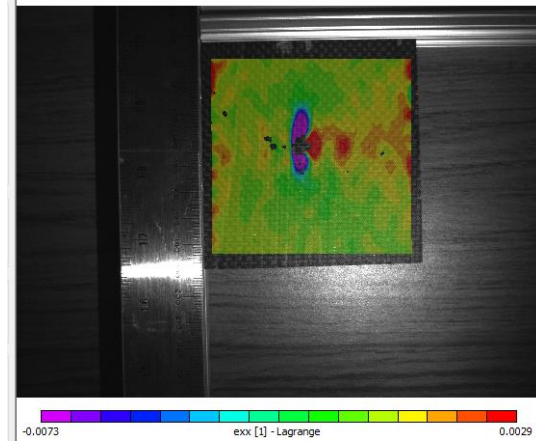


Sample 4 – First Impact 10J – 2 in diameter head with center impact

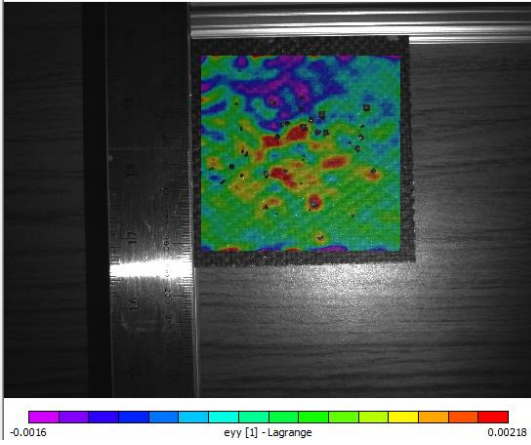
Front Inside – Exx



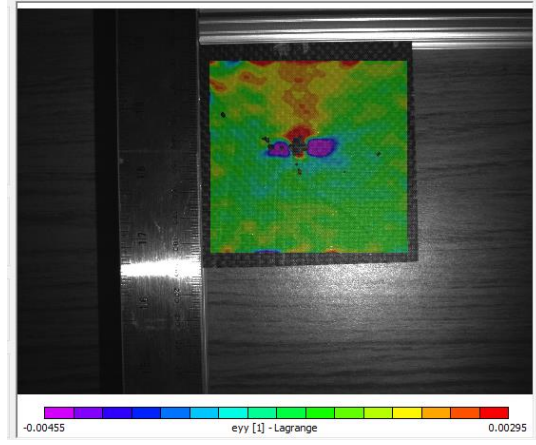
Back Inside – Exx



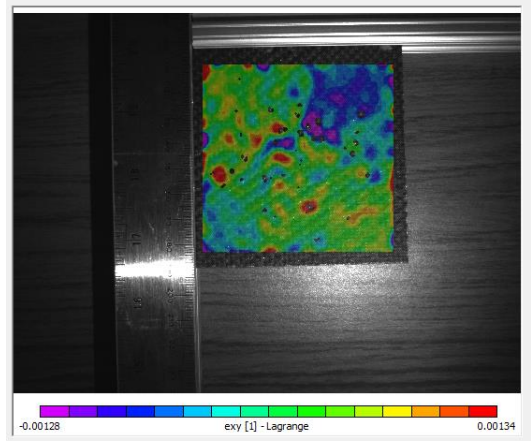
Front Inside – Eyy



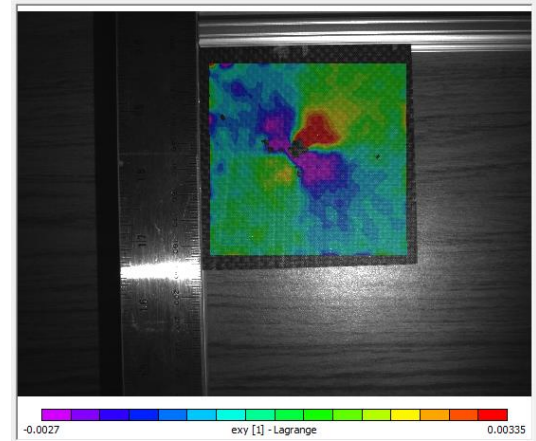
Back Inside – Eyy



Front Inside – Exy

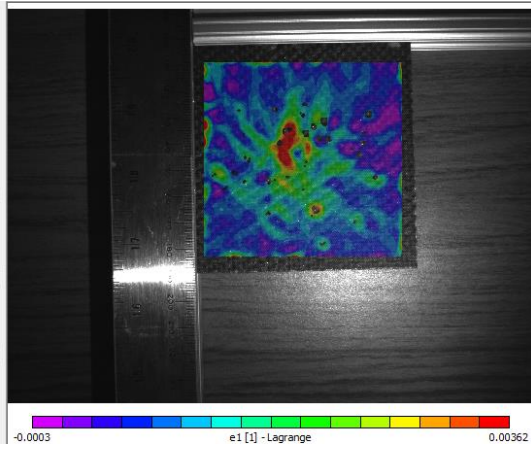


Back Inside – Exy

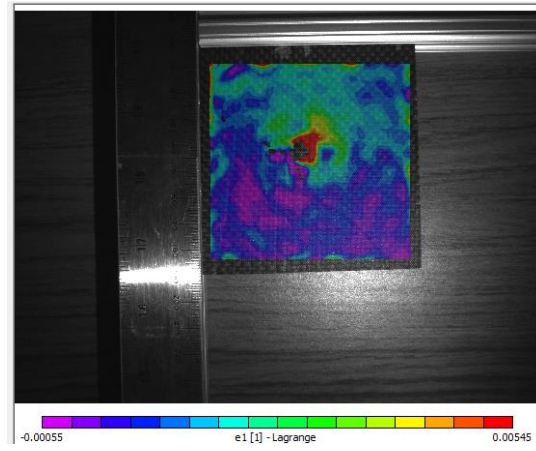




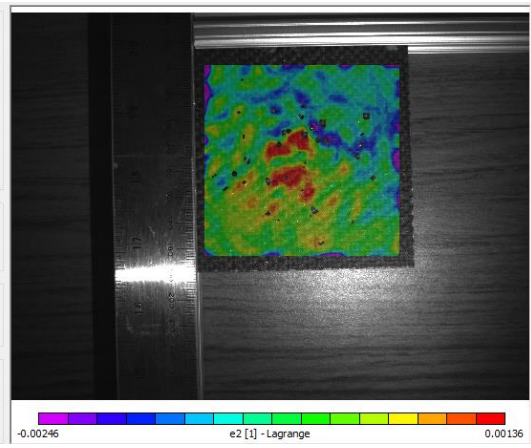
Front Inside – E1



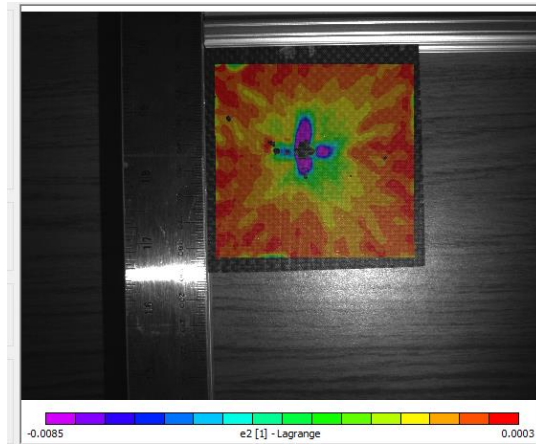
Back Inside – E1



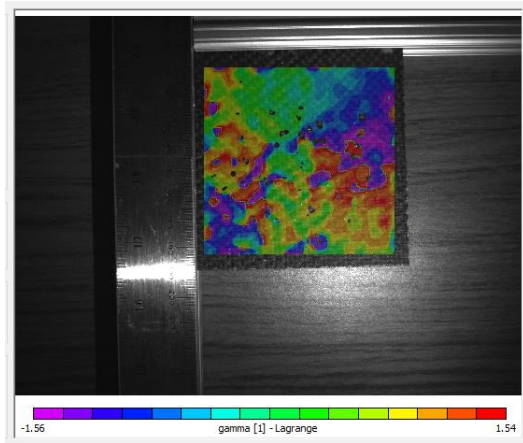
Front Inside – E2



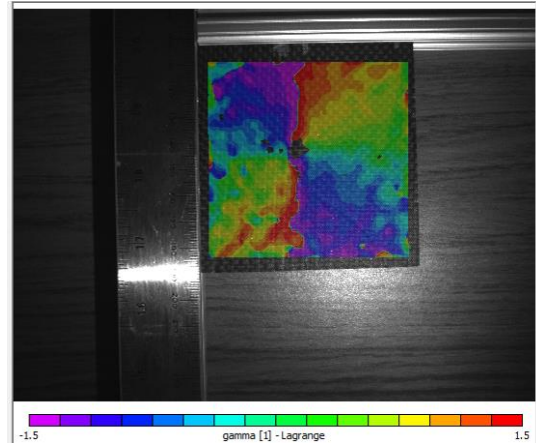
Back Inside – E2



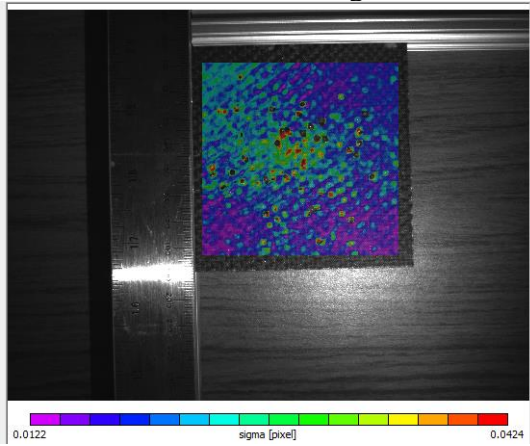
Front Inside – Gamma



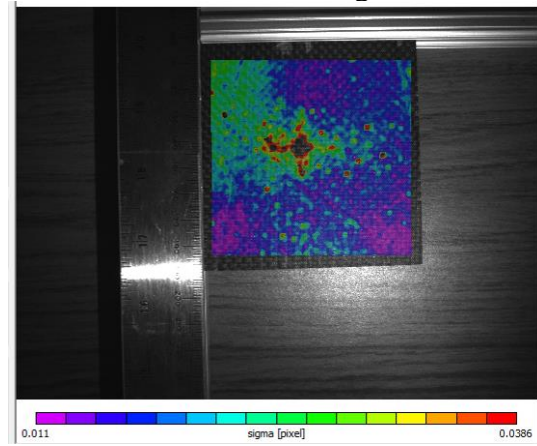
Back Inside – Gamma



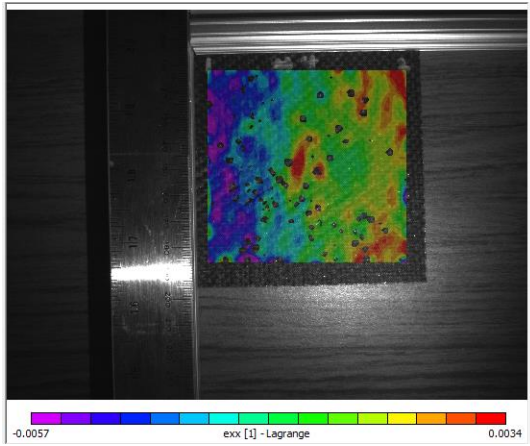
Front Inside – Sigma



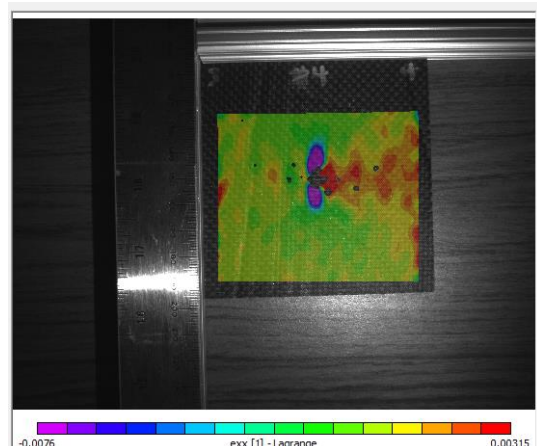
Back Inside – Sigma



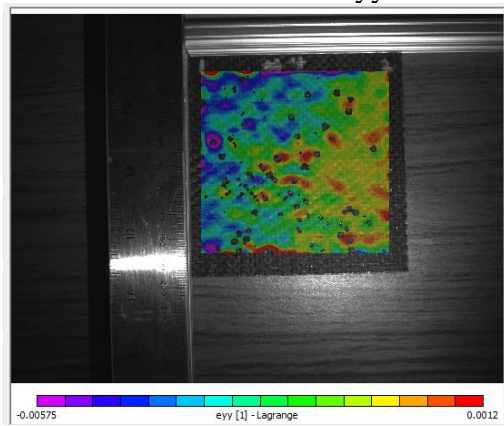
Front Outside -Exx



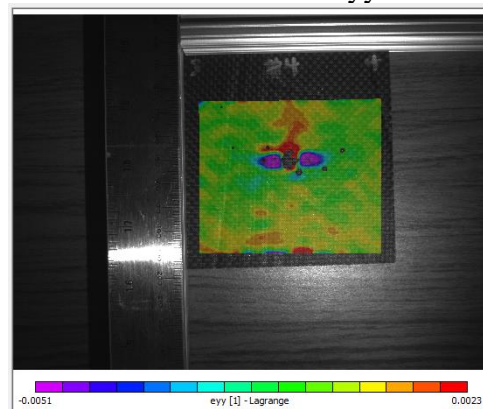
Back Outside – Exx



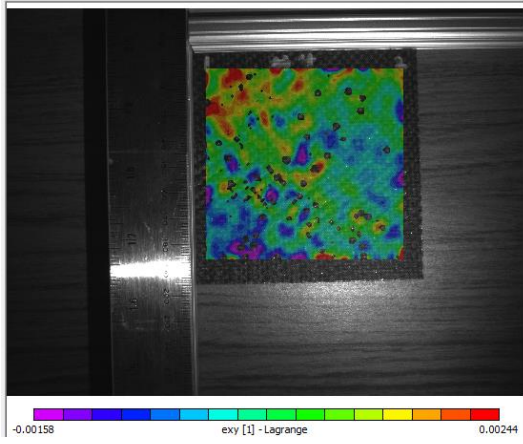
Front Outside – Eyy



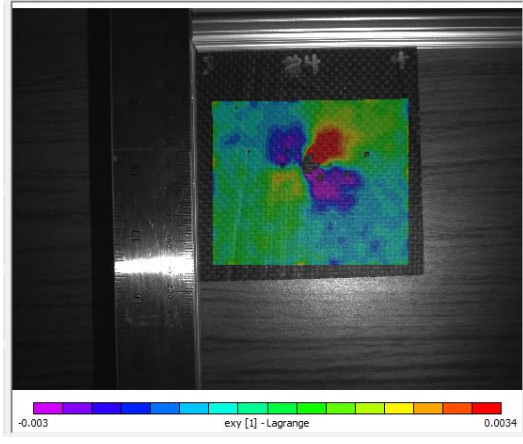
Back Outside – Eyy



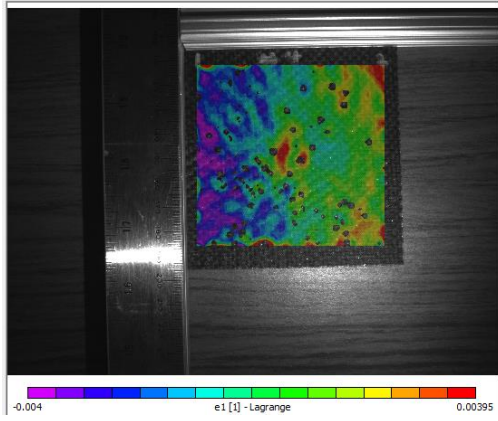
Front Outside – Exy



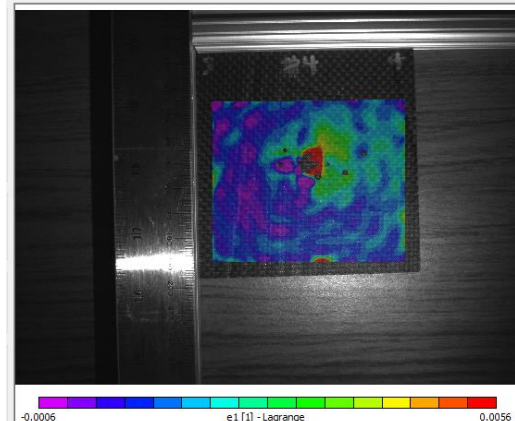
Back Outside – Exy



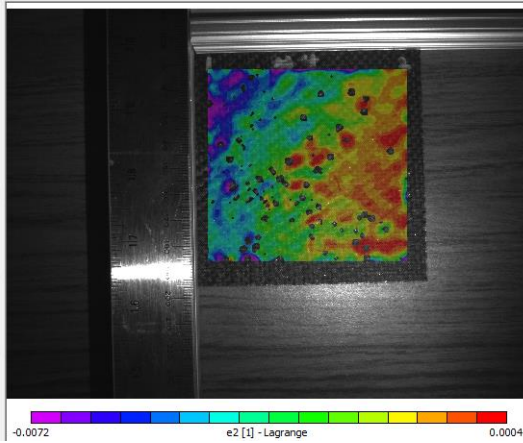
Front Outside – E1



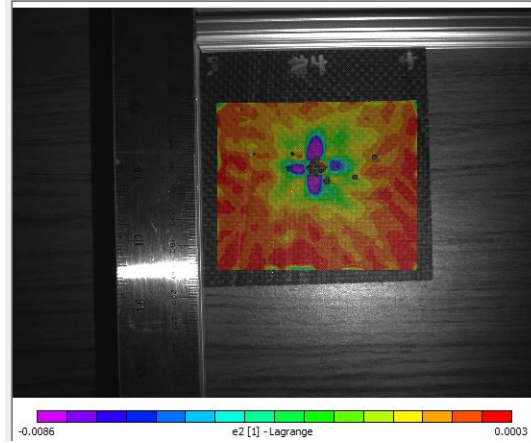
Back Outside – E1



Front Outside – E2

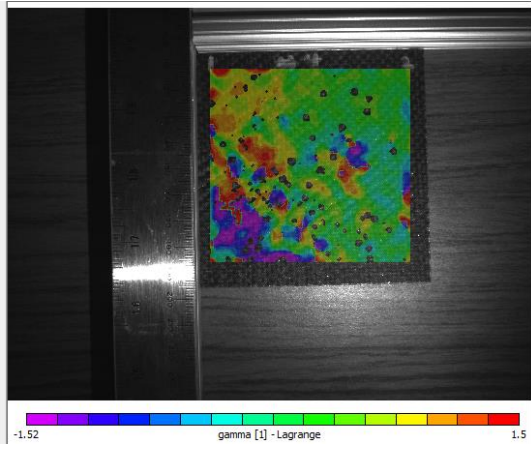


Back Outside – E2

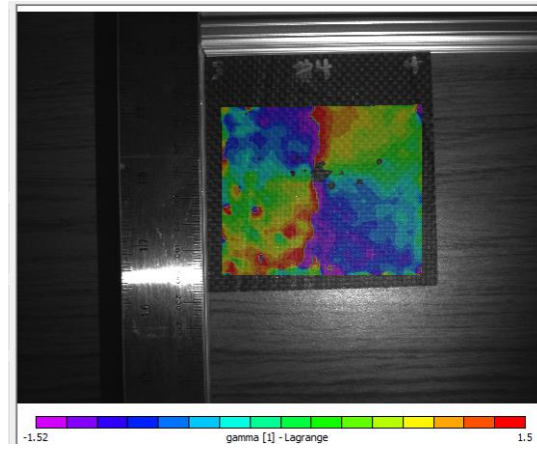




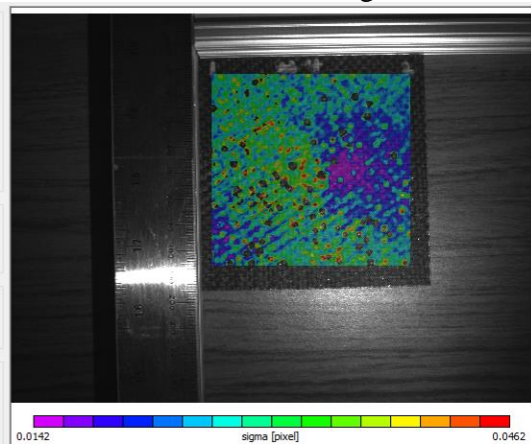
Front Outside – Gamma



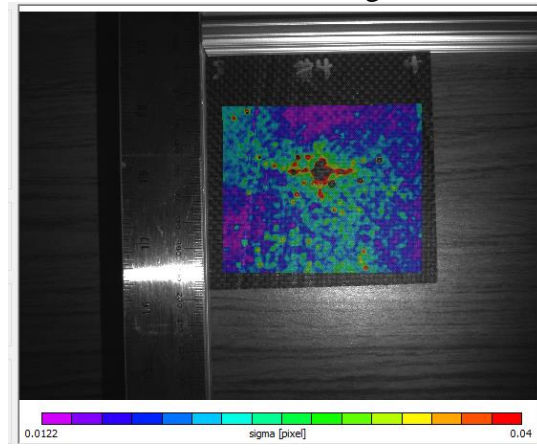
Back Outside – Gamma



Front Outside – Sigma

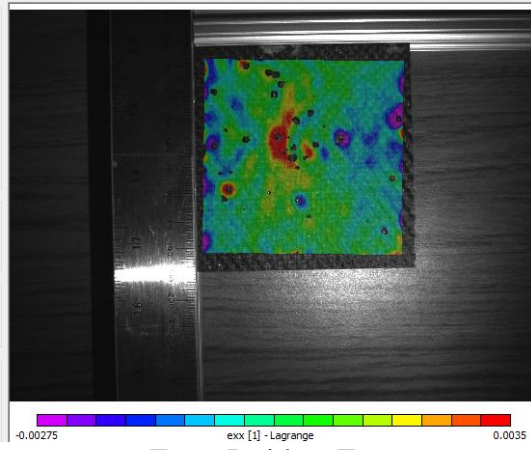


Back Outside – Sigma

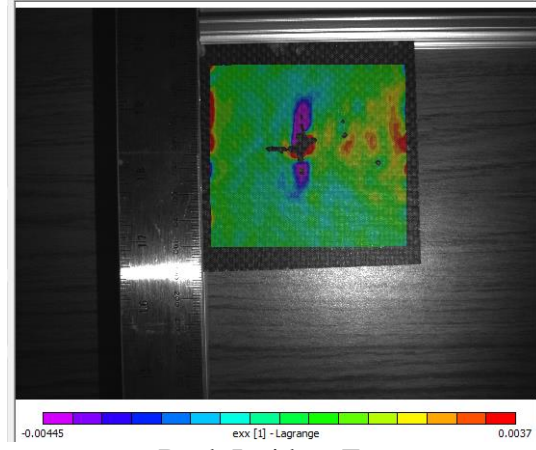


Sample 5 – First Impact 10J – 2 in diameter head with center impact

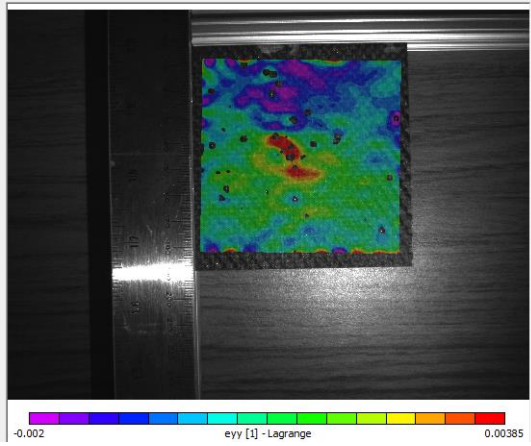
Front Inside – Exx



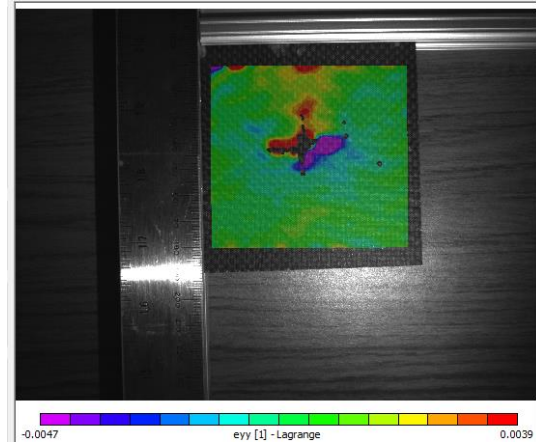
Back Inside – Exx



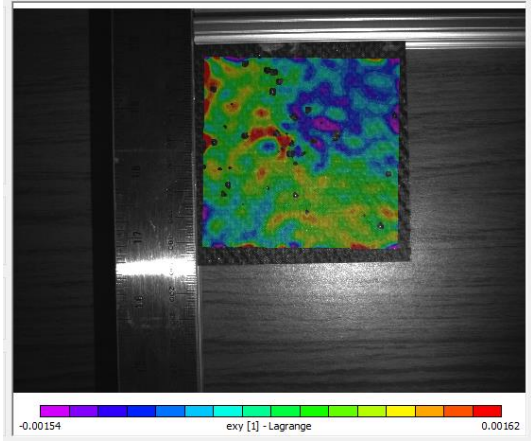
Front Inside – Eyy



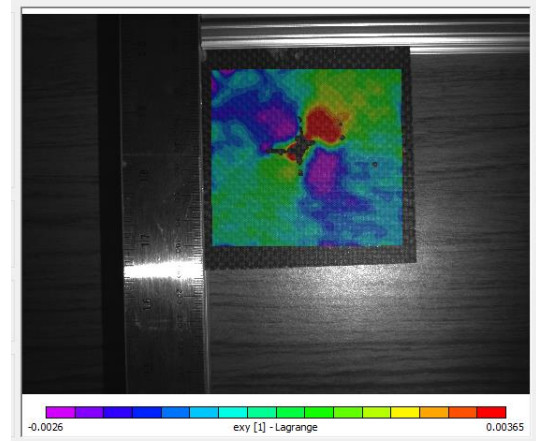
Back Inside – Eyy



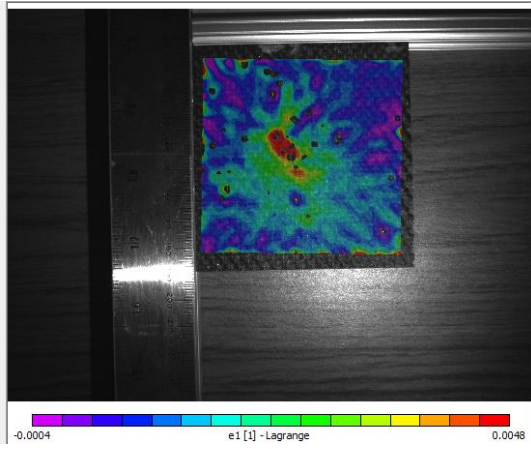
Front Inside – Exy



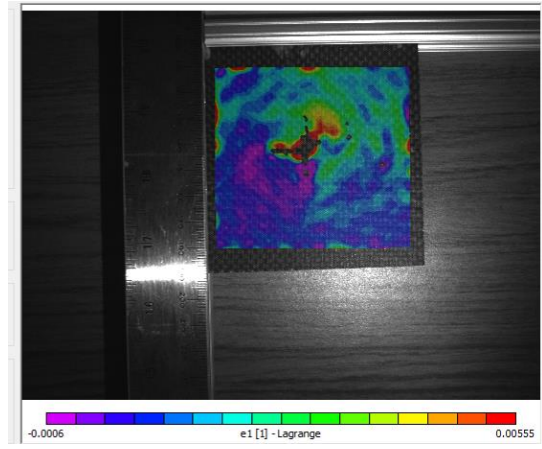
Back Inside – Exy



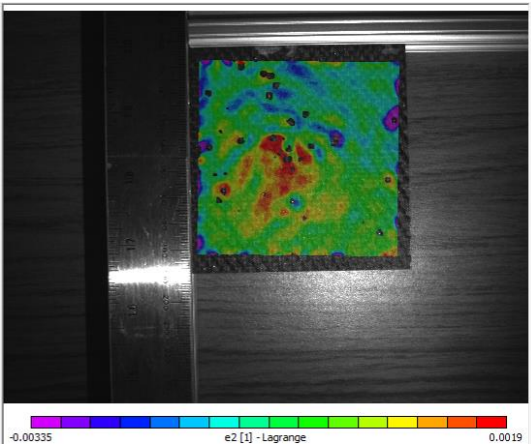
Front Inside – E1



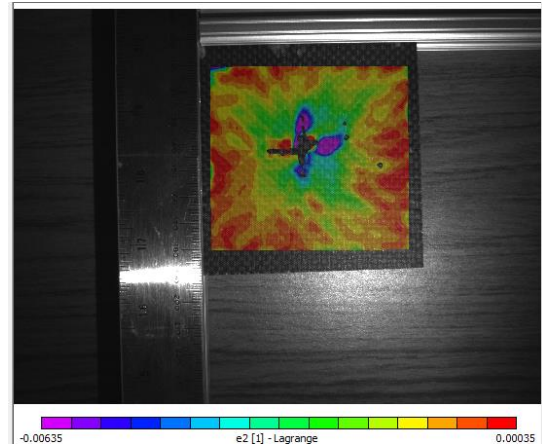
Back Inside – E1



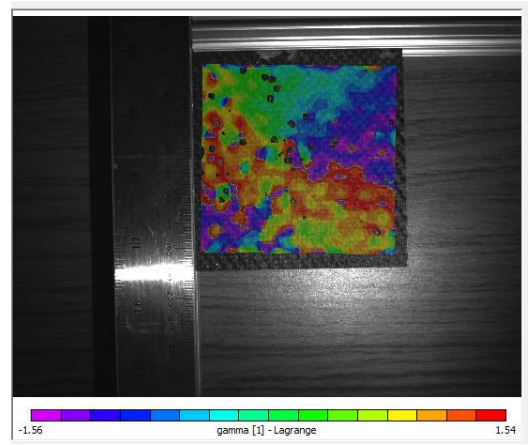
Front Inside – E2



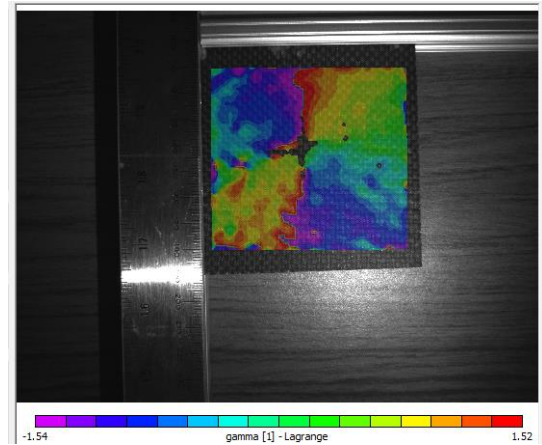
Back Inside – E2



Front Inside – Gamma

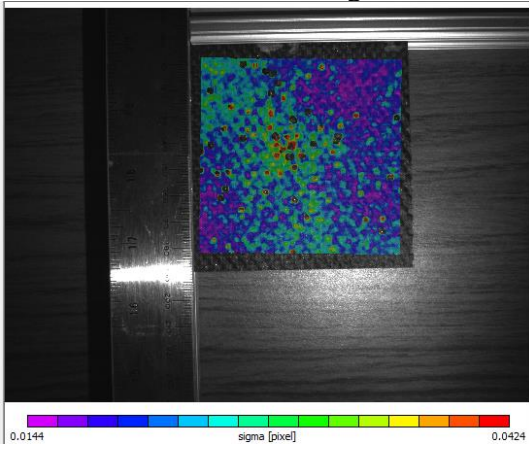


Back Inside – Gamma

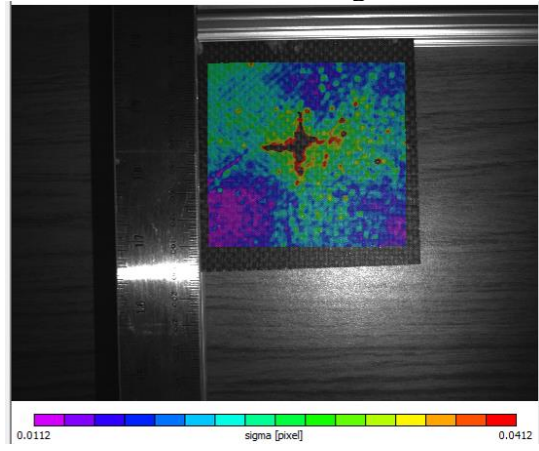




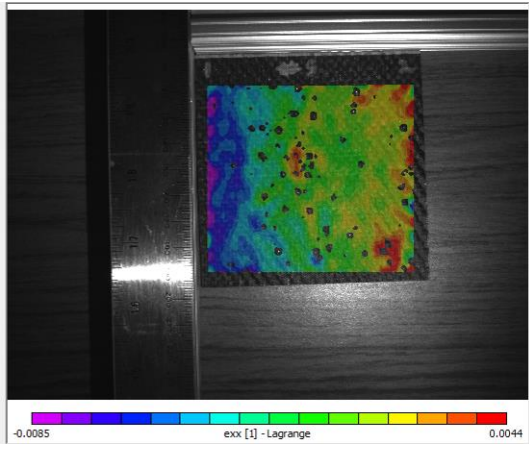
Front Inside – Sigma



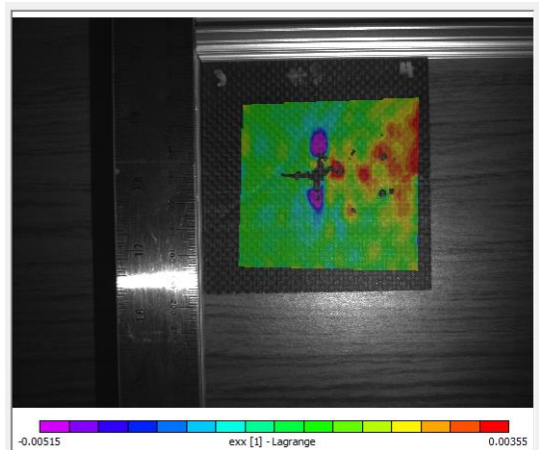
Back Inside – Sigma



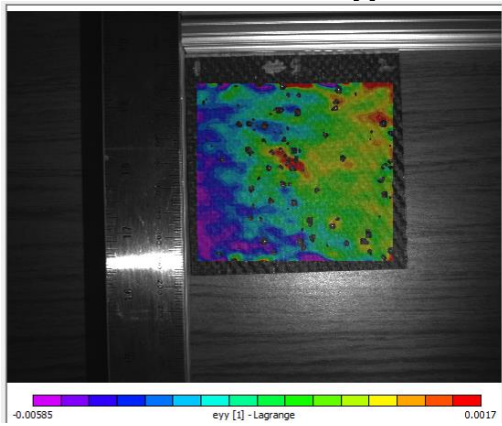
Front Outside -Exx



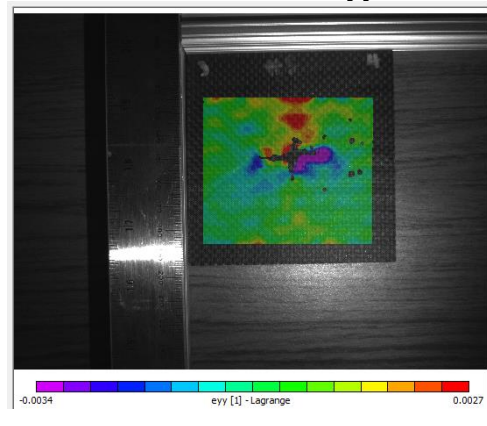
Back Outside – Exx



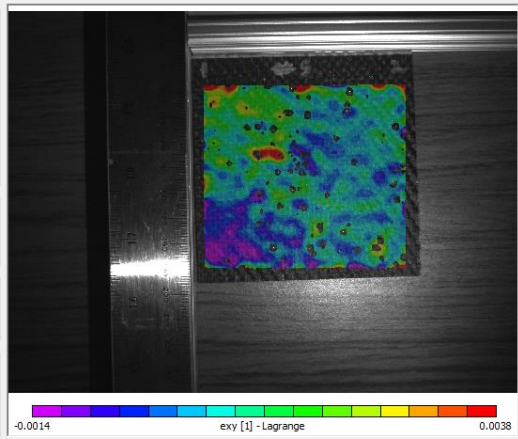
Front Outside – Eyy



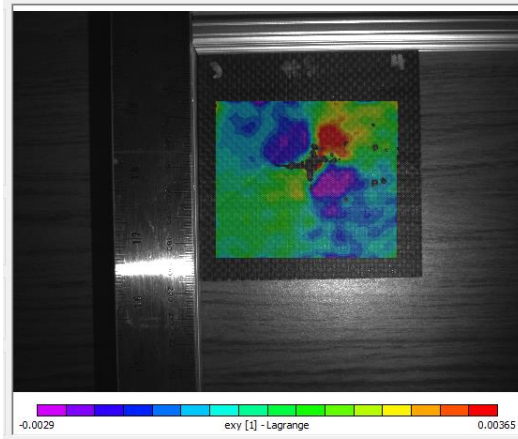
Back Outside – Eyy



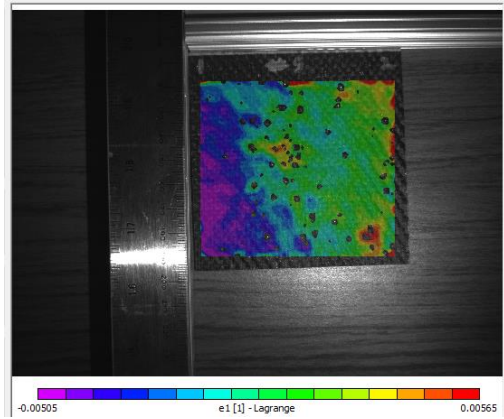
Front Outside – Exy



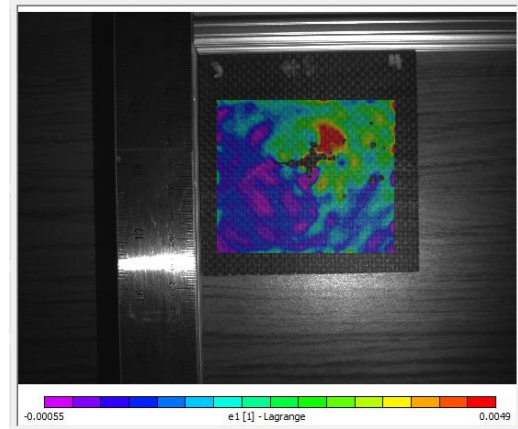
Back Outside – Exy



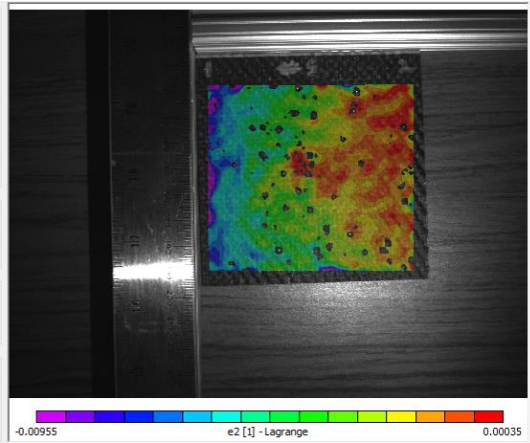
Front Outside – E1



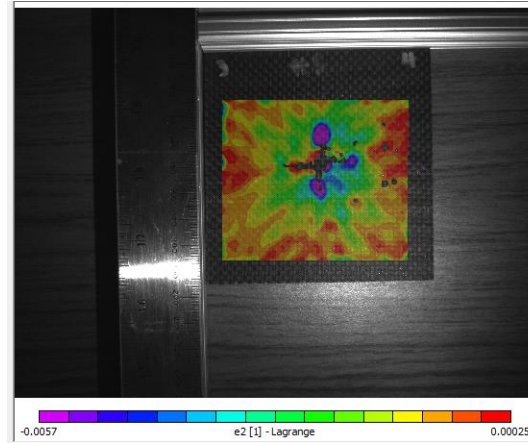
Back Outside – E1



Front Outside – E2

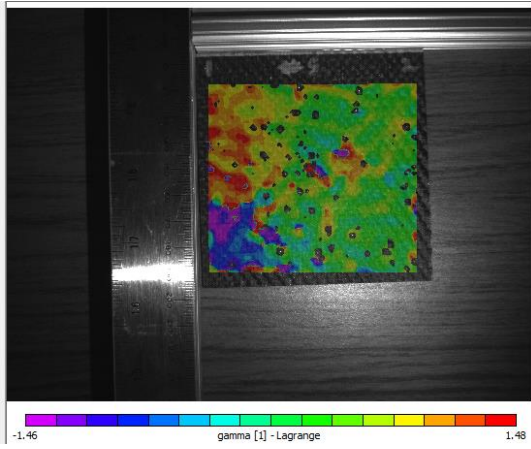


Back Outside – E2

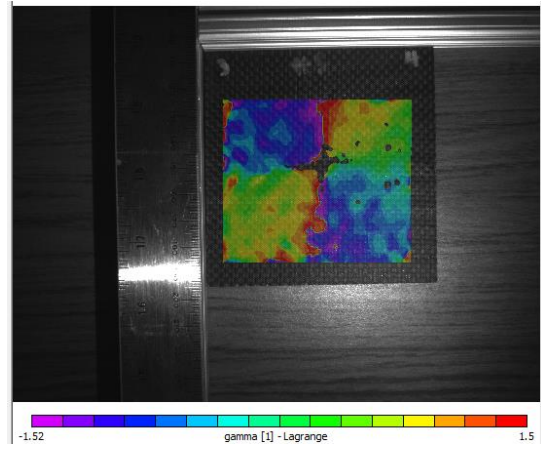




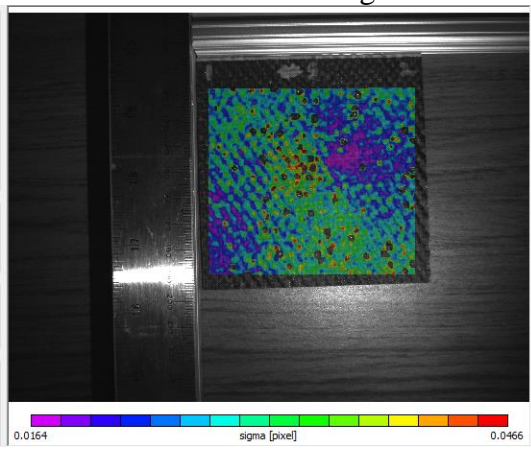
Front Outside – Gamma



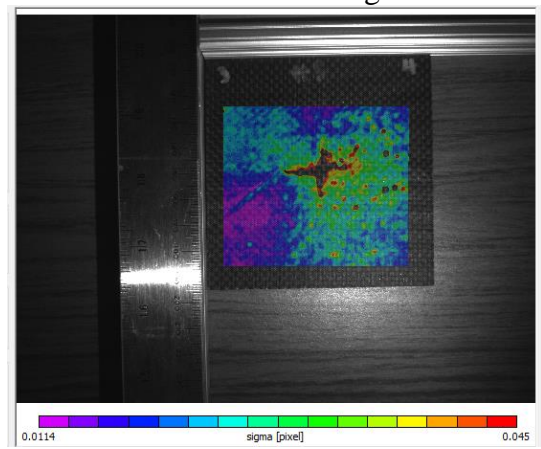
Back Outside – Gamma



Front Outside – Sigma

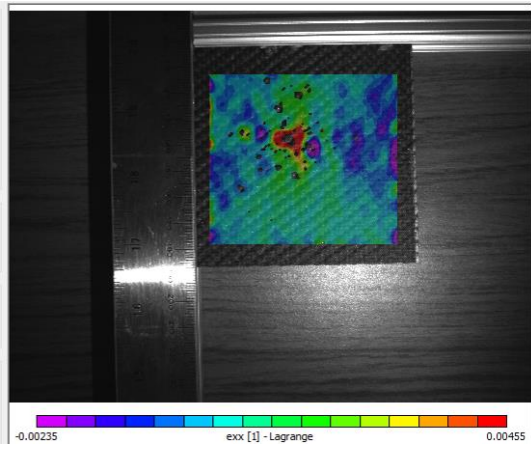


Back Outside – Sigma

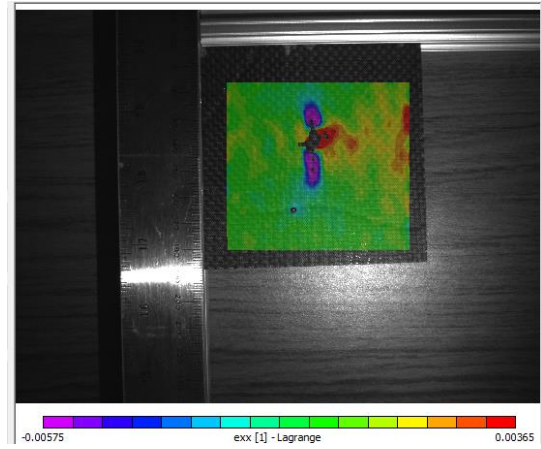


Sample 6 – First Impact 10J – 2 in diameter head with center impact

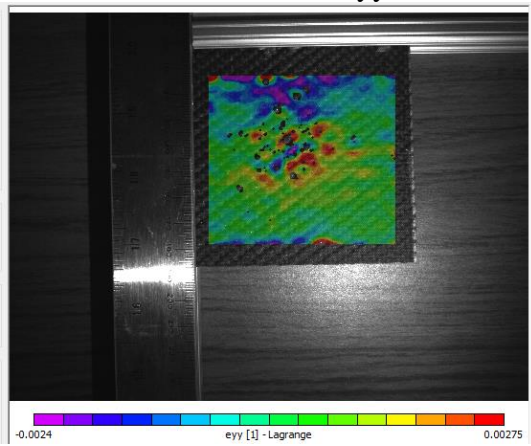
Front Inside – Exx



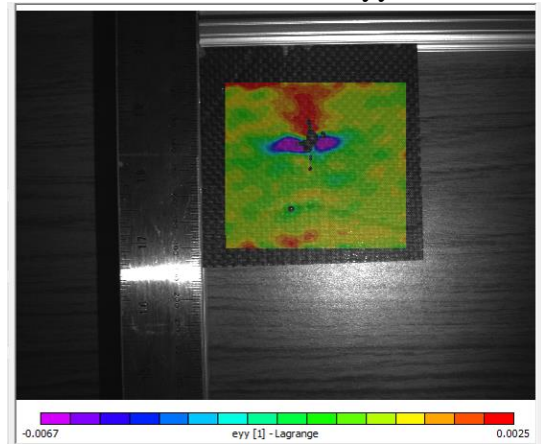
Back Inside – Exx



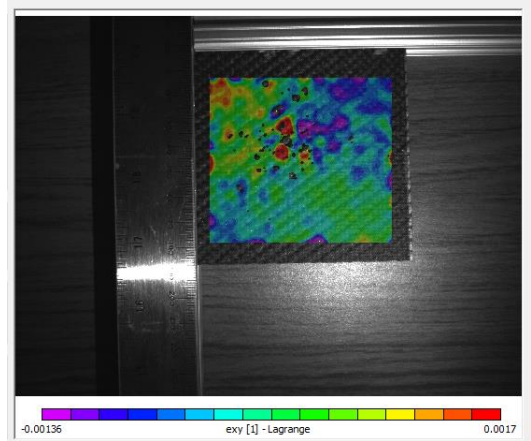
Front Inside – Eyy



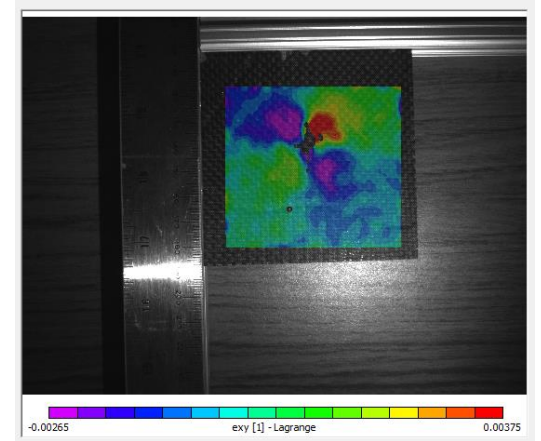
Back Inside – Eyy



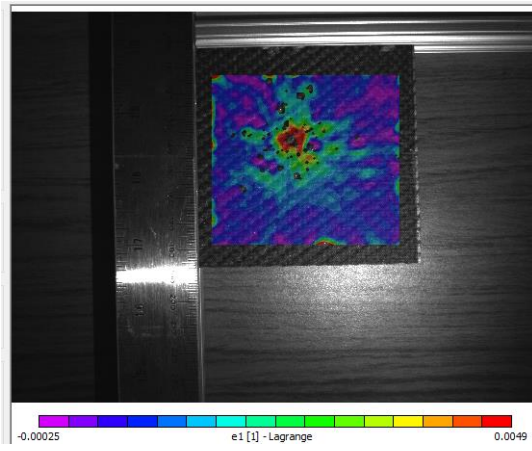
Front Inside – Exy



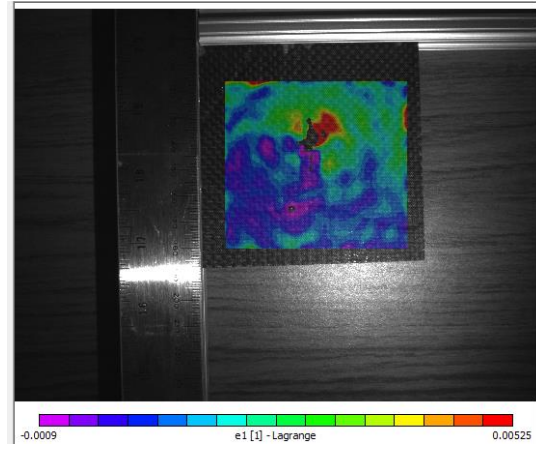
Back Inside – Exy



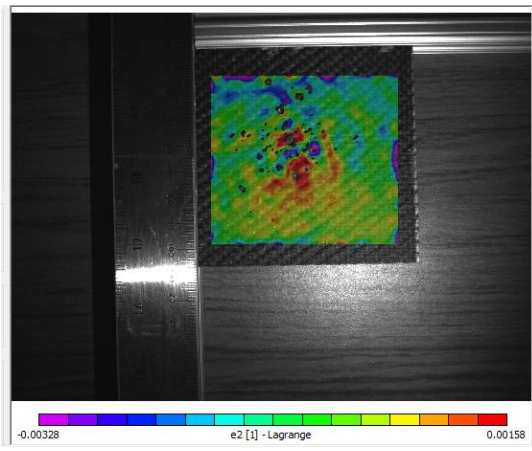
Front Inside – E1



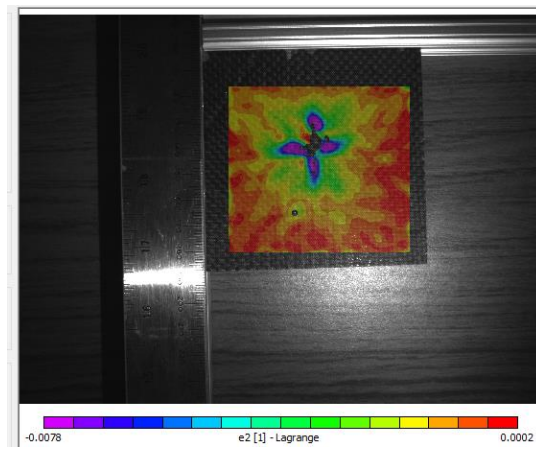
Back Inside – E1



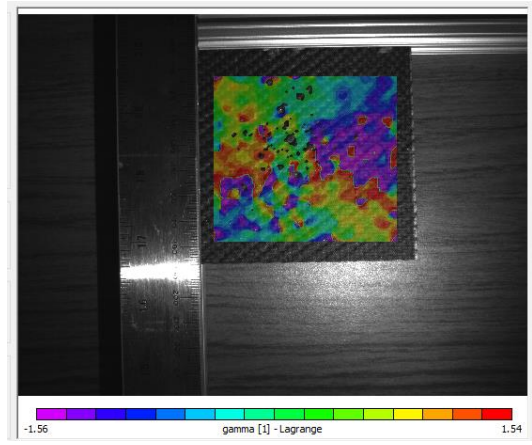
Front Inside – E2



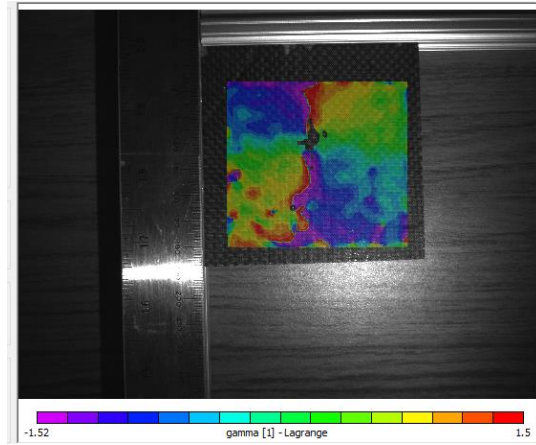
Back Inside – E2



Front Inside – Gamma

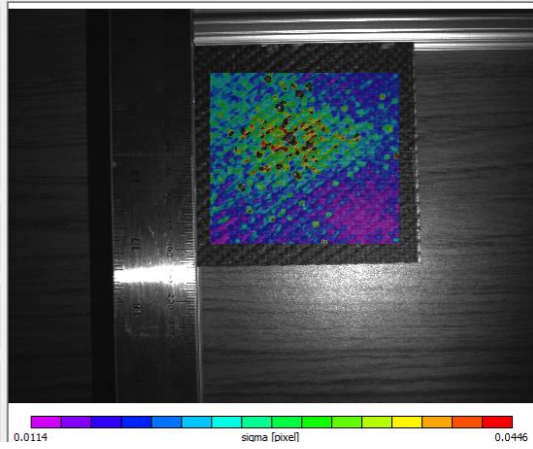


Back Inside – Gamma

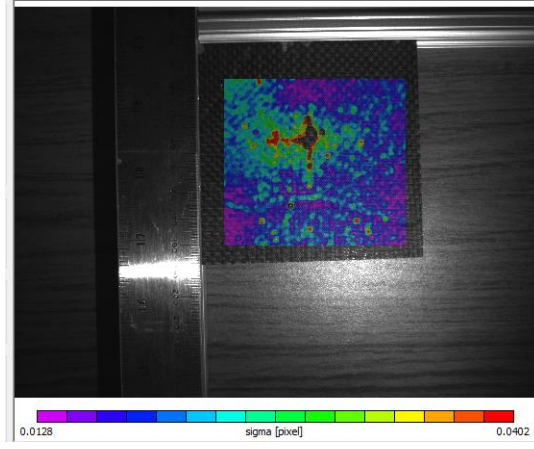




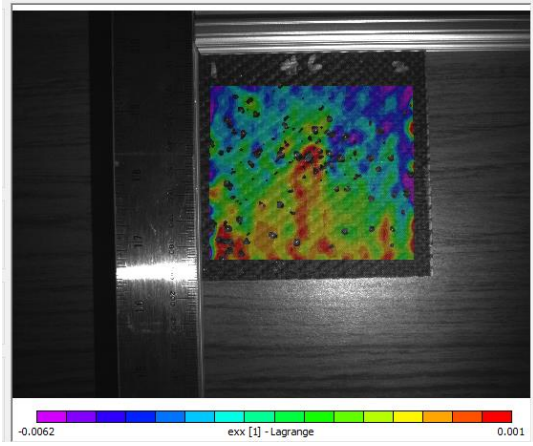
Front Inside – Sigma



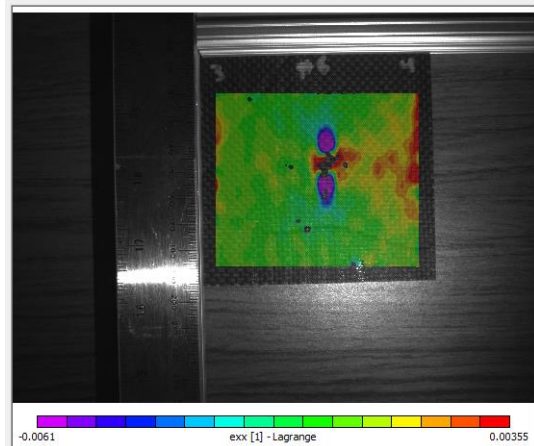
Back Inside – Sigma



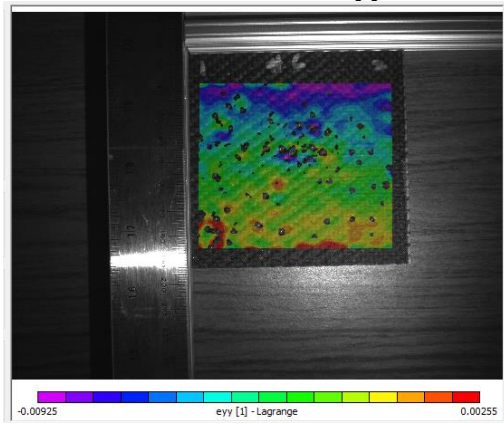
Front Outside -Exx



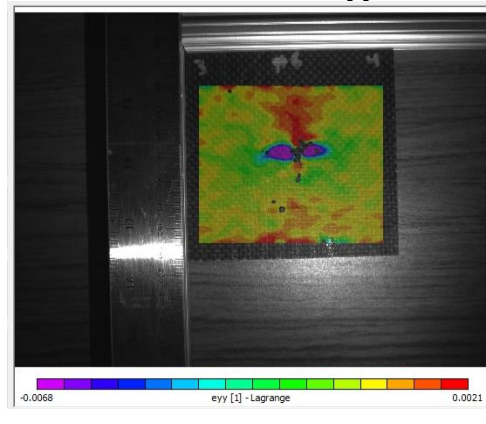
Back Outside – Exx



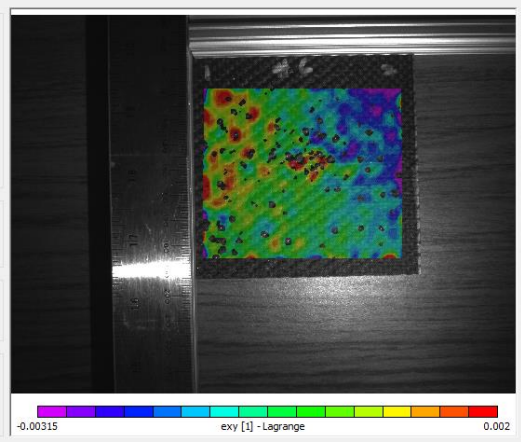
Front Outside – Eyy



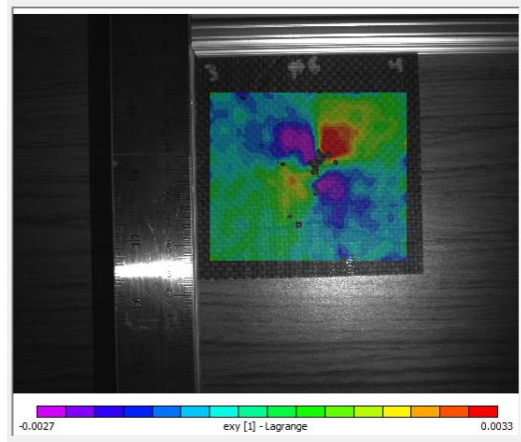
Back Outside – Eyy



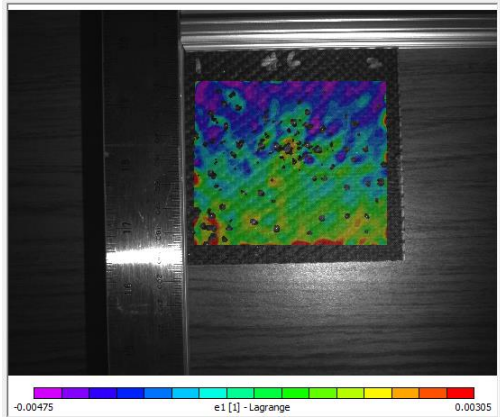
Front Outside – Exy



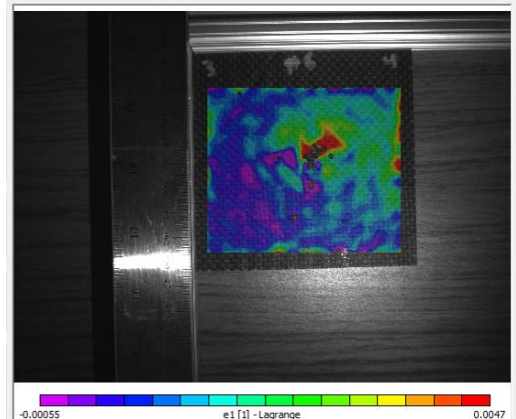
Back Outside – Exy



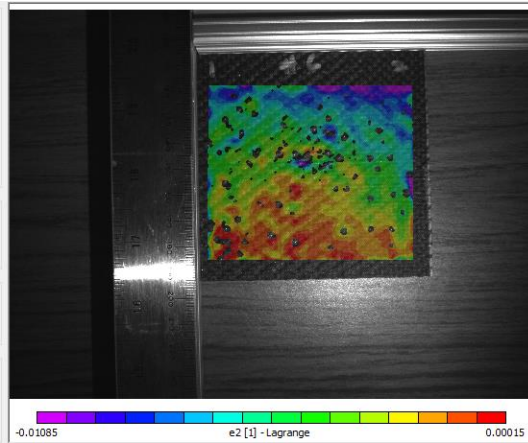
Front Outside – E1



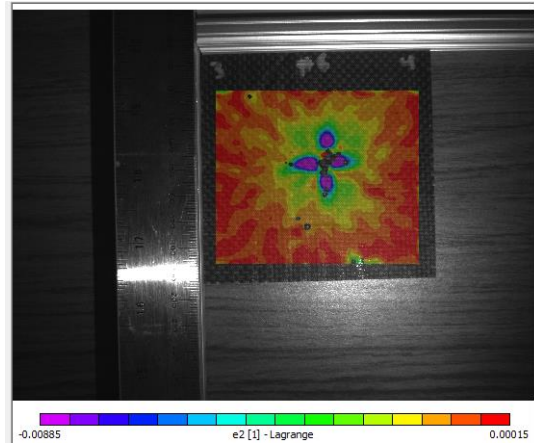
Back Outside – E1



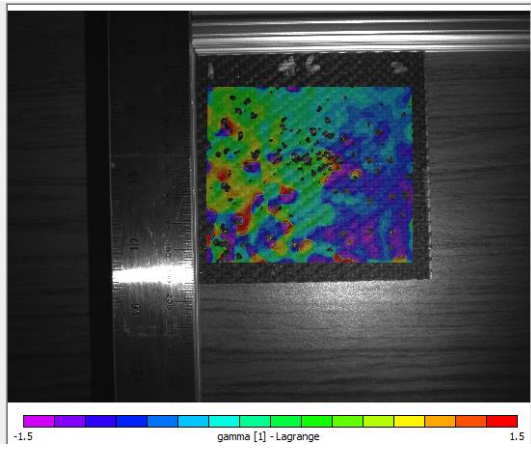
Front Outside – E2



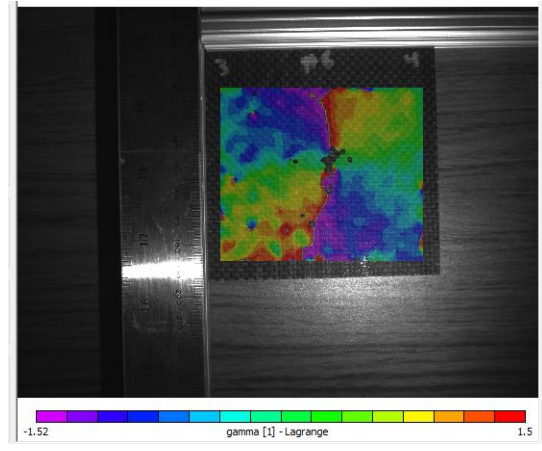
Back Outside – E2



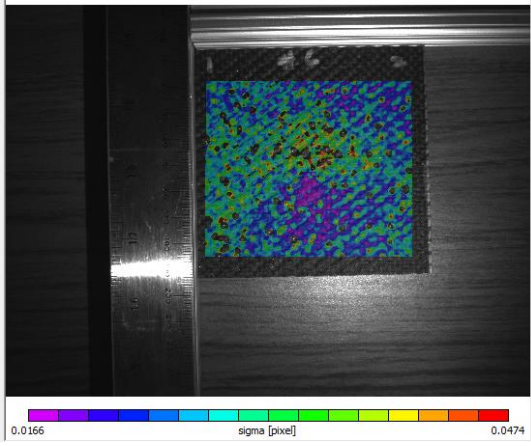
Front Outside – Gamma



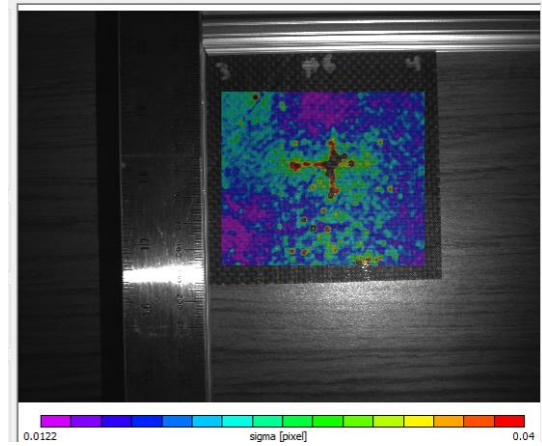
Back Outside – Gamma



Front Outside – Sigma



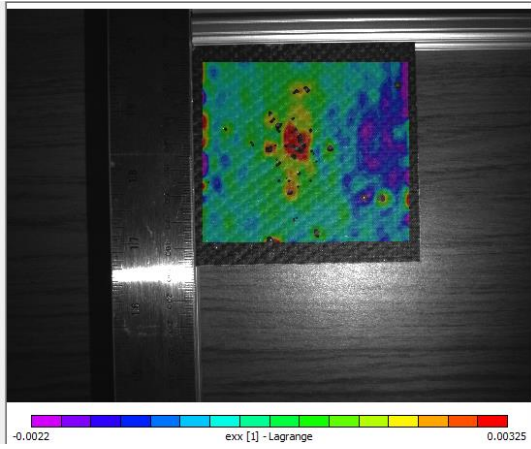
Back Outside – Sigma



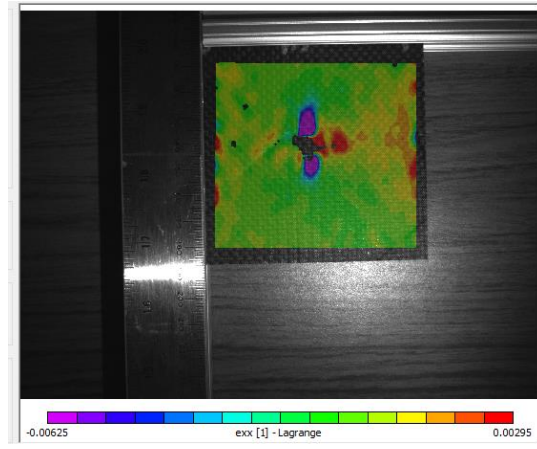


Sample 7– First Impact 10J – 2 in diameter head with center impact

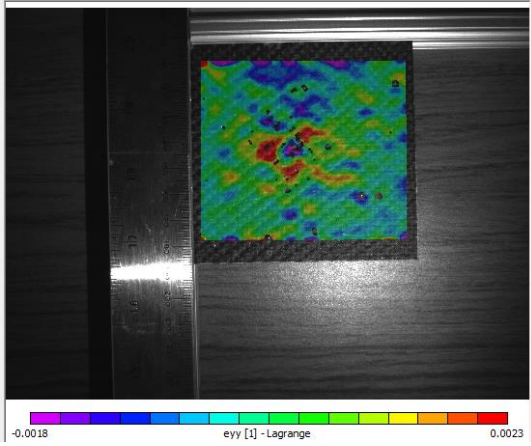
Front Inside – Exx



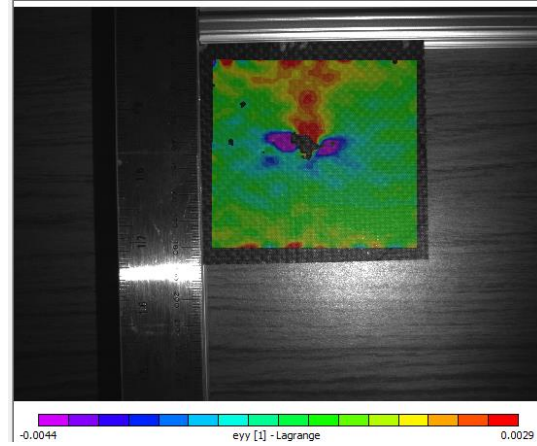
Back Inside – Exx



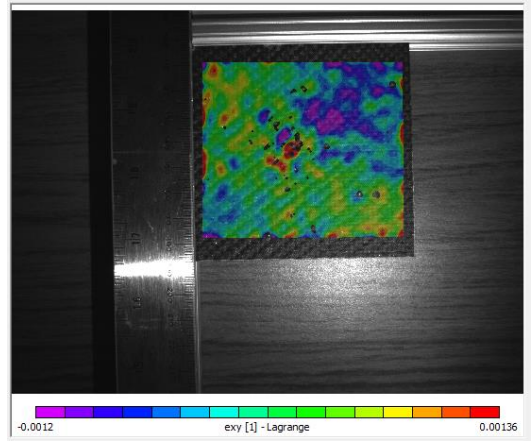
Front Inside – Eyy



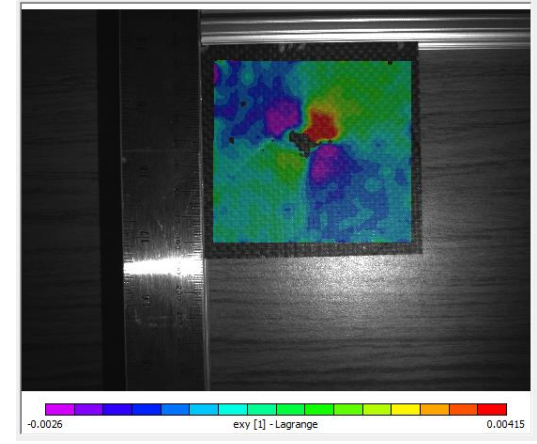
Back Inside – Eyy



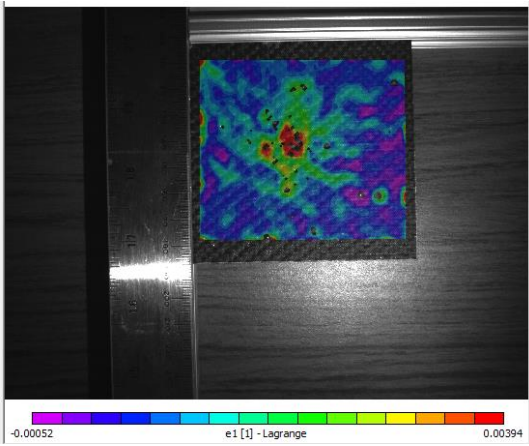
Front Inside – Exy



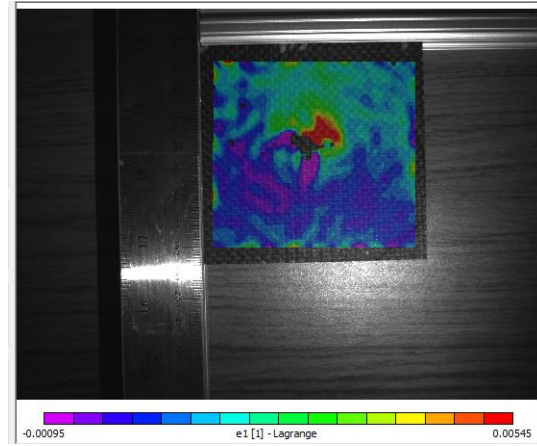
Back Inside – Exy



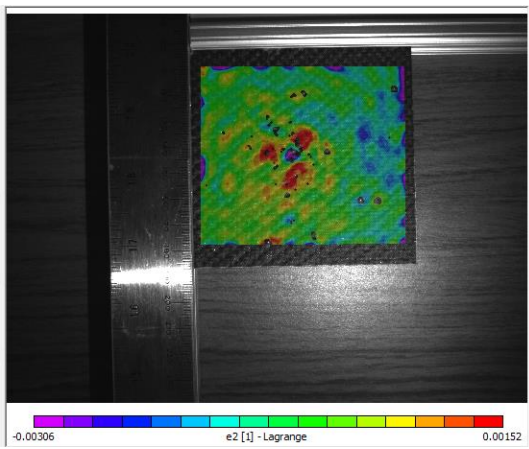
Front Inside – E1



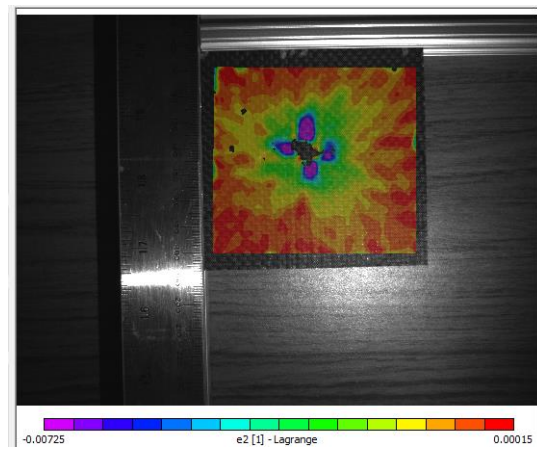
Back Inside – E1



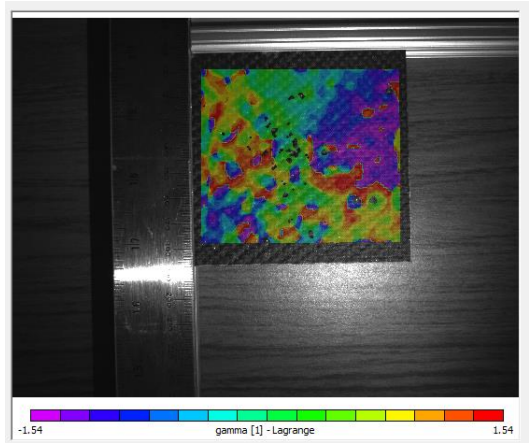
Front Inside – E2



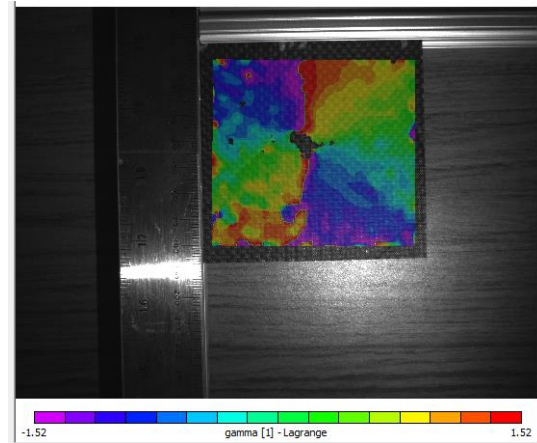
Back Inside – E2



Front Inside – Gamma

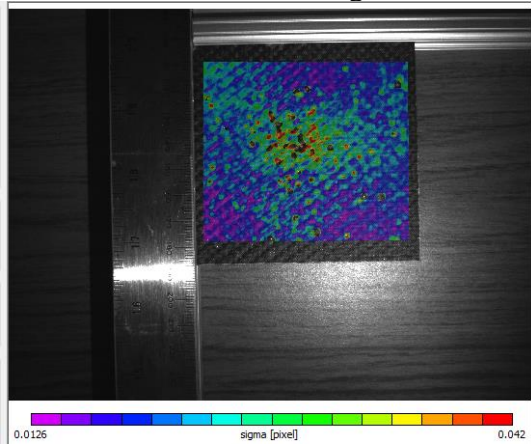


Back Inside – Gamma

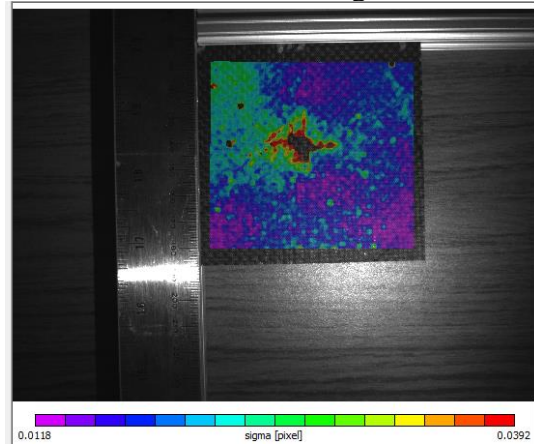




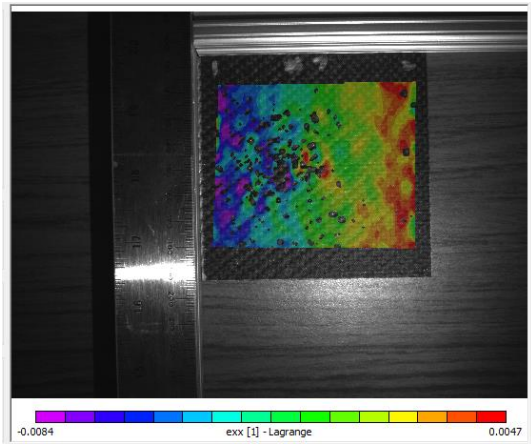
Front Inside – Sigma



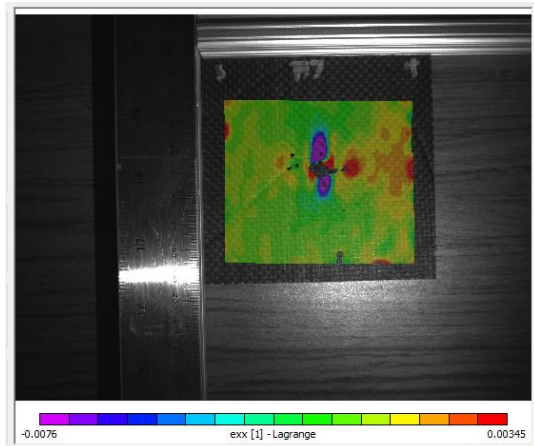
Back Inside – Sigma



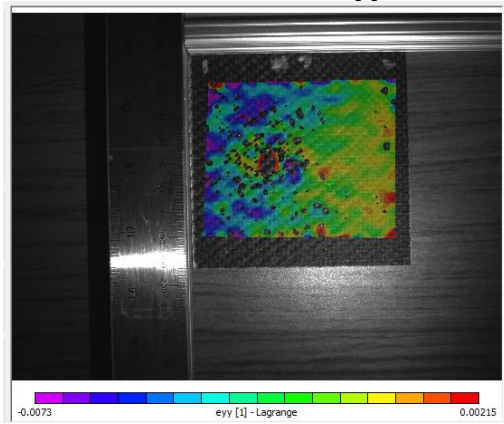
Front Outside -Exx



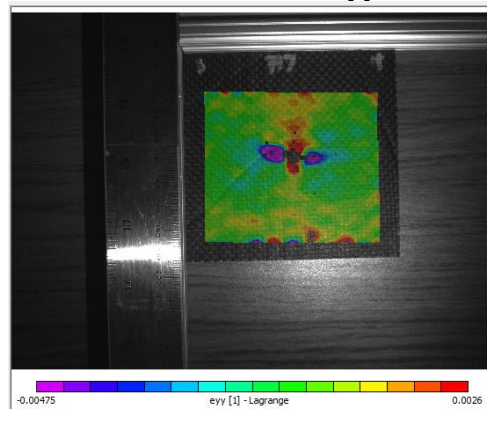
Back Outside – Exx



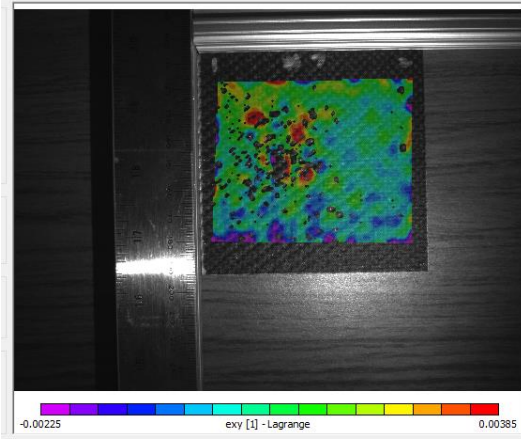
Front Outside – Eyy



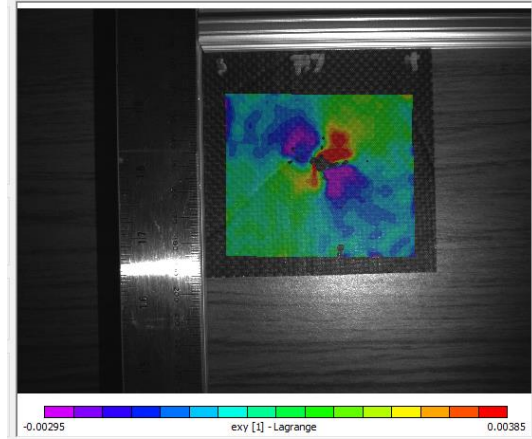
Back Outside – Eyy



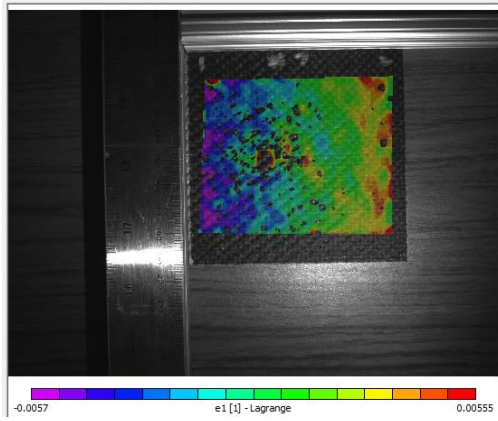
Front Outside – Exy



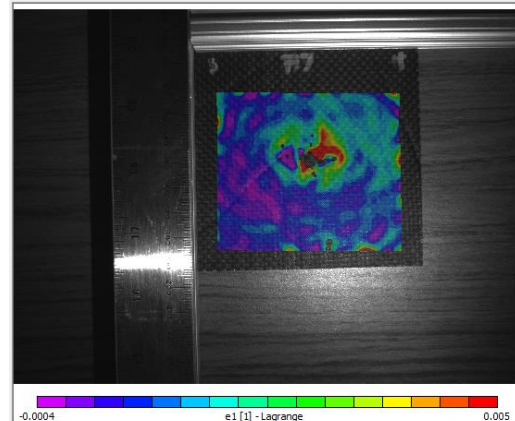
Back Outside – Exy



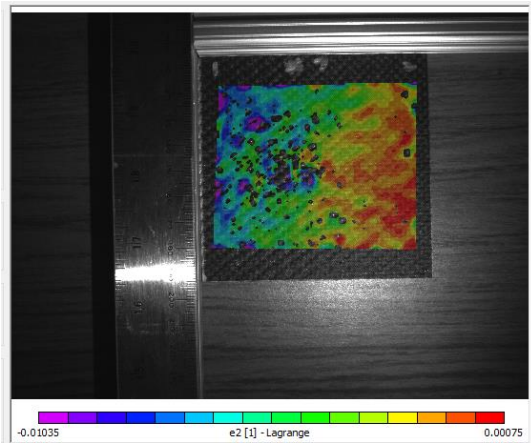
Front Outside – E1



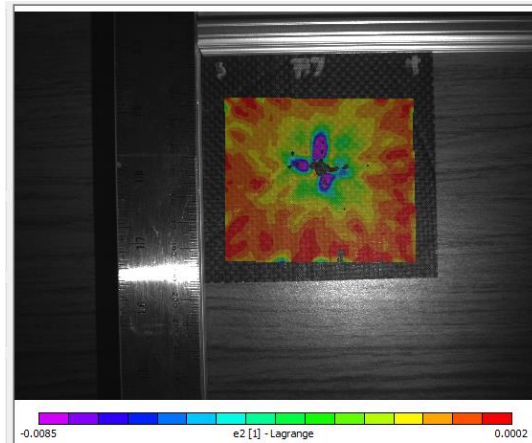
Back Outside – E1



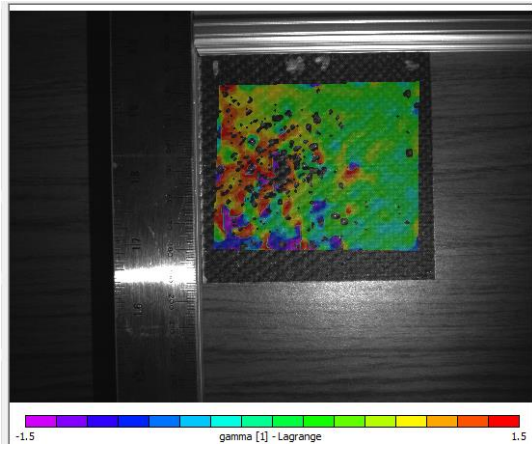
Front Outside – E2



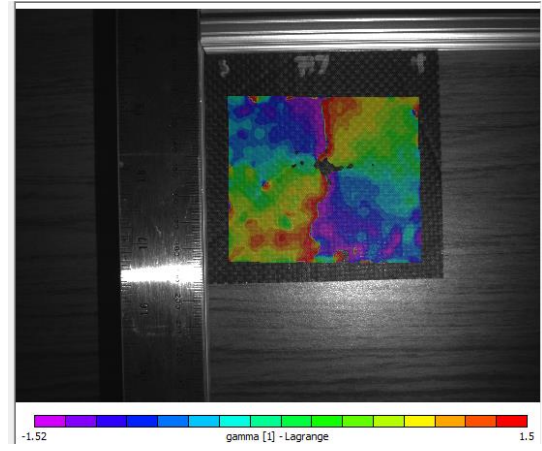
Back Outside – E2



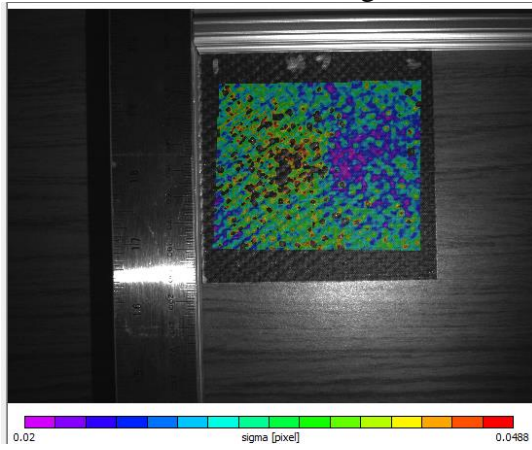
Front Outside – Gamma



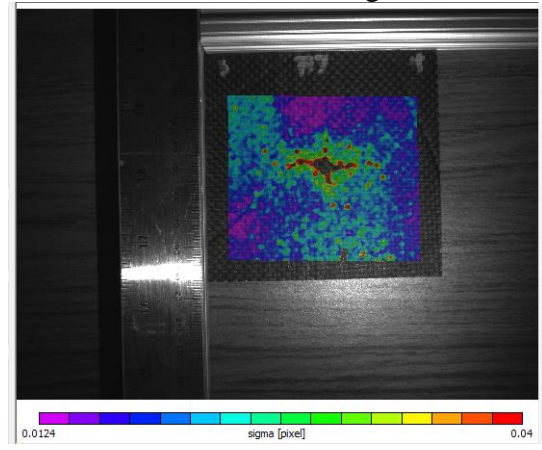
Back Outside – Gamma



Front Outside – Sigma



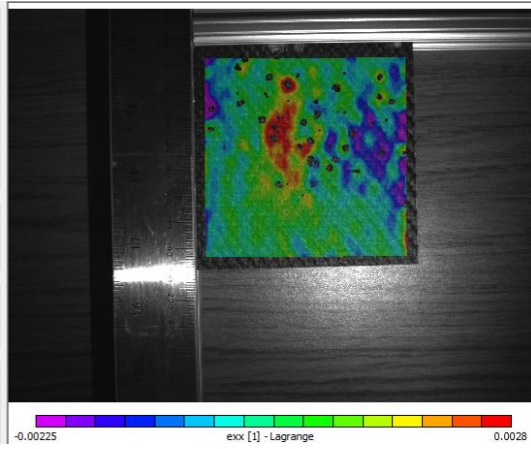
Back Outside – Sigma



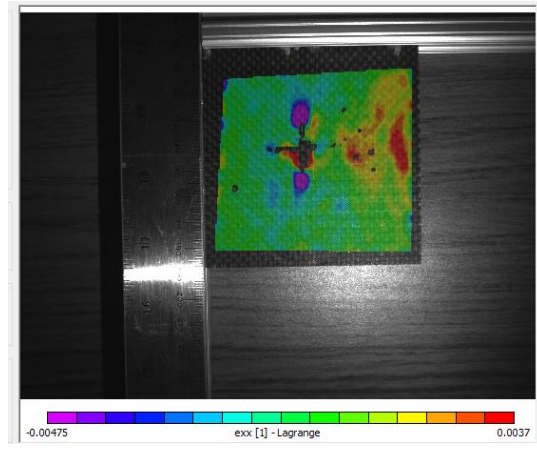


Sample 8 – First Impact 10J – 2 in diameter head with center impact

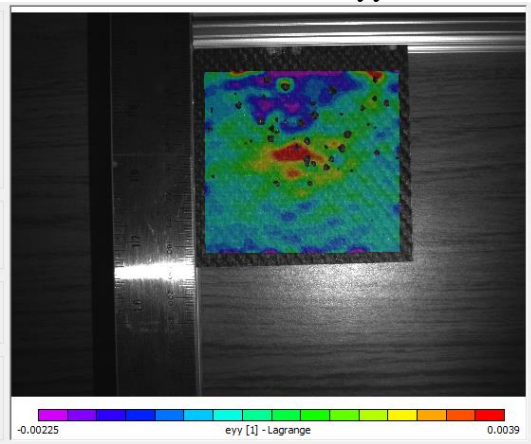
Front Inside – Exx



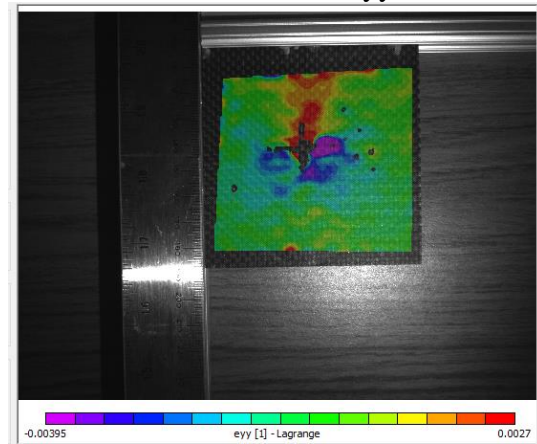
Back Inside – Exx



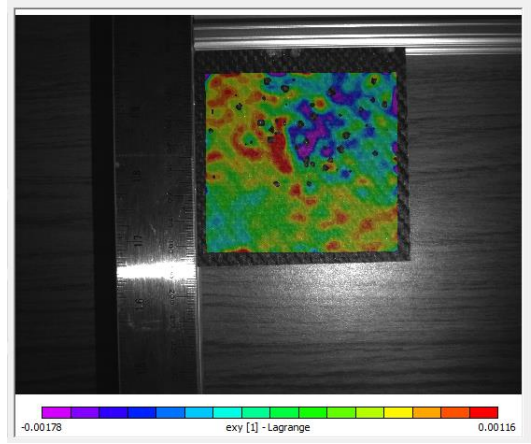
Front Inside – Eyy



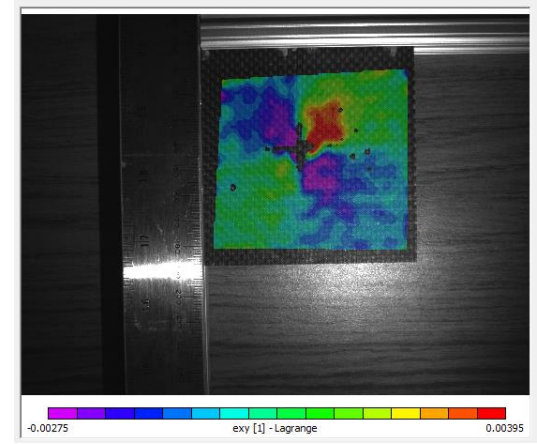
Back Inside – Eyy



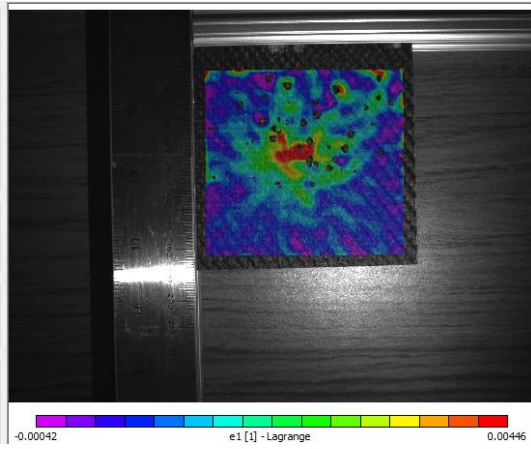
Front Inside – Exy



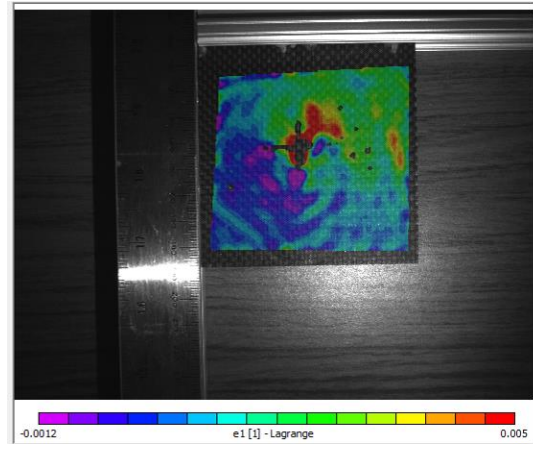
Back Inside – Exy



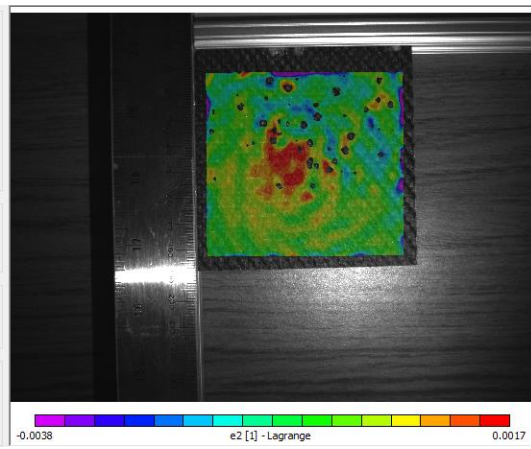
Front Inside – E1



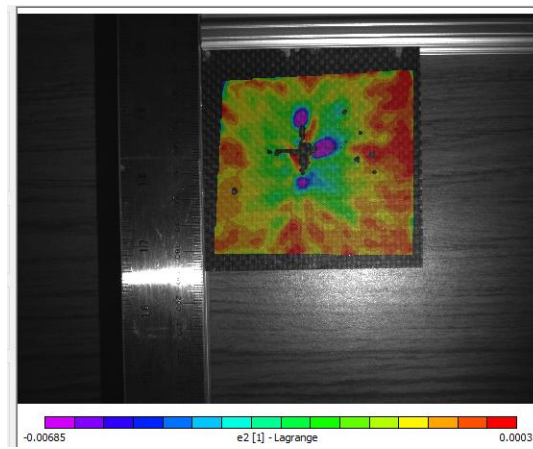
Back Inside – E1



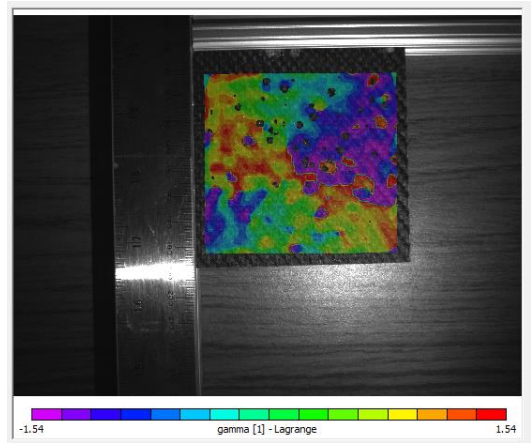
Front Inside – E2



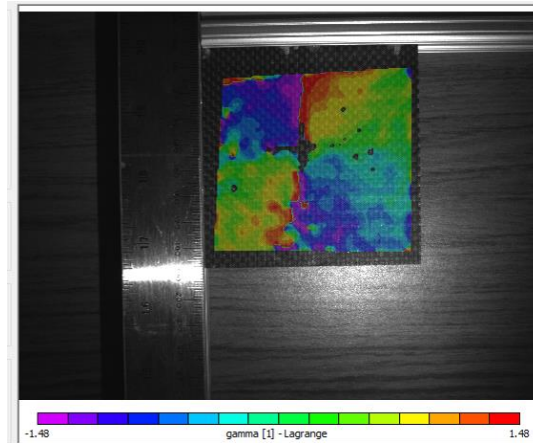
Back Inside – E2



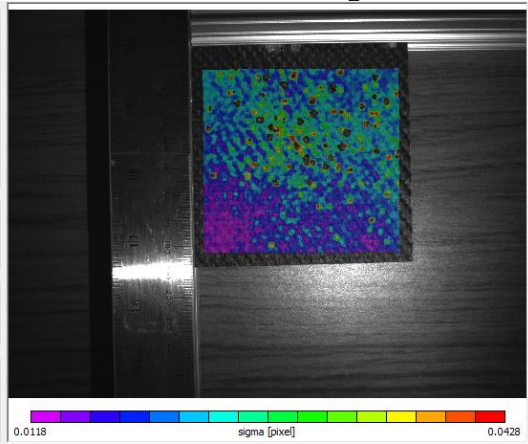
Front Inside – Gamma



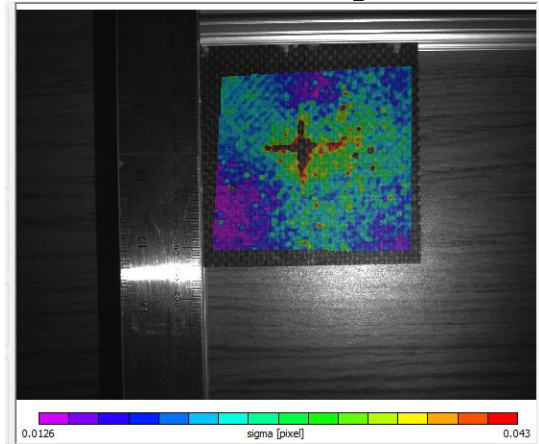
Back Inside – Gamma



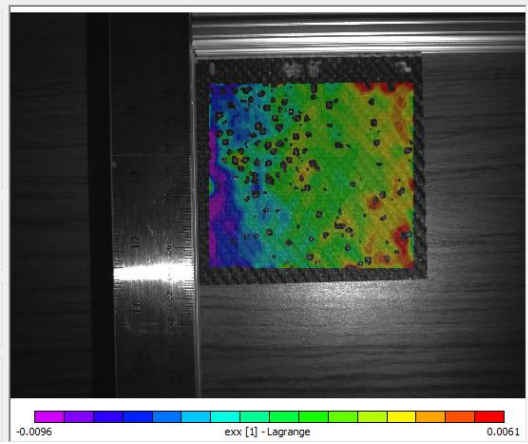
Front Inside – Sigma



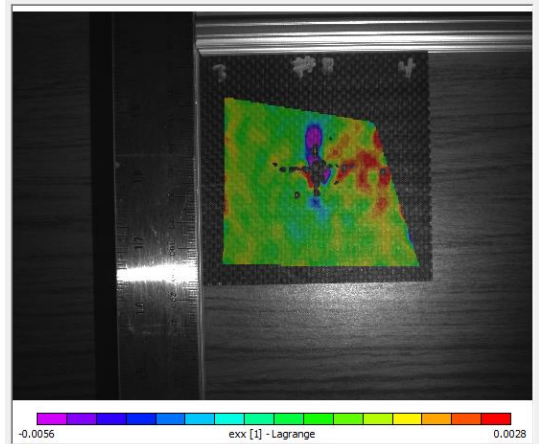
Back Inside – Sigma



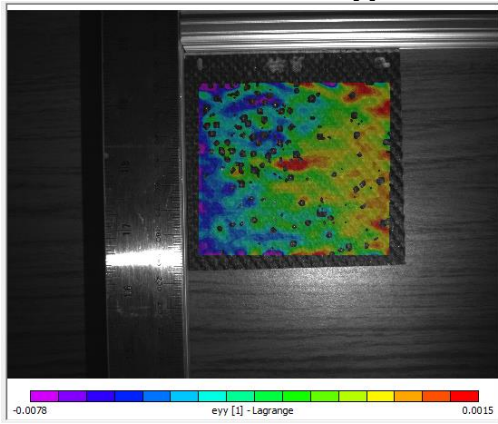
Front Outside -Exx



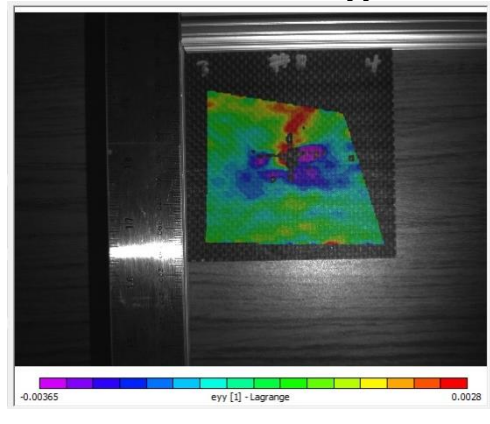
Back Outside – Exx



Front Outside – Eyy

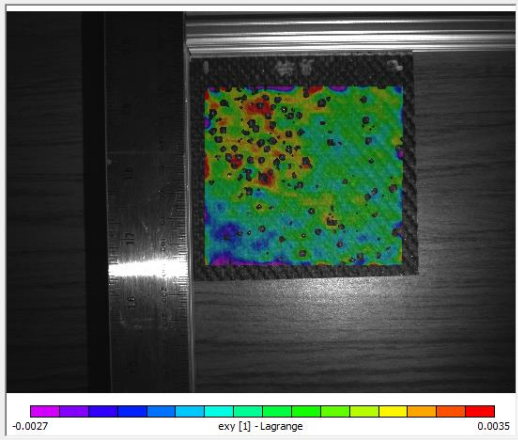


Back Outside – Eyy

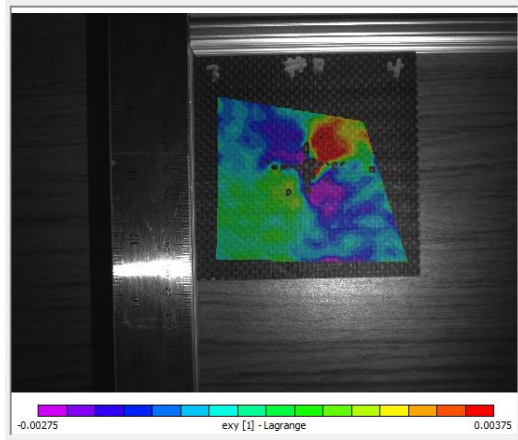




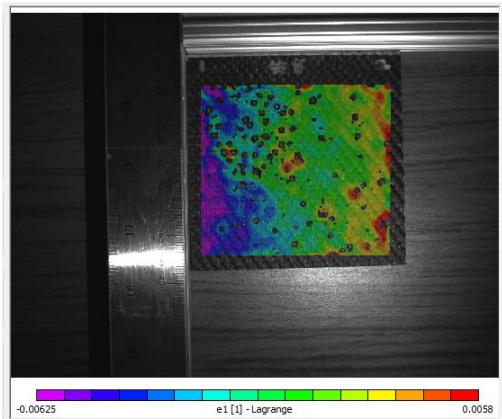
Front Outside – Exy



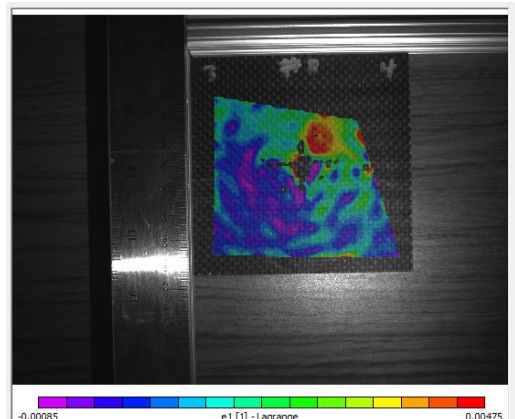
Back Outside – Exy



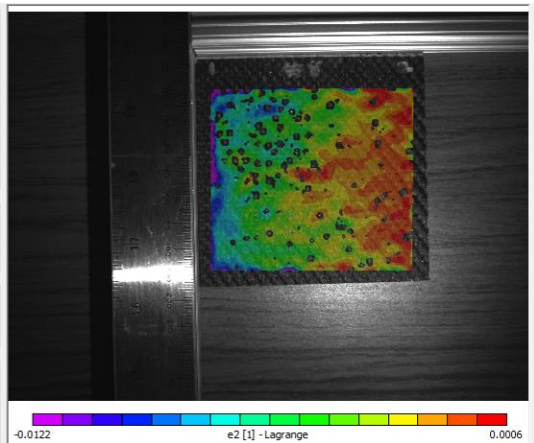
Front Outside – E1



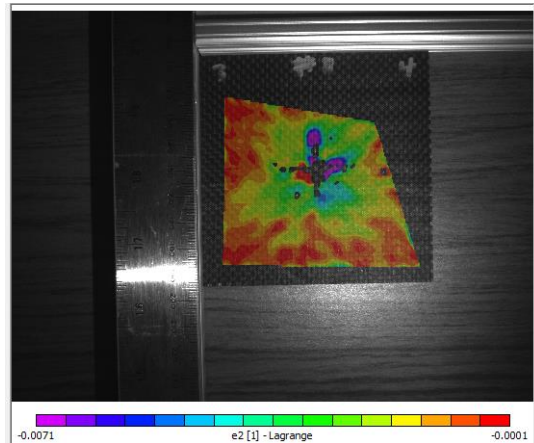
Back Outside – E1



Front Outside – E2

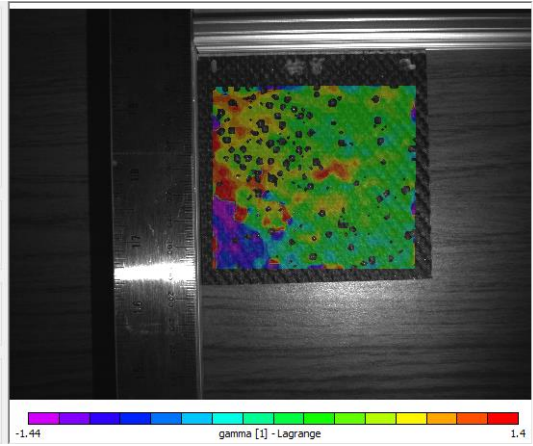


Back Outside – E2

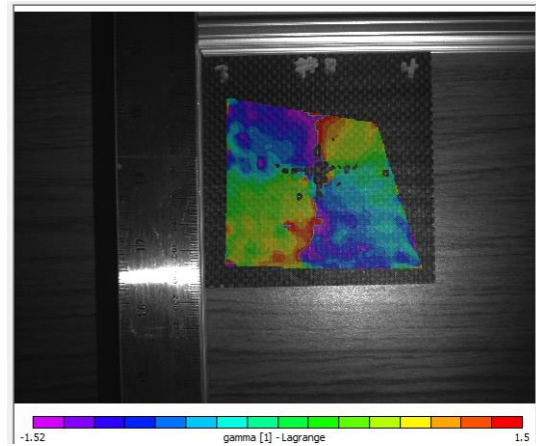




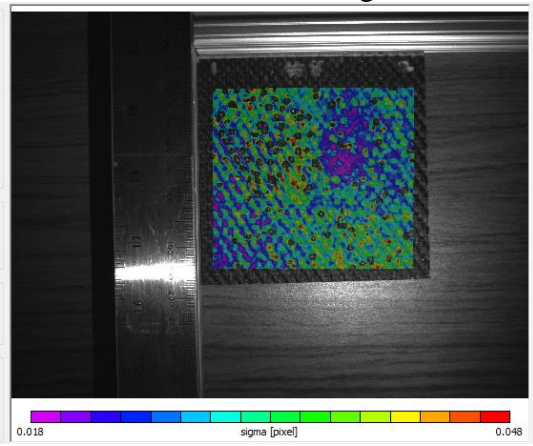
Front Outside – Gamma



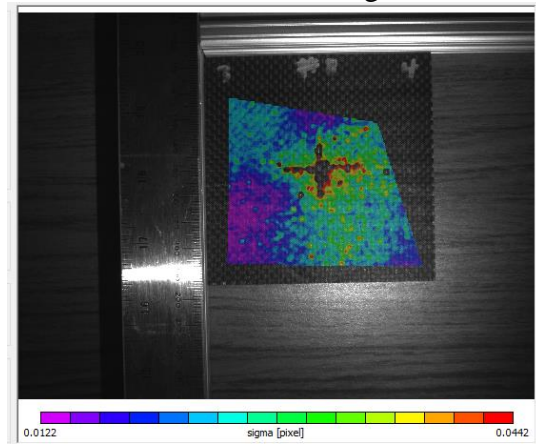
Back Outside – Gamma



Front Outside – Sigma

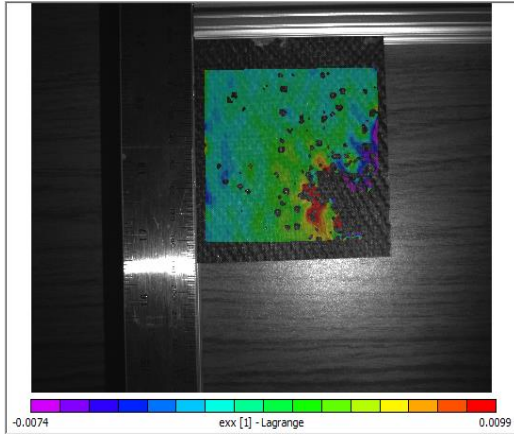


Back Outside – Sigma

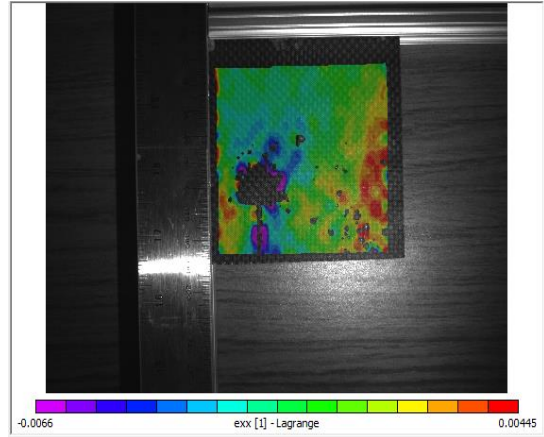


Sample 5 – Second Impact 10J – 1 in diameter head with lower right impact

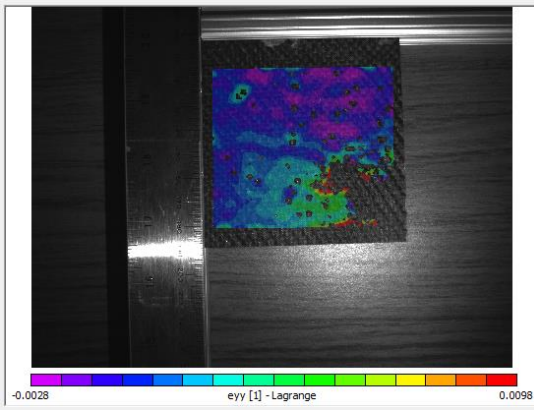
Front Inside – Exx



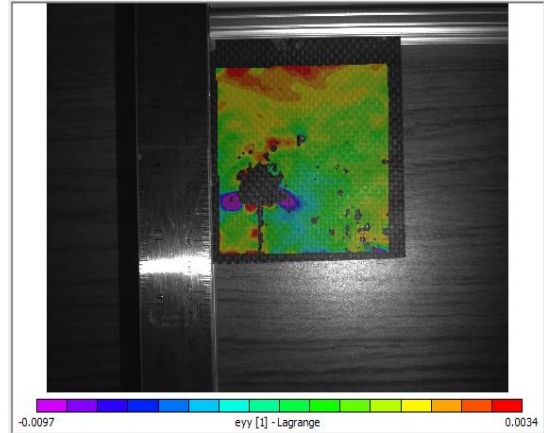
Back Inside – Exx



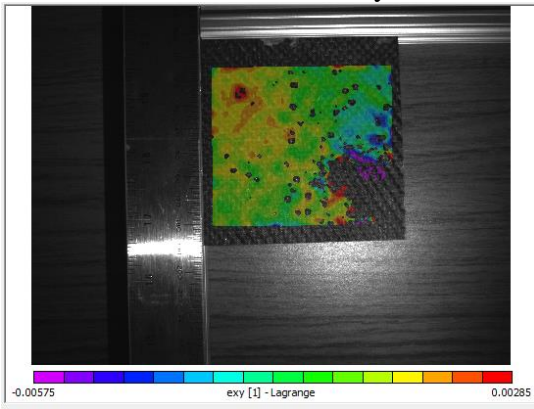
Front Inside – Eyy



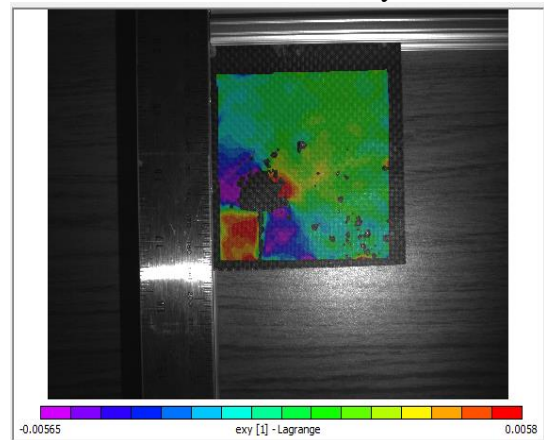
Back Inside – Eyy



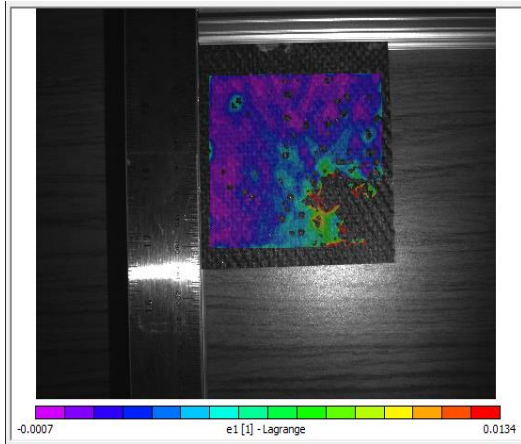
Front Inside – Exy



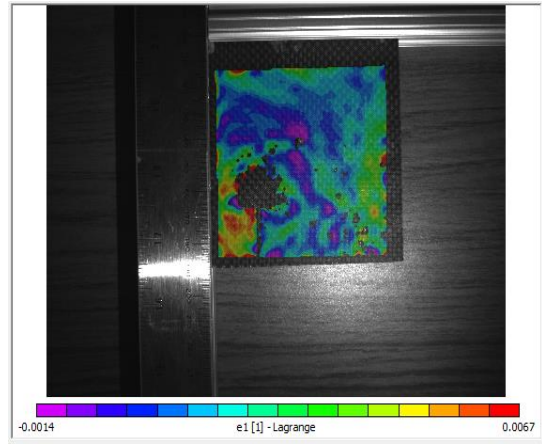
Back Inside – Exy



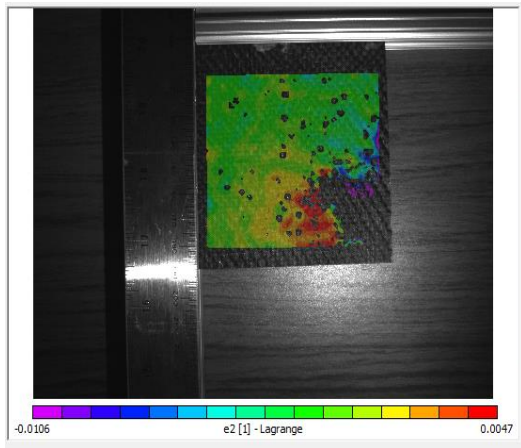
Front Inside – E1



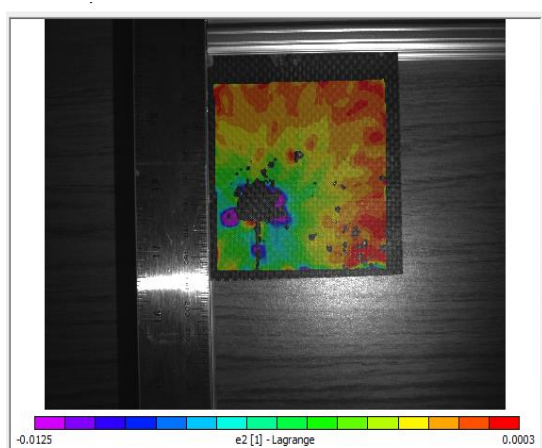
Back Inside – E1



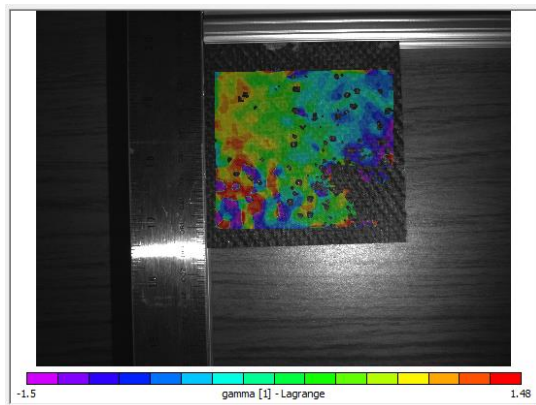
Front Inside – E2



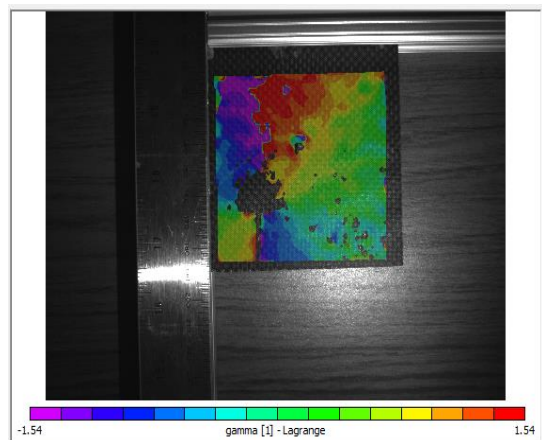
Back Inside – E2



Front Inside – Gamma

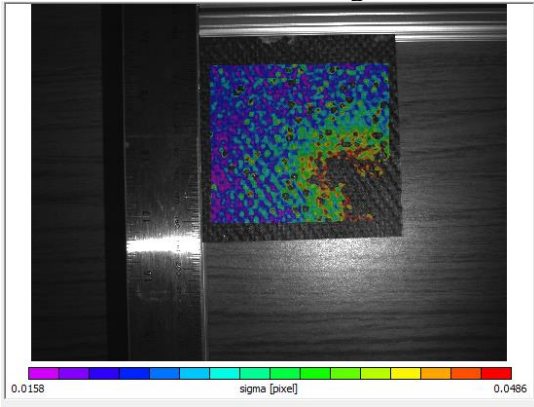


Back Inside – Gamma

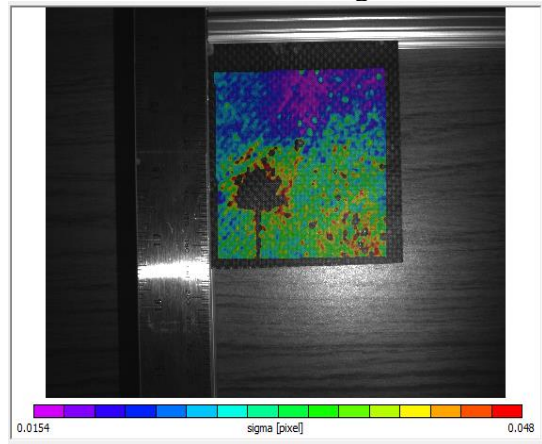




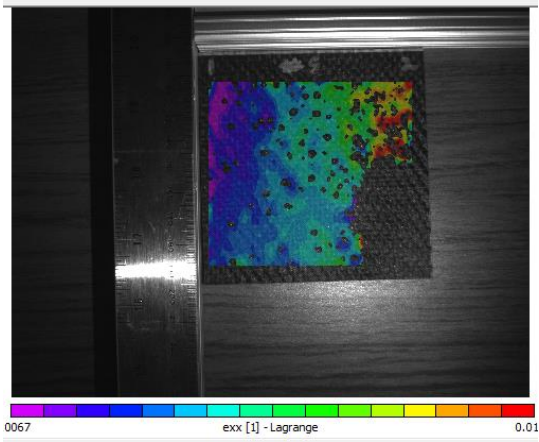
Front Inside – Sigma



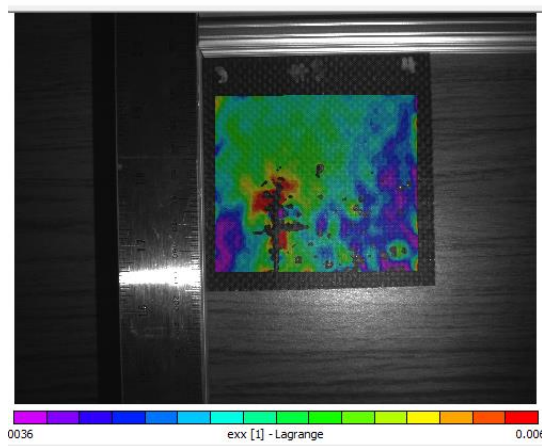
Back Inside – Sigma



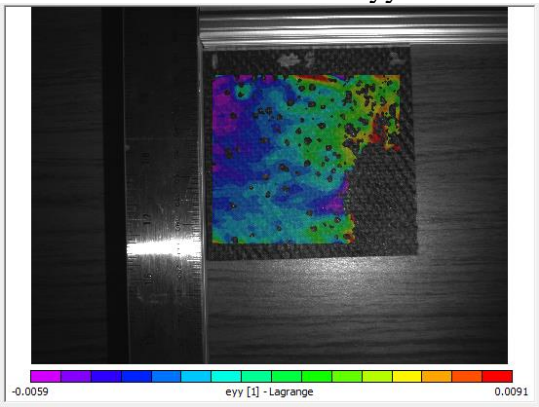
Front Outside -Exx



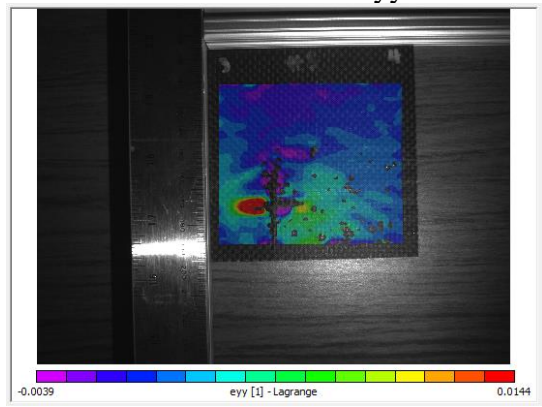
Back Outside – Exx



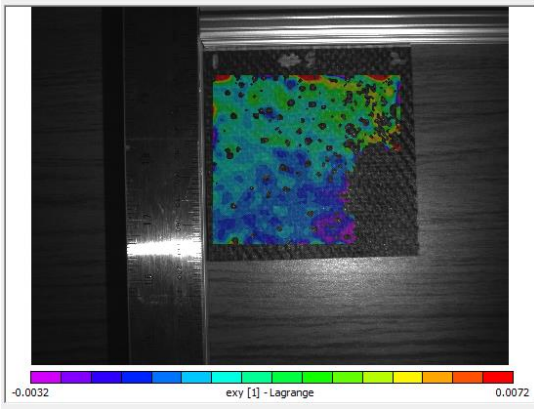
Front Outside – Eyy



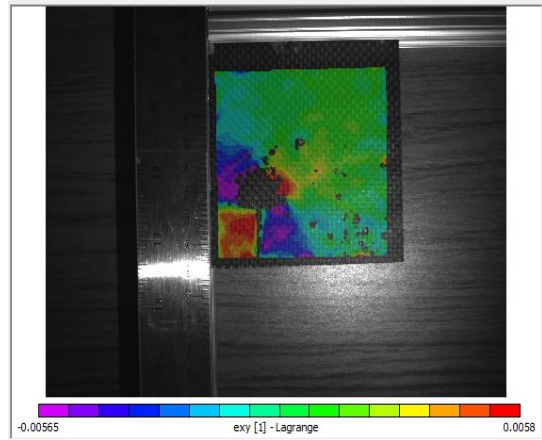
Back Outside – Eyy



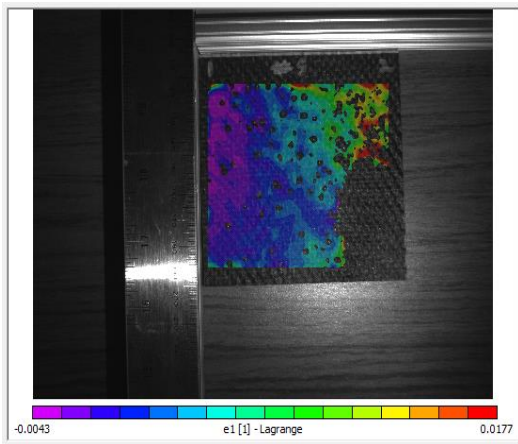
Front Outside – Exy



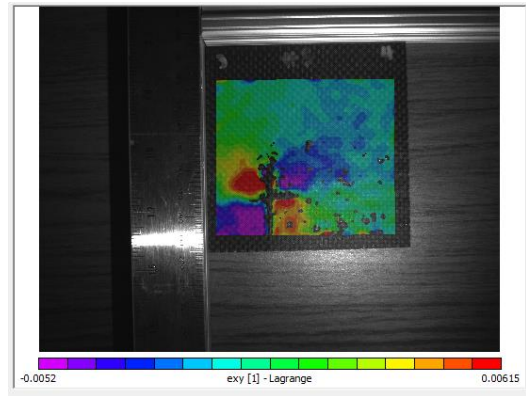
Back Outside – Exy



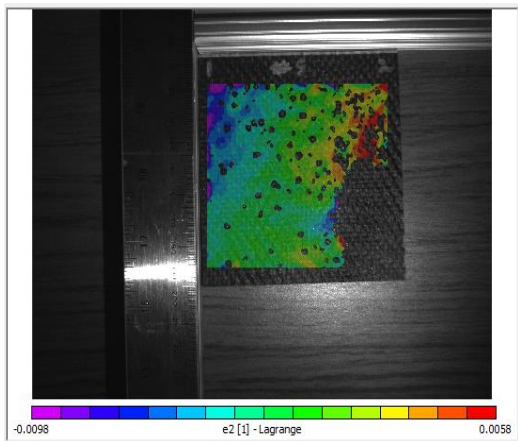
Front Outside – E1



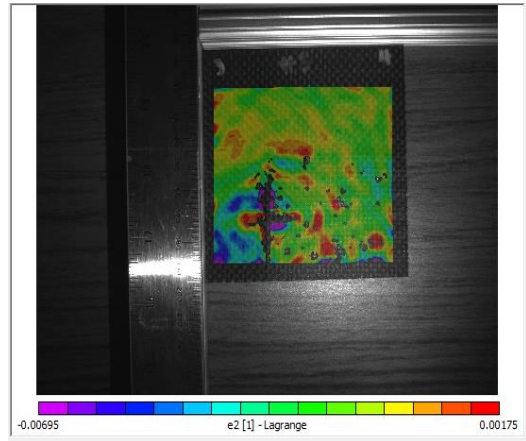
Back Outside – E1



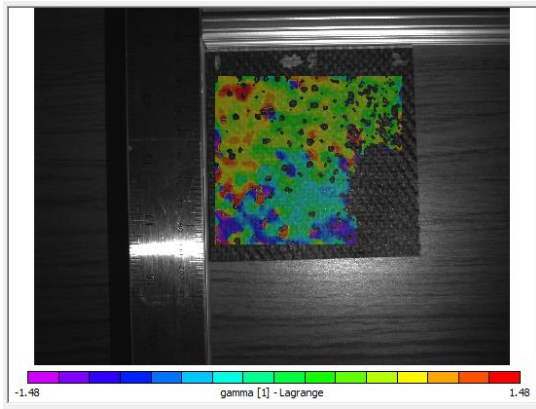
Front Outside – E2



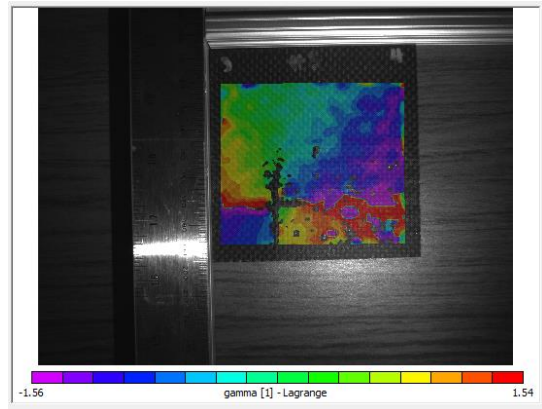
Back Outside – E2



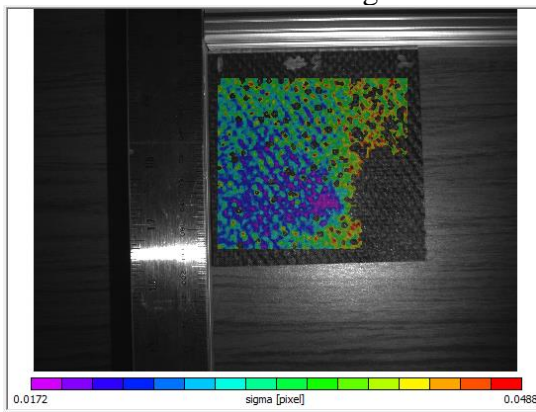
Front Outside – Gamma



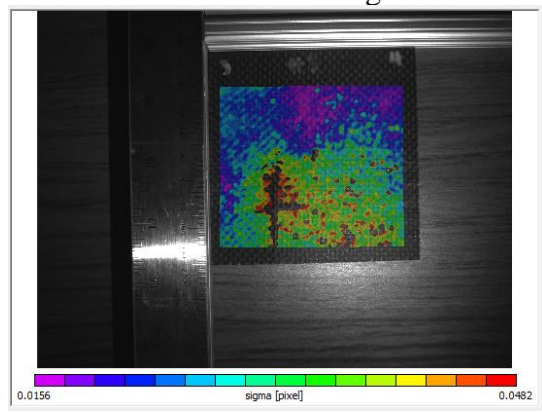
Back Outside – Gamma



Front Outside – Sigma



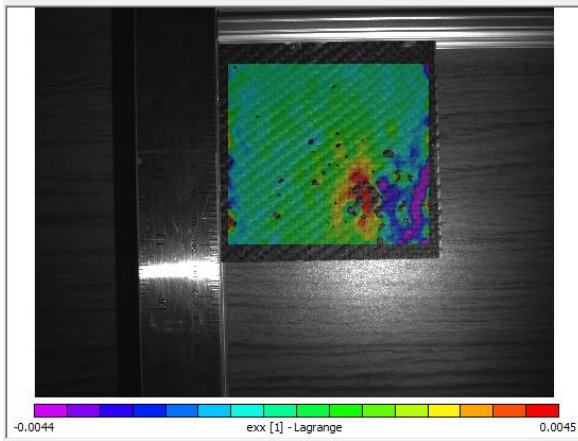
Back Outside – Sigma



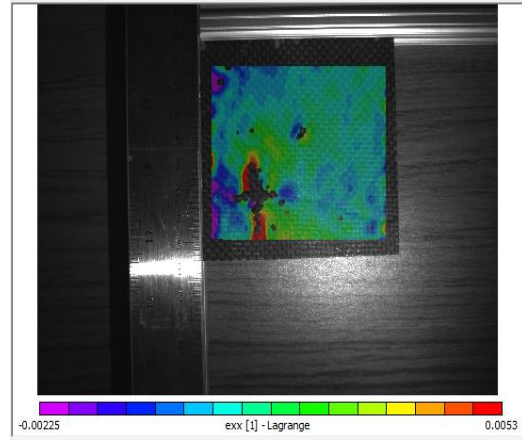


Sample 6 – Second Impact 10J – 1 in diameter head with lower right impact

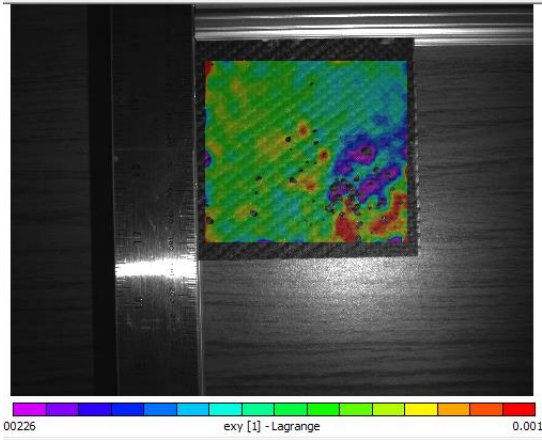
Front Inside – Exx



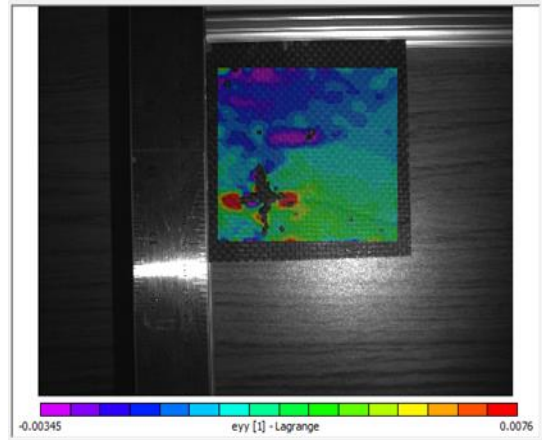
Back Inside – Exx



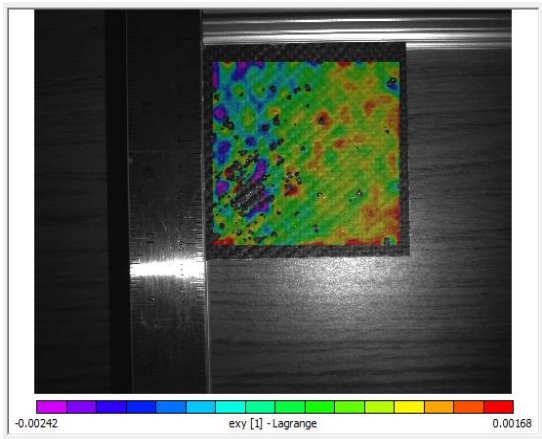
Front Inside – Eyy



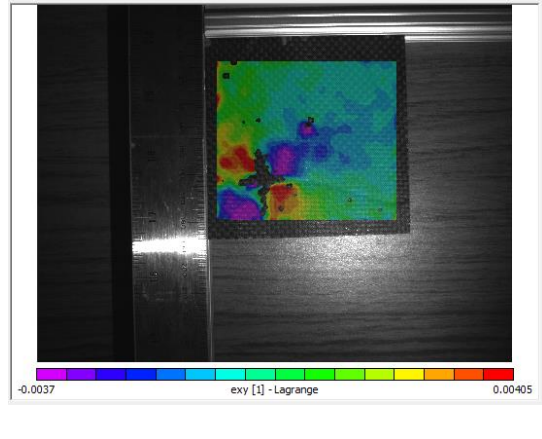
Back Inside – Eyy



Front Inside – Exy

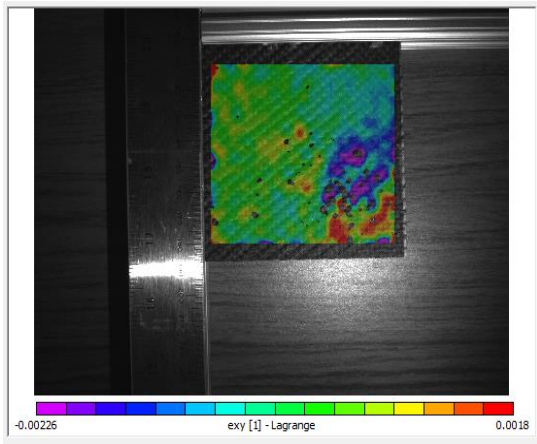


Back Inside – Exy

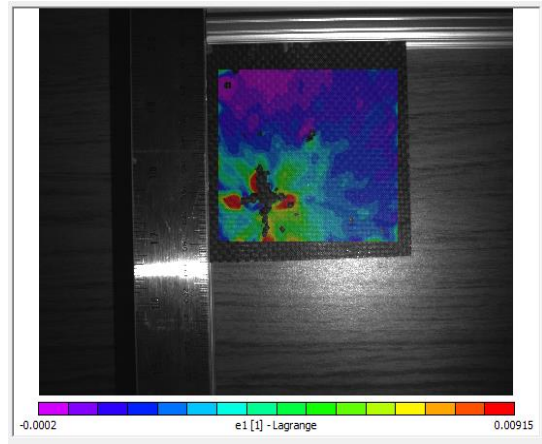




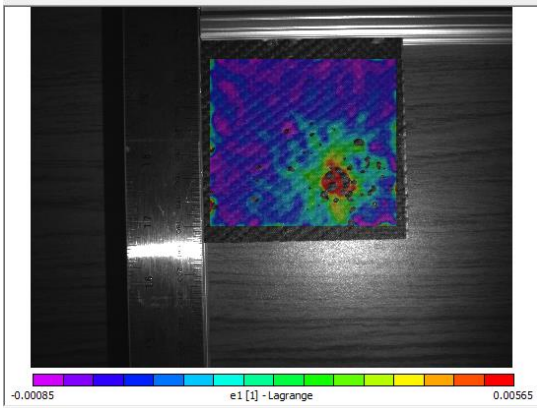
Front Inside – E1



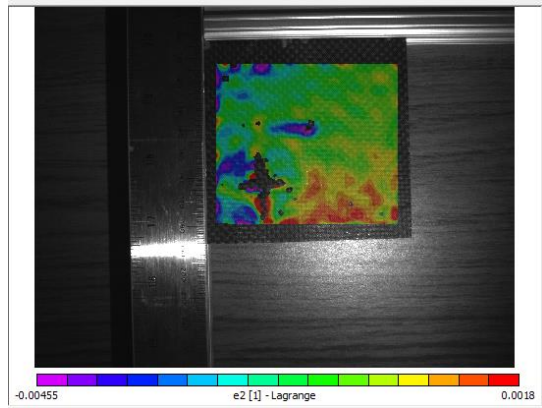
Back Inside – E1



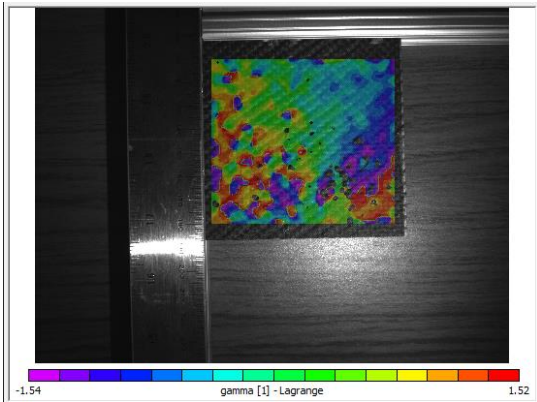
Front Inside – E2



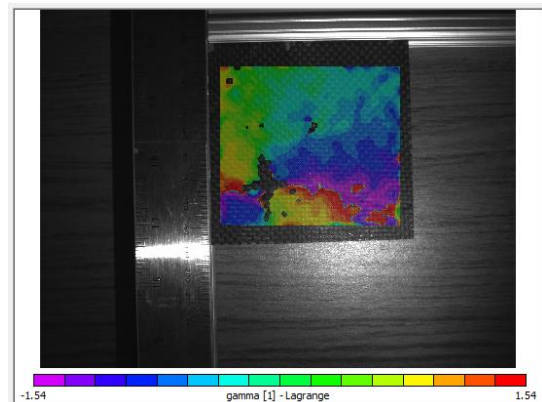
Back Inside – E2



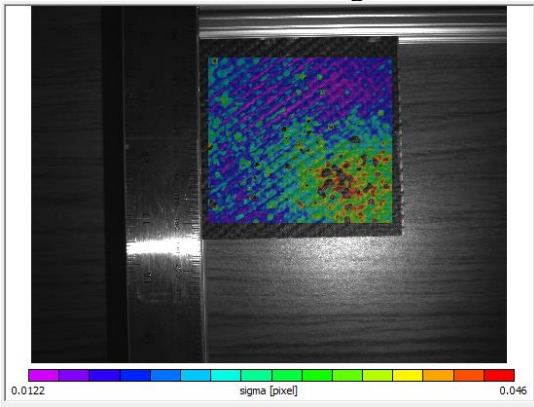
Front Inside – Gamma



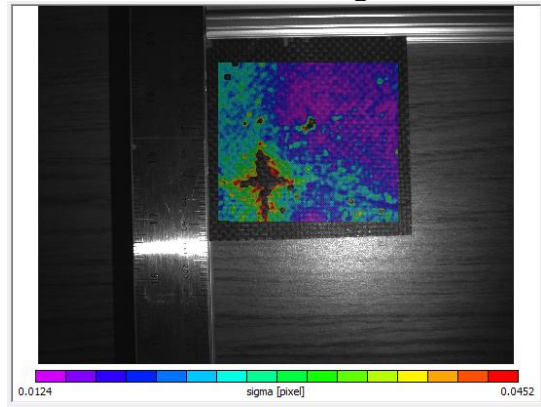
Back Inside – Gamma



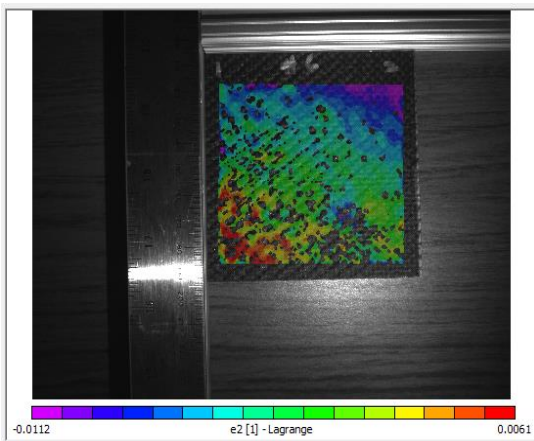
Front Inside – Sigma



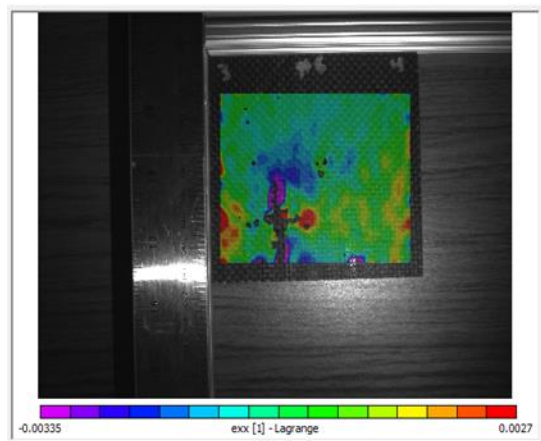
Back Inside – Sigma



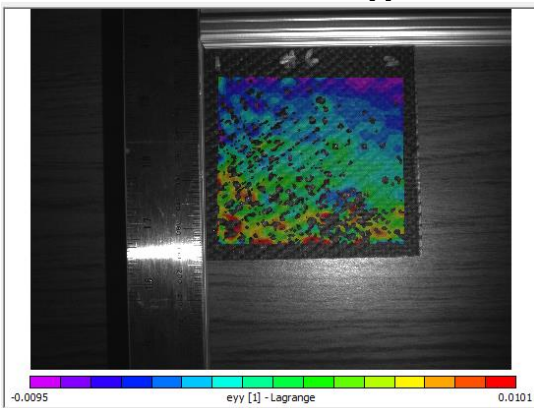
Front Outside -Exx



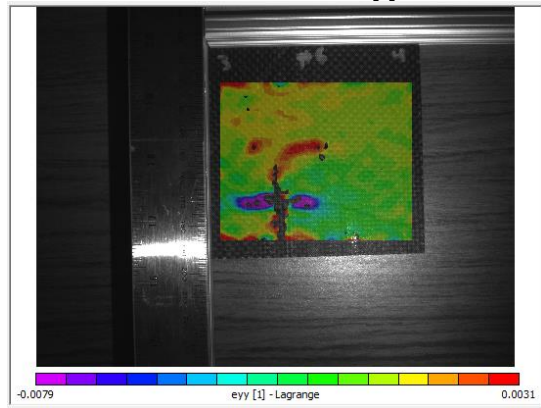
Back Outside – Exx



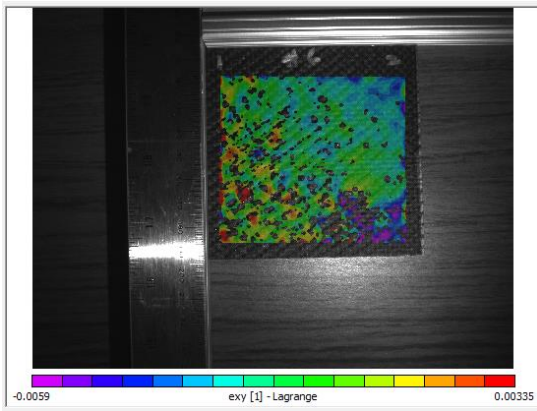
Front Outside – Eyy



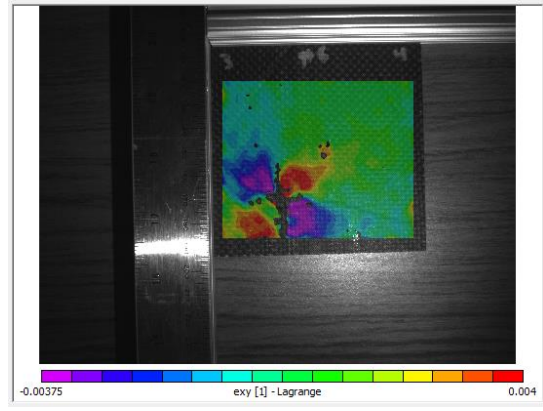
Back Outside – Eyy



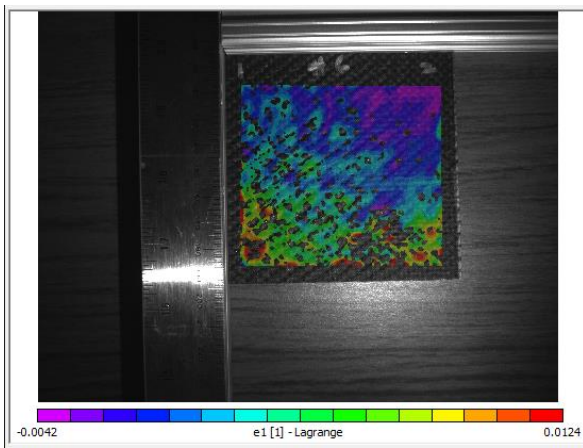
Front Outside – Exy



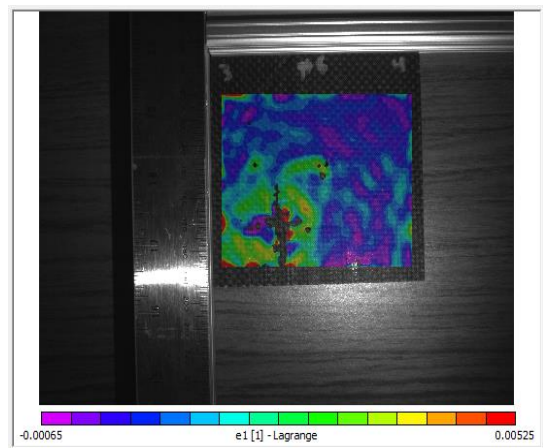
Back Outside – Exy



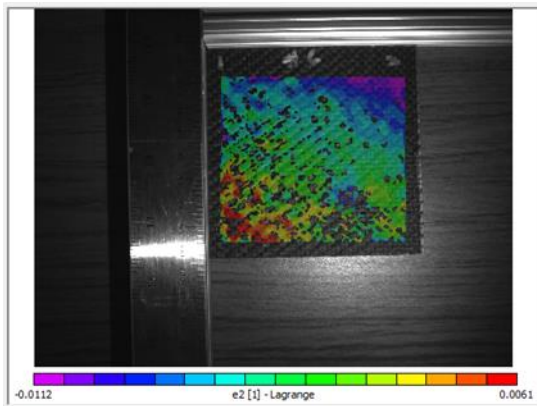
Front Outside – E1



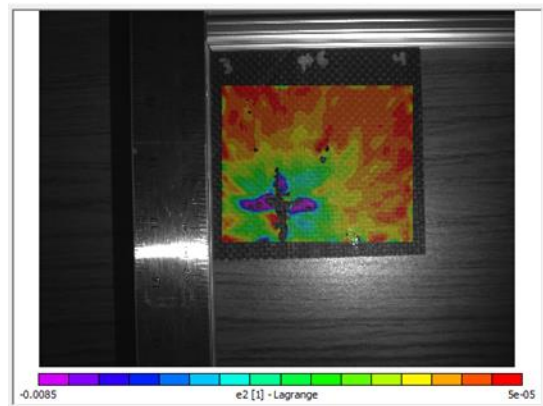
Back Outside – E1



Front Outside – E2

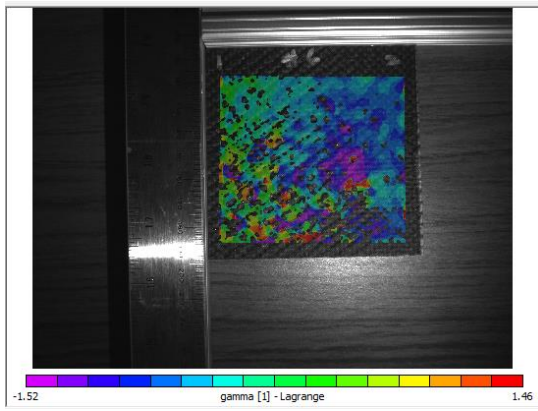


Back Outside – E2

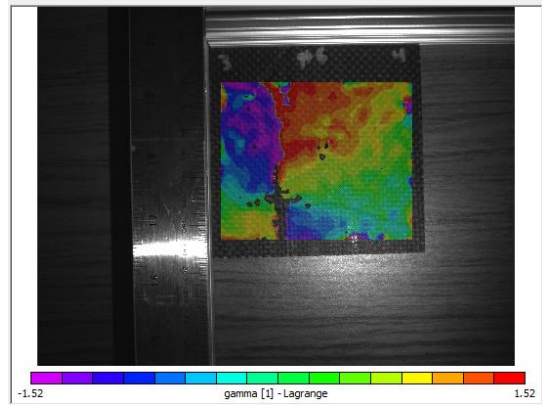




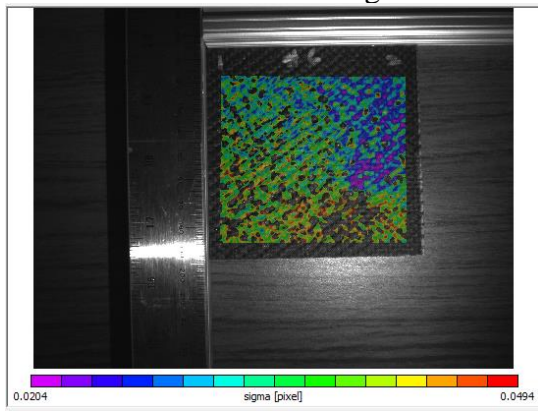
Front Outside – Gamma



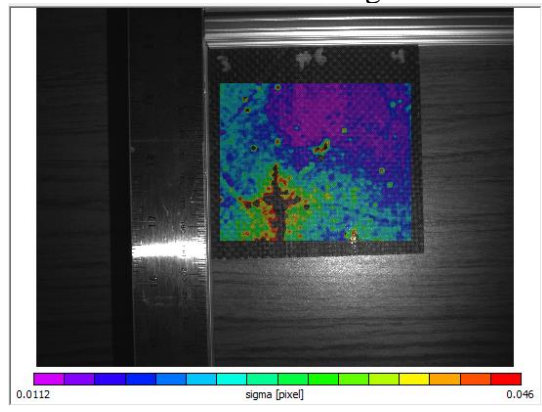
Back Outside – Gamma



Front Outside – Sigma

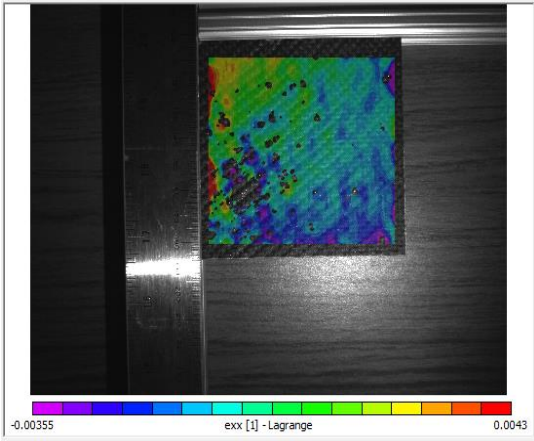


Back Outside – Sigma

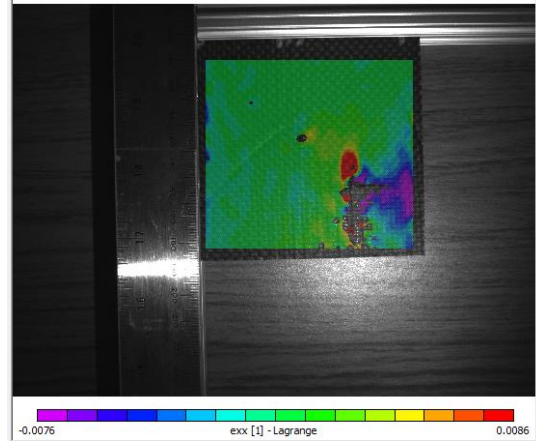


Sample 7 – Second Impact 10J – 1 in diameter head with bottom left impact

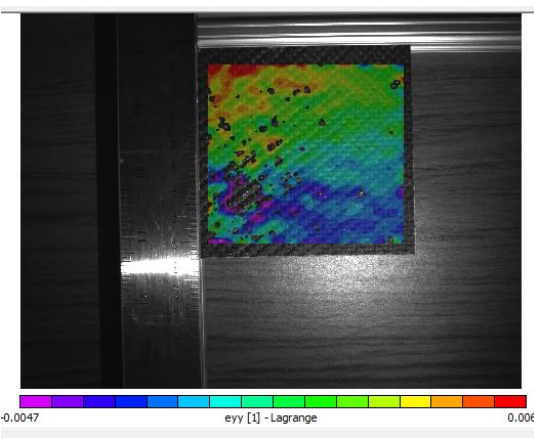
Front Inside – Exx



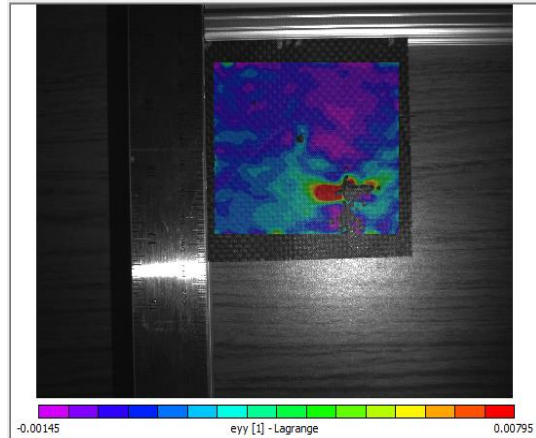
Back Inside – Exx



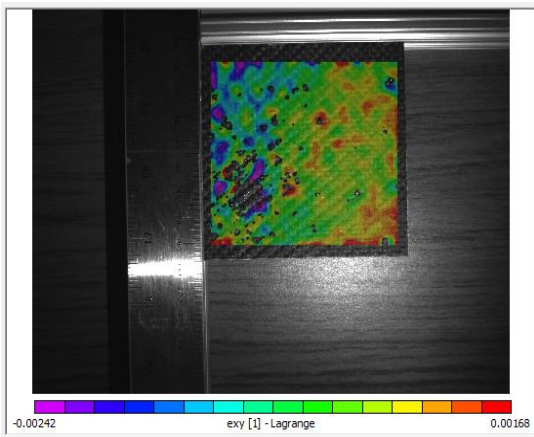
Front Inside – Eyy



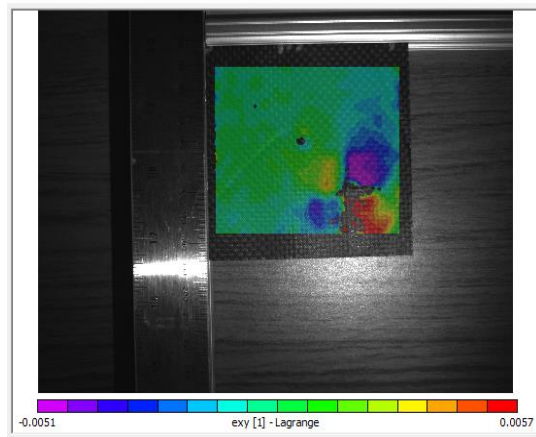
Back Inside – Eyy



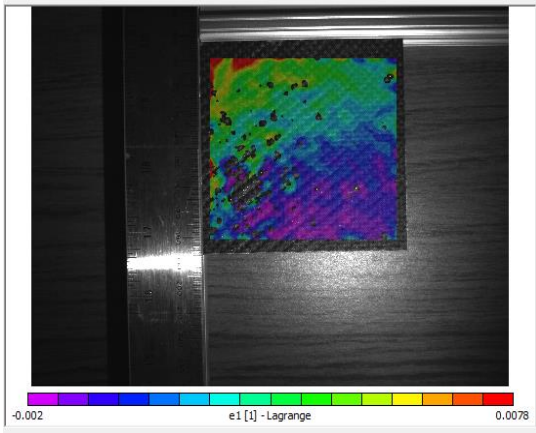
Front Inside – Exy



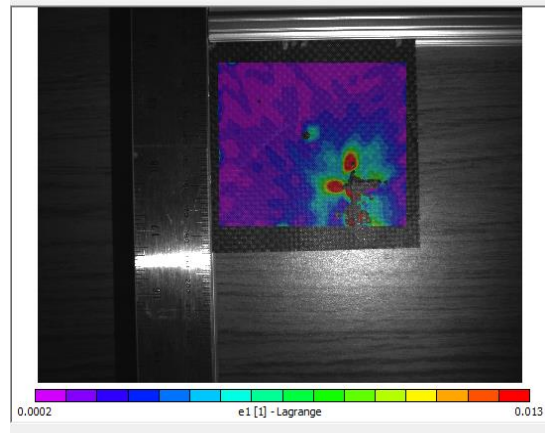
Back Inside – Exy



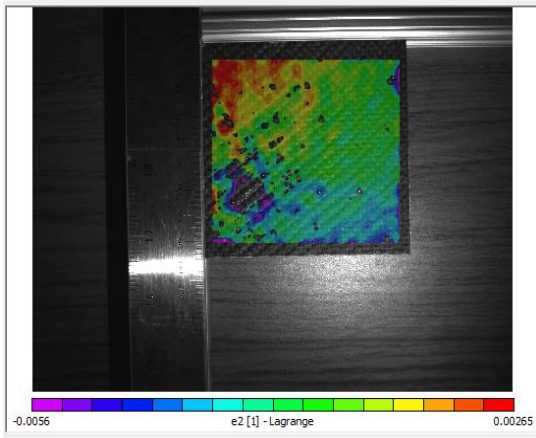
Front Inside – E1



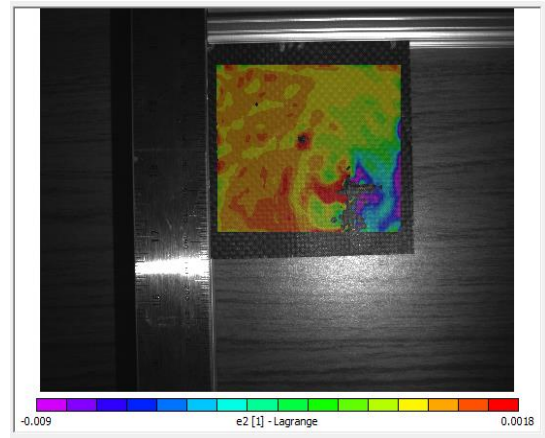
Back Inside – E1



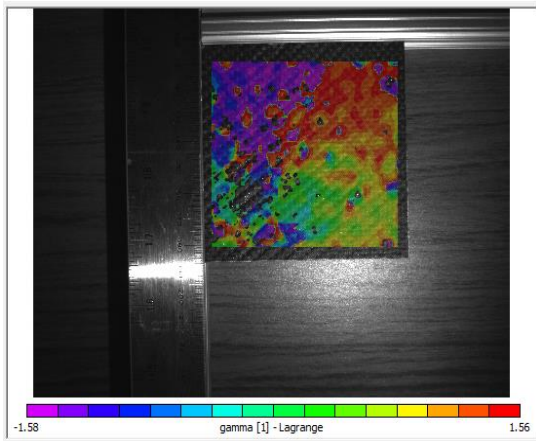
Front Inside – E2



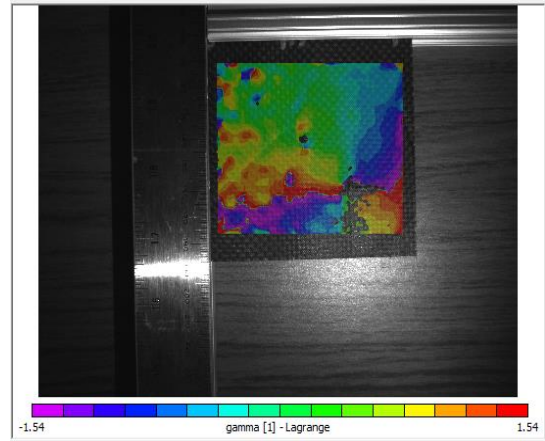
Back Inside – E2



Front Inside – Gamma

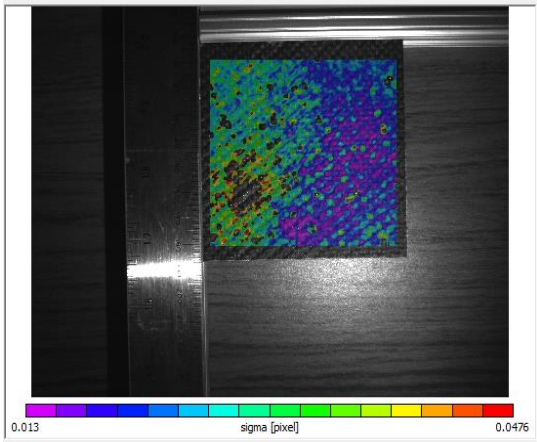


Back Inside – Gamma

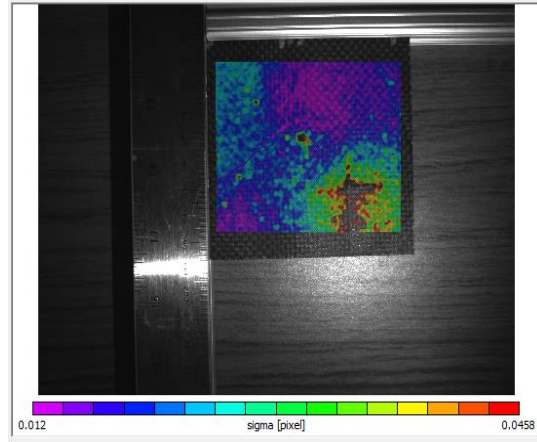




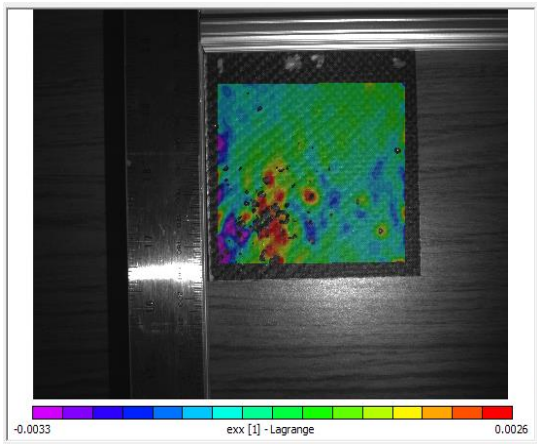
Front Inside – Sigma



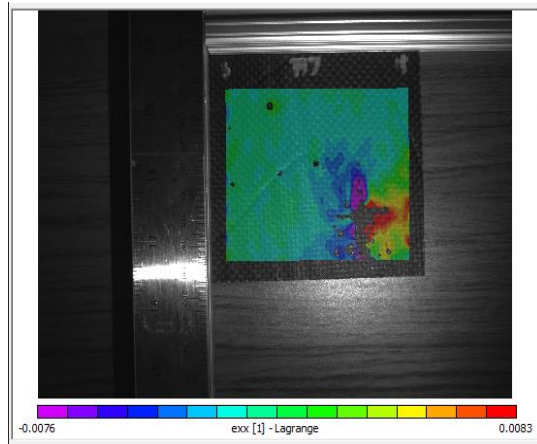
Back Inside – Sigma



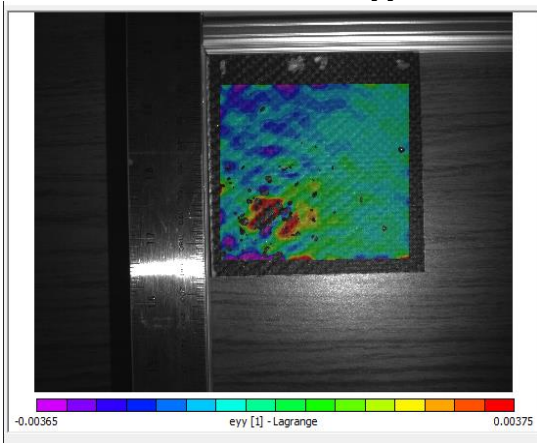
Front Outside -Exx



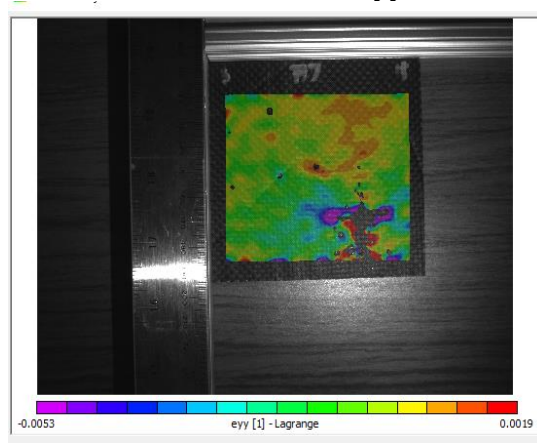
Back Outside – Exx



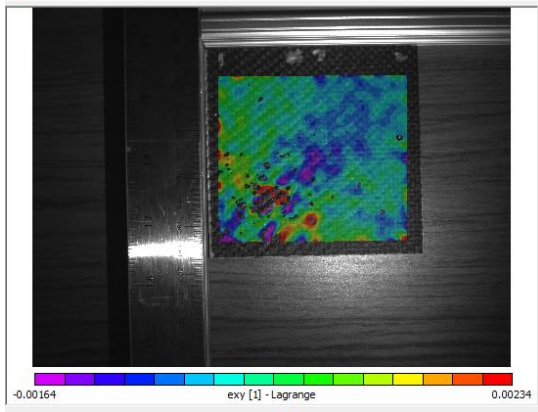
Front Outside – Eyy



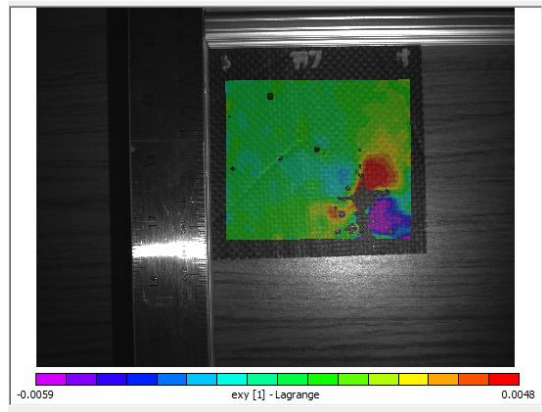
Back Outside – Eyy



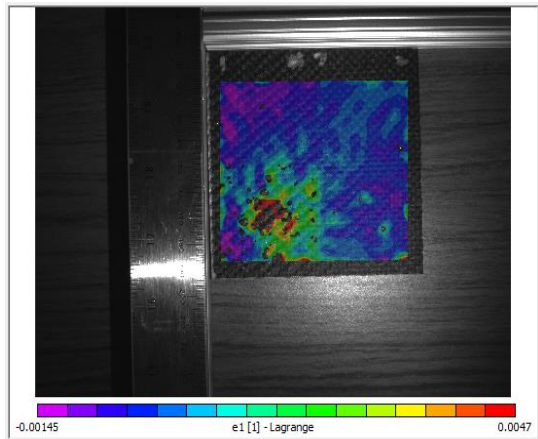
Front Outside – Exy



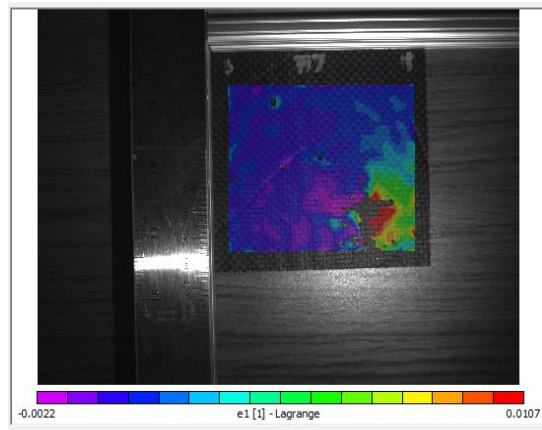
Back Outside – Exy



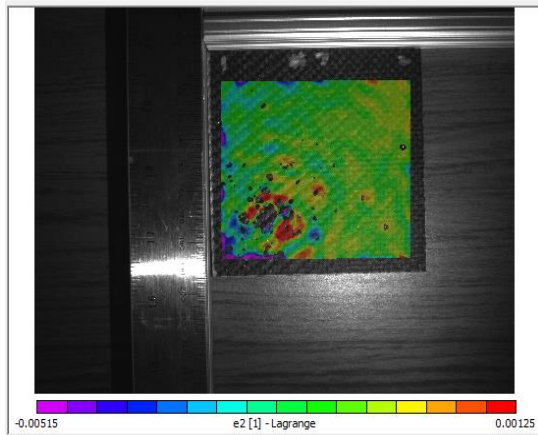
Front Outside – E1



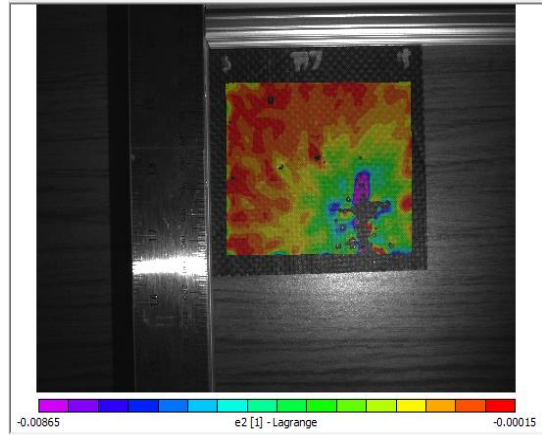
Back Outside – E1



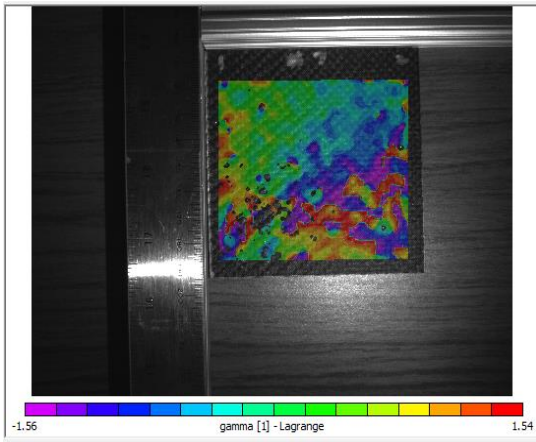
Front Outside – E2



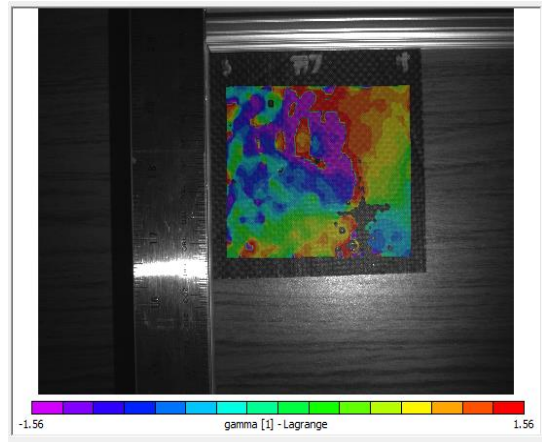
Back Outside – E2



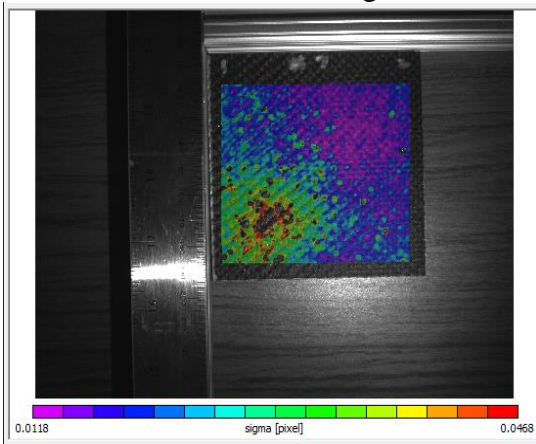
Front Outside – Gamma



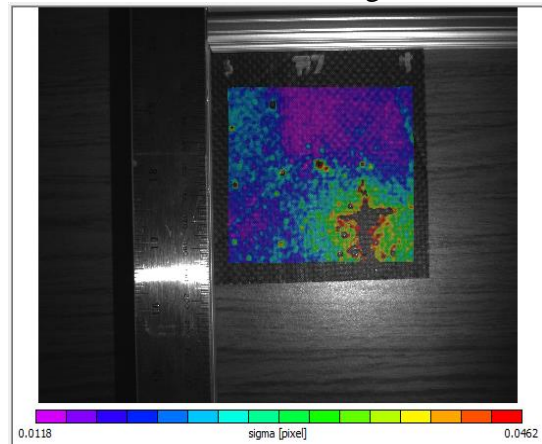
Back Outside – Gamma



Front Outside – Sigma



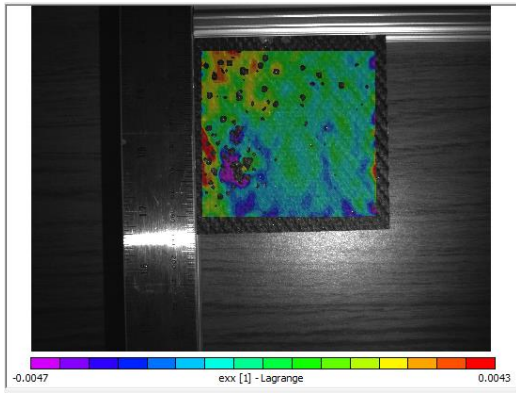
Back Outside – Sigma



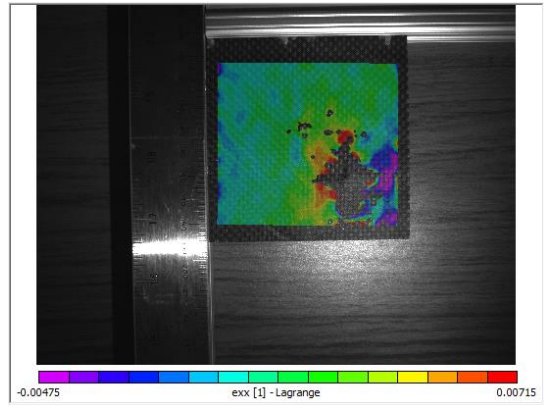


Sample 8 – Second Impact 10J – 1 in diameter head with bottom left impact

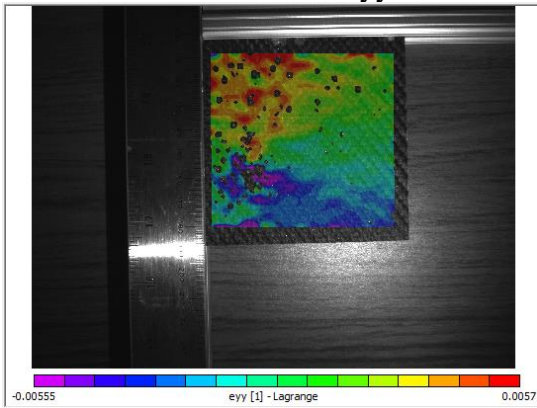
Front Inside – Exx



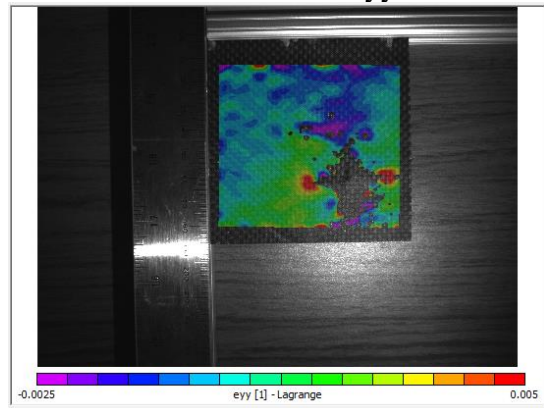
Back Inside – Exx



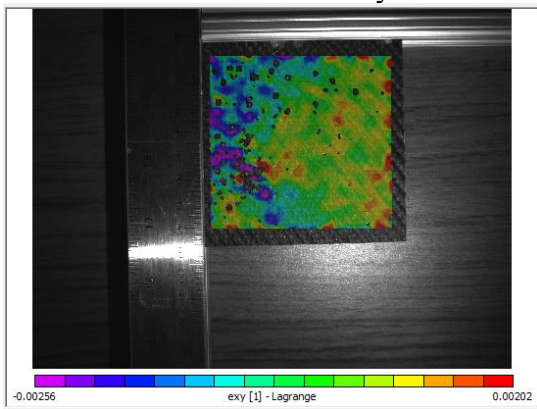
Front Inside – Eyy



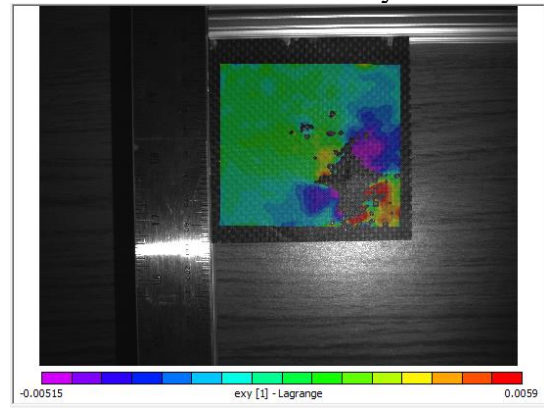
Back Inside – Eyy



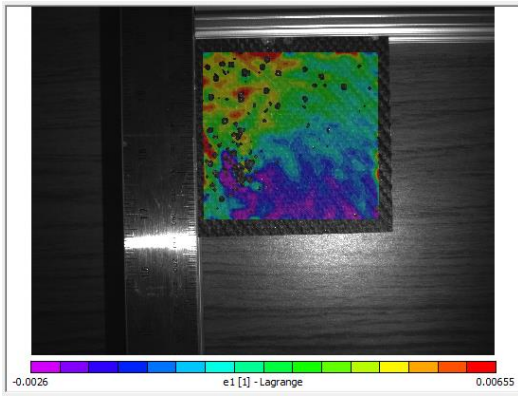
Front Inside – Exy



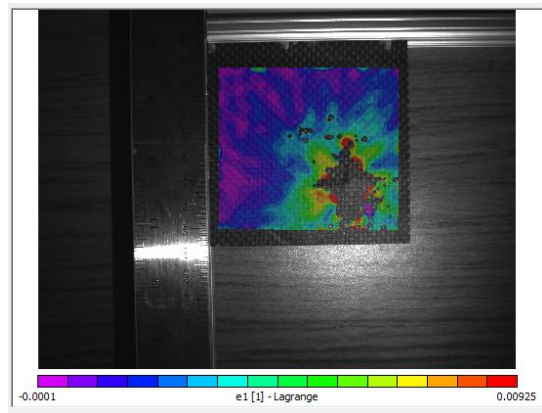
Back Inside – Exy



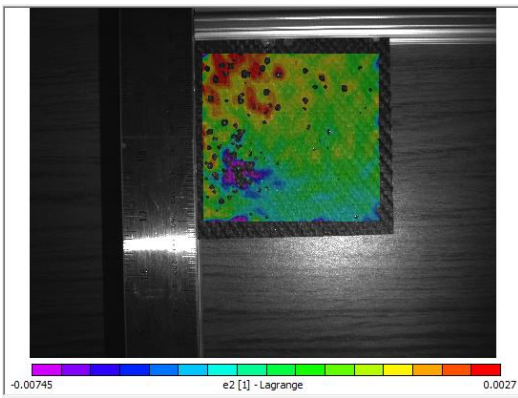
Front Inside – E1



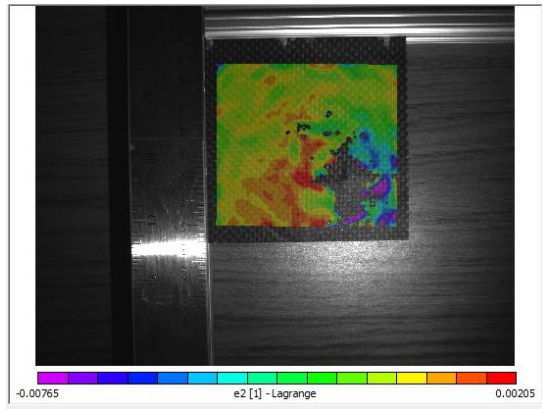
Back Inside – E1



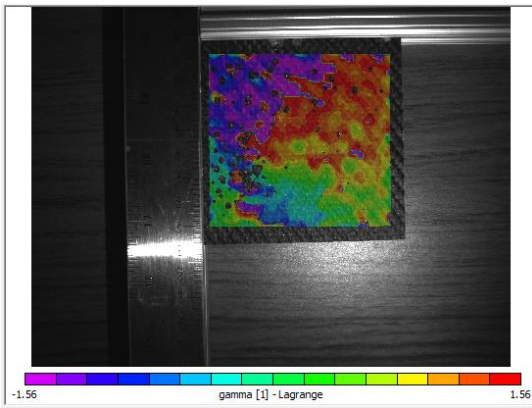
Front Inside – E2



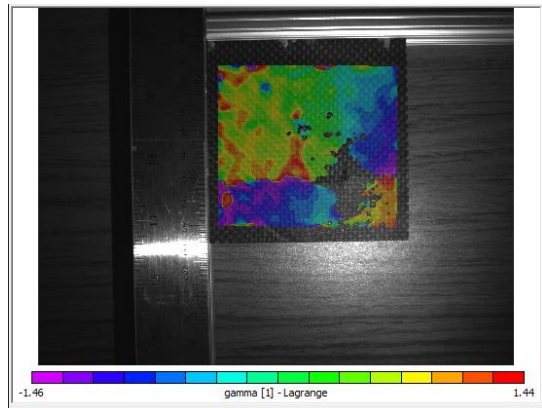
Back Inside – E2



Front Inside – Gamma

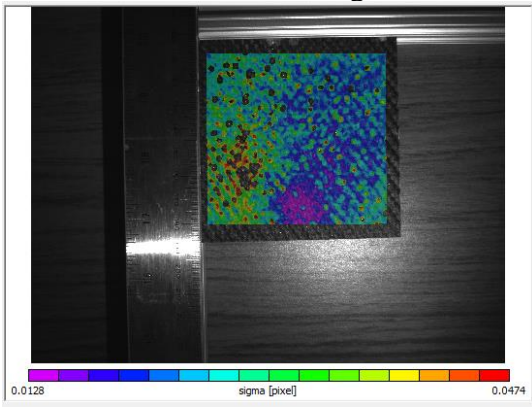


Back Inside – Gamma

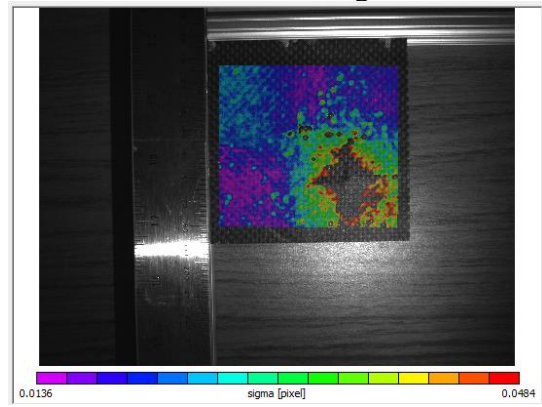




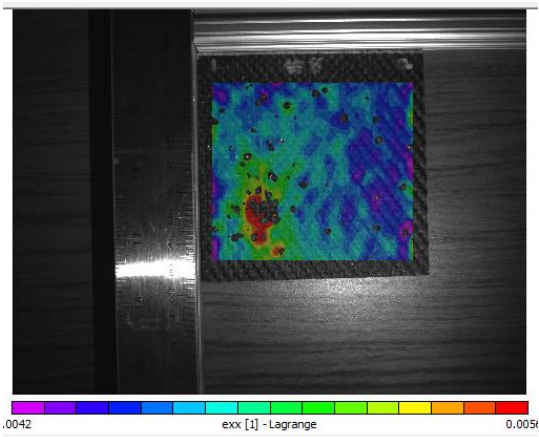
Front Inside – Sigma



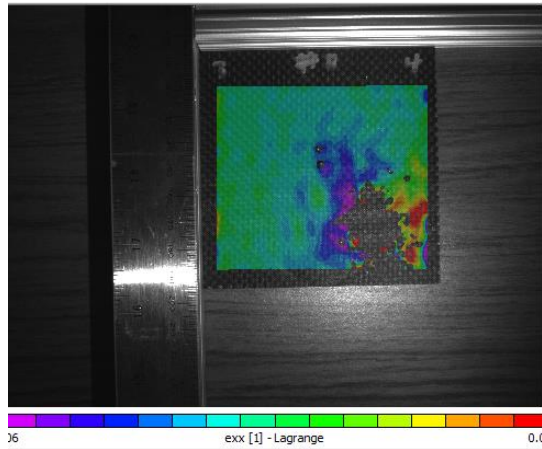
Back Inside – Sigma



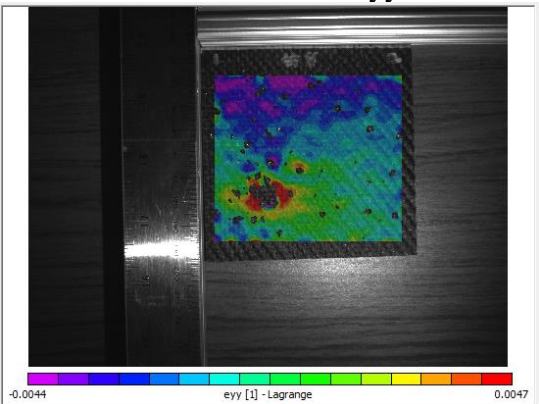
Front Outside -Exx



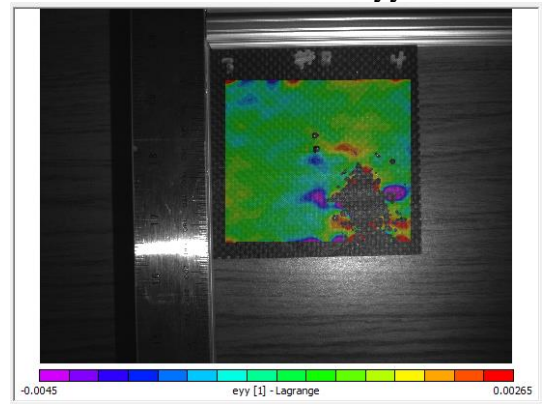
Back Outside – Exx



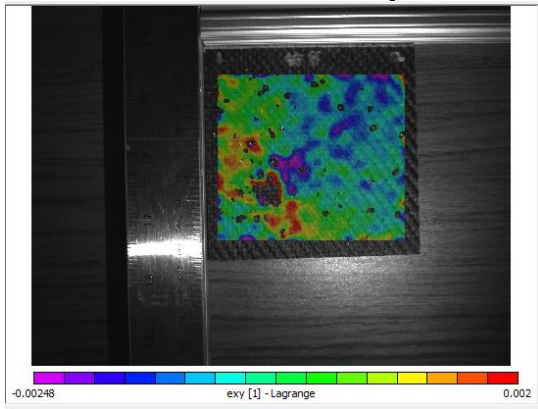
Front Outside – Eyy



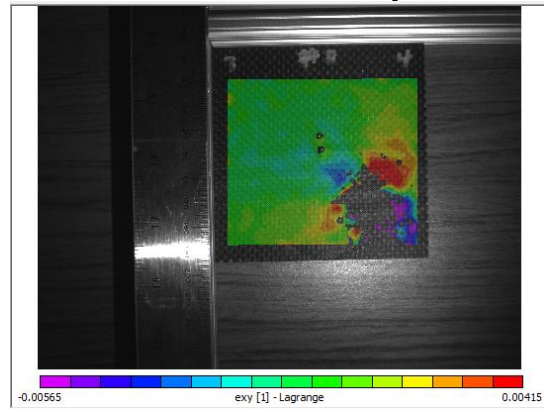
Back Outside – Eyy



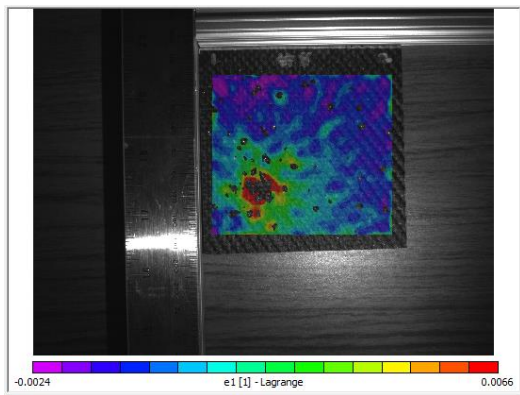
Front Outside – Exy



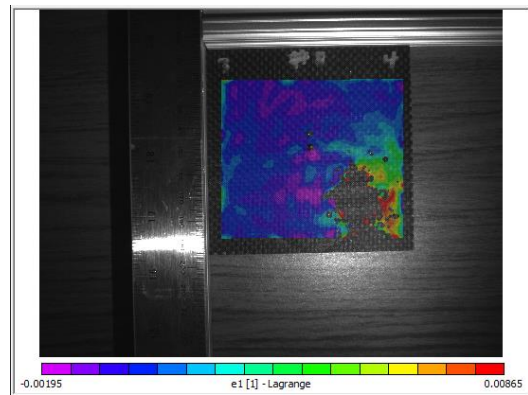
Back Outside – Exy



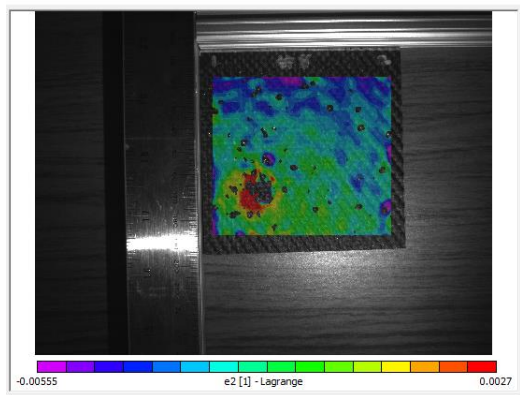
Front Outside – E1



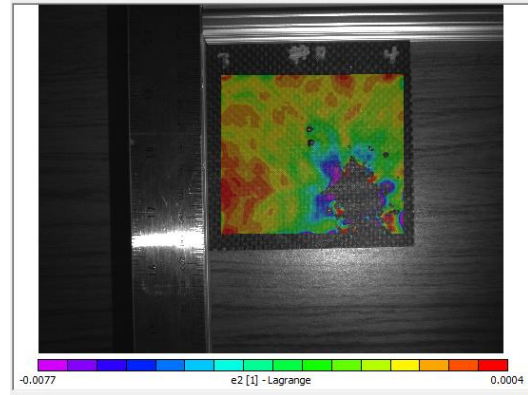
Back Outside – E1



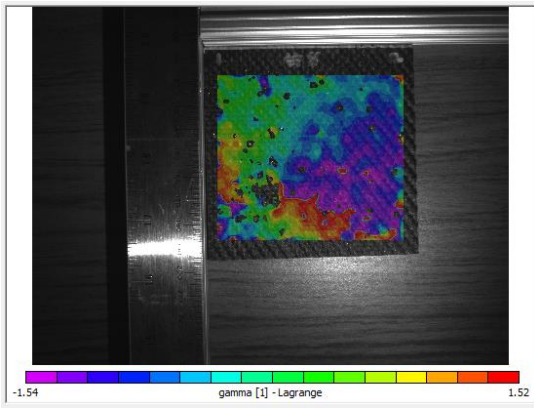
Front Outside – E2



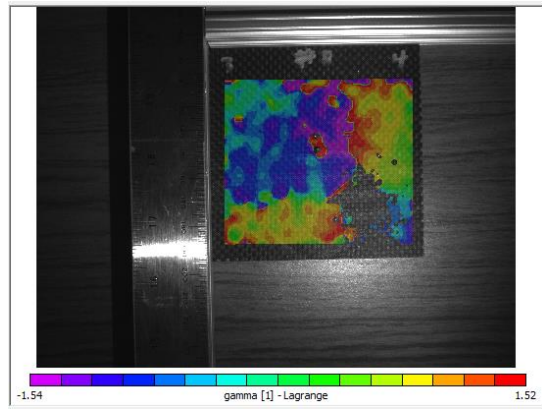
Back Outside – E2



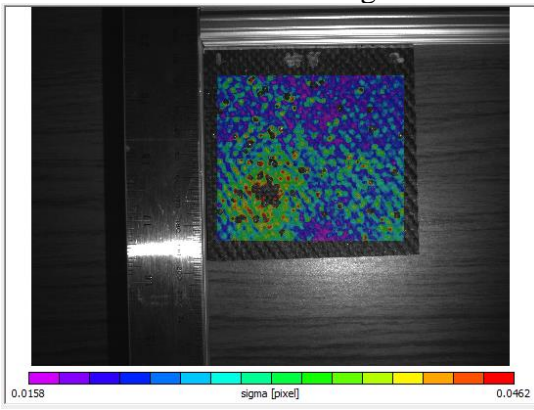
Front Outside – Gamma



Back Outside – Gamma



Front Outside – Sigma



Back Outside – Sigma

